DEVELOPMENT OF A HYDROGEL-BASED CARBON DIOXIDE SENSOR

A TOOL FOR DIAGNOSING GASTROINTESTINAL ISCHEMIA

The described research has been carried out at the “Miniaturized Systems For Biomedical And Environmental Applications” group (BIOS) of the MESA+ Research Institute at the University of Twente, Enschede, the Netherlands. The research was financially supported by the Dutch Technology Foundation, STW, project TTF.5439.

Samenstelling promotiecommissie:

Voorzitter	
prof. dr. ir. J. van Amerongen	Universiteit Twente
Promotor	
prof. dr. ir. P. Bergveld	Universiteit Twente
Co-promotor	
prof. dr. ir. A. van den Berg	Universiteit Twente
Assistent promotor	
dr. ir. W. Olthuis	Universiteit Twente
Leden	
prof. dr. J.F.J. Engbersen	Universiteit Twente
prof. dr.-ing. habil G. Gerlach	Technische Universität Dresden
dr. J.J. Kolkman	Medisch Spectrum Twente
prof. P.F. Gibson	Royal Academy of Engineering

Title: DEVELOPMENT OF A HYDROGEL-BASED CARBON DIOXIDE SENSOR - a tool for diagnosing gastrointestinal ischemia

Cover: Front-side: artist impression of the hydrogel-based carbon dioxide sensor. Back-side: some relevant pictures and scientific notations collected during the research

Author: Sebastiaan Herber

ISBN: 90-365-2144-0

Printing: Febodruk B.V. Enschede

DEVELOPMENT OF A HYDROGEL-BASED CARBON DIOXIDE SENSOR

A TOOL FOR DIAGNOSING GASTROINTESTINAL ISCHEMIA

PROEFSCHRIFT

ter verkrijging van
de graad van doctor aan de Universiteit Twente,
op gezag van rector magnificus,
prof. dr. W.H.M. Zijm,
volgens besluit van het College voor Promoties
in het openbaar te verdedigen
op vrijdag 13 mei 2005 om 13:15 uur

door

Sebastiaan Herber
geboren op 1 februari 1979
te Utrecht

Dit proefschrift is goedgekeurd door

promotor: prof. dr. ir. Piet Bergveld
co-promotor: prof. dr. ir. Albert van den Berg
assistent promotor: dr. ir. Wouter Olthuis

Aan mijn ouders

"Always learn from history
To be sure you make the same mistakes again
Dig with bare hands or a silver spoon
But never change the masterplan"

Johan Edlund

TIAMAT

Song: Angel Holograms

TABLE OF CONTENTS

Chapter 1
Introduction

The first chapter starts with presenting some medical background information on gastrointestinal ischemia. This form of ischemia can be diagnosed by measuring the gastric/intestinal CO_2 concentration. The research goal, i.e. the development of an alternative gastric CO_2 sensor, is described, followed by an overview of other CO_2 sensor application areas and existing detection principles. The chapter ends with an outline of this thesis.

1.1 Motivation

The BIOS chair of the Faculty of Electrical Engineering, Mathematics and Computer Science at the University of Twente aims at the research and development of miniaturized systems for biomedical and environmental applications, and Lab-on-a-Chip systems. The BIOS research program, embedded in the MESA$^+$ research institute, is broad but its main competence is found in micro/nanofluidics, micro/nanofabrication and electrochemical sensor technologies. Research goals of BIOS are bridging the gap between physical, chemical, biomedical and life-sciences fields, and the development of the necessary new micro- and nanotechnologies. Other goals are to increase the knowledge and understanding of nanofluidics, and to demonstrate the potential of Lab-on-a-Chip applications.

In 1998 Dr. J.J. Kolkman (gastroenterologist at the Medical Spectrum Twente hospital, Enschede, The Netherlands) contacted Prof. Dr. Ir. P. Bergveld of the BIOS group with a request to develop a miniature sensor for

the intracorporeal detection of carbon dioxide in the stomach to diagnose gastrointestinal ischemia. Ultimately, this led to the origination of a new PhD project (financed by the Dutch funding agency for university research, STW) in May 2001 with this thesis as result.

1.2 Gastrointestinal ischemia

1.2.1 Description

Gastrointestinal ischemia occurs when blood flow is insufficient to deliver oxygen (O_2) to the stomach and intestines necessary for maintaining cell integrity[1-3]. In figure 1.1 the human digestive system is shown.

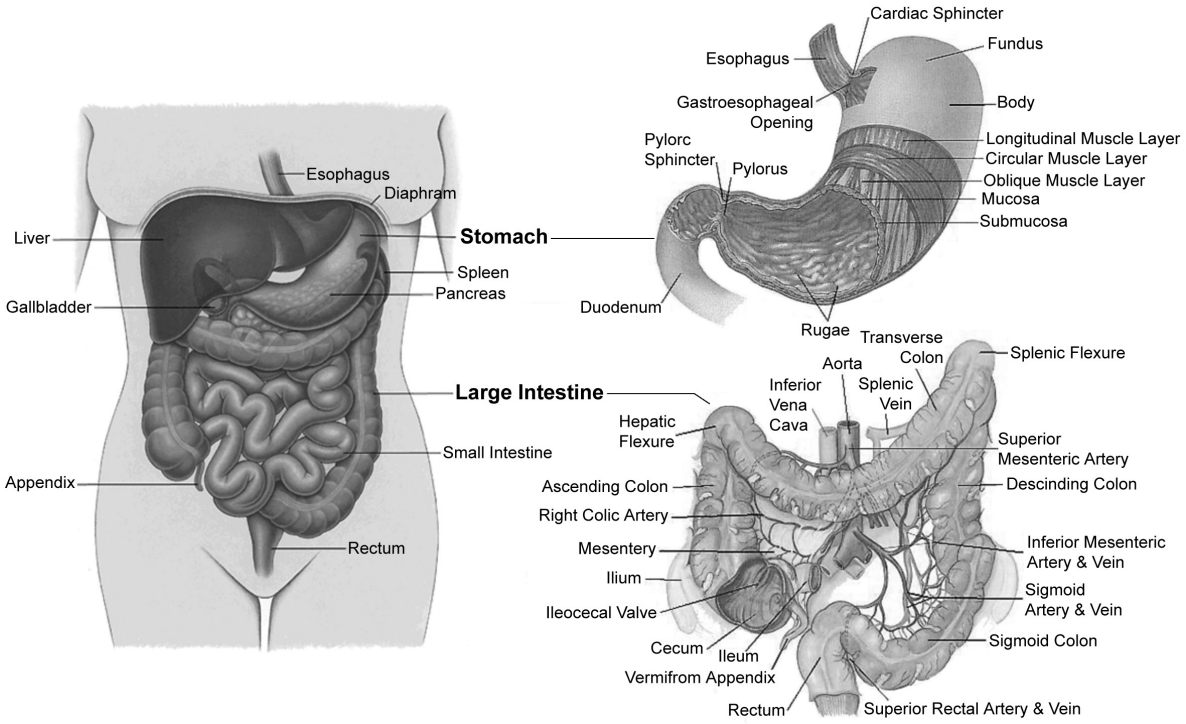

Figure 1.1. The human digestive system (photo courtesy of Thibodeau).

Under normal conditions 10% of the cardiac output goes through the splanchnic (intestinal) vessels (fig. 1.1). After eating, the gut demands more oxygen and therefore the blood flow is increased. With sufficient blood flow, enough oxygen enters the cells and is used for carbohydrate oxygenation, the so-called aerobic metabolism. This glycolysis is a metabolic process that

breaks down carbohydrates and sugars through a series of reactions to lactic acid and releases energy for the body in the form of adenosine triphosphate (ATP). Together with the lactic acid, carbon dioxide is released, which is removed by the blood flow. The mechanism is schematically represented in figure 1.2a.

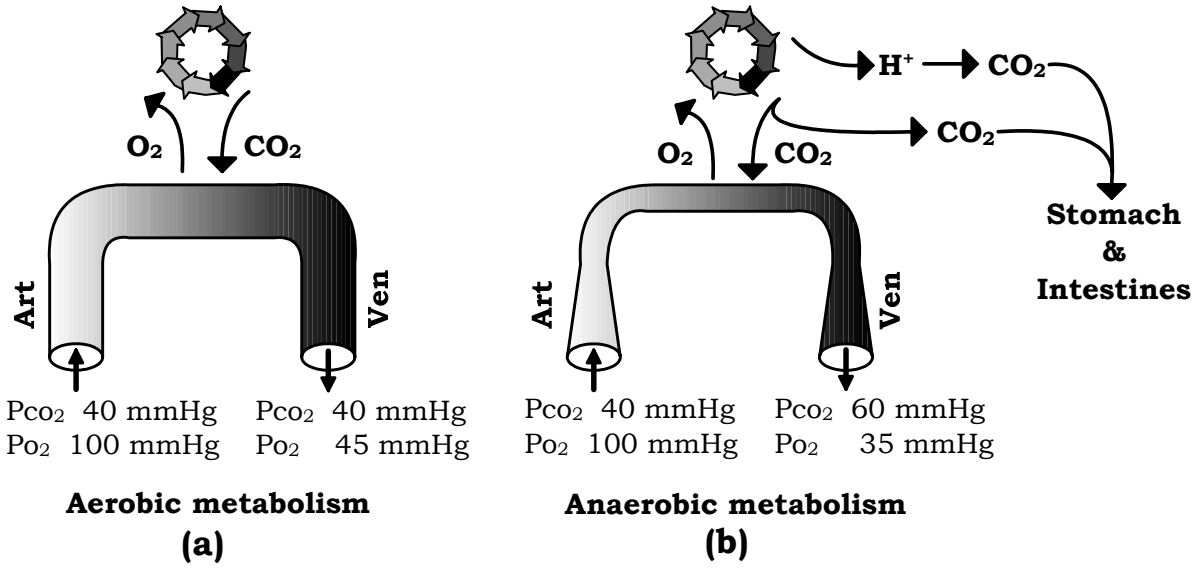

Figure 1.2. (a) Normal organ perfusion (b) Severe organ hypoperfusion (figure courtesy of J.J. Kolkman, dept gastroenterology MST Enschede).

When the blood flow decreases (hypoperfusion) and oxygen is delivered below demands, the production of lactic acid by the bowel is increased as result of anaerobic glycolysis in the cells (figure 1.2b). The lactate production is accompanied by hydrolysis of ATP and liberation of H^+ ions. The protons react with local bicarbonate to carbon dioxide and water,

$$H^+ + HCO_3^- \rightarrow H_2CO_3 \rightarrow CO_2 + H_2O\,. \qquad (1.1)$$

Consequently, the partial pressure of carbon dioxide (Pco_2) increases. Additionally, there is a decreased CO_2 clearance due to the reduced blood flow. The remaining carbon dioxide accumulates within the wall of the intestines and stomach (intramural) and diffuses readily over the gastrointestinal mucosa (membrane lining all body passages that communicate with the exterior, fig 1.1) leading to unusually high concentration of carbon dioxide in the intestines and stomach (intraluminal

hypercapnia). Note that due to the decreased blood flow in case of anaerobic metabolism the uptake of oxygen per blood volume is increased, which results in a lower Po_2 (35 mmHg) than in the case of aerobic metabolism (45 mmHg).

1.2.2 Etiology

Gastrointestinal ischemia results from two fundamentally different types of disorders. The first type is occlusive ischemia which is the result of disrupted gastrointestinal blood flow, such as by strangulation, volvulus (abnormal twisting of the intestine) or venous/arterial thrombosis (formation or presence of a clot of coagulated blood, or so-called thrombus). It is assumed that this type of ischemia is relatively rare compared to the one discussed below.

The second type is non-occlusive ischemia. This ischemia results from systematic conditions such as circulatory shock, sepsis (a toxic condition resulting from the spread of bacteria or their products from a focus of infection), or cardiac insufficiency. The syndrome is due to impaired splanchnic circulation and can be found relatively frequent in post-operative and critically ill patients. Clinical signs may range from ileus (intestinal obstruction causing colic, vomiting, and constipation) and intolerance to enteral nutrients to ovurt ulceration (a lesion of the mucous membrane with loss of surface tissue, disintegration and necrosis of epithelial tissue, and often pus) and bleeding.

1.2.3 Clinical features

Clinical features of gastrointestinal ischemia can be divided into three types. The first is acute gastrointestinal ischemia which is an acute termination of blood flow to the gut. Main causes are arterial thrombosis, venous thrombosis or non-occlusive ischemia. Patients can suffer from acute abdominal pain, severe nausea, vomiting and hypotension.

Another type is chronic gastrointestinal ischemia which can be caused by splanchnic atherosclerosis, celiac artery syndrome, venous thrombosis or small vessel disease. Symptoms are pain after having meal, weight loss and audible abdominal bruit.

The last type is colonic ischemia which occurs at the large intestine extending from the cecum to the rectum (fig. 1.1). This type of ischemia is

most often due to non-occlusive disease with normal major splanchnic vessels. The features are crampy abdominal pain of sudden onset, diarrhea often with blood loss.

1.2.4 Diagnosis

Splanchnic perfusion and ischemia can be evaluated with several diagnostic methods such as splanchnic angiography, blood markers, duplex sonography, endoluminal laser Doppler flowmetry and endoluminal puls oximetry. A particularly interesting method is tonometry of intraluminal Pco_2 which is extensively used at the local hospital of Enschede (Medical Spectrum Twente, MST Enschede) [4].

Tonometry is based on the assumption that gastrointestinal ischemia causes intraluminal hypercapnia. The high concentration of carbon dioxide in the intestines and stomach can be measured with a tonometer. There are two types of tonometry: saline tonometry and air tonometry[5,6]. Saline tonometry has a multitude of practical problems and will therefore not be discussed. Air tonometry involves a catheter equipped with a gas-permeable silicone balloon at its tip which is introduced nasogastrically to the stomach or jejunum. In figure 1.3 a common tonometer catheter is shown and in figure 1.4 a picture of the tonometry catheter placed in the stomach.

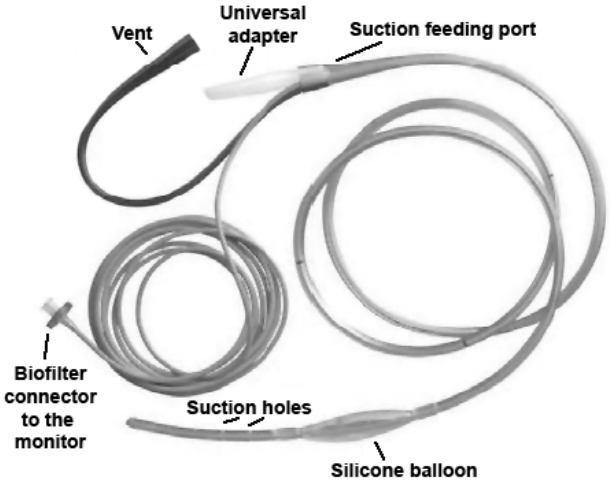

Figure 1.3. Picture of a common tonometry catheter (photo courtesy of Datex-Ohmeda).

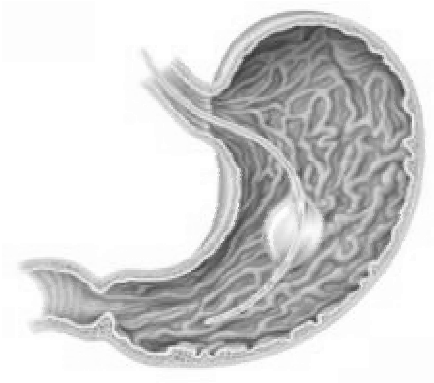

Figure 1.4. The tonometry catheter placed in the stomach (photo courtesy of Datex-Ohmeda).

The tonometer catheter is connected to a Tonocap, a modified capnograph allowing for automated inflation and aspiration from air into or out of the tonometer catheter. After positioning of the catheter, the balloon is automatically inflated with 5 ml room air and carbon dioxide equilibrates between the stomach and the content of the balloon. After ten minutes the balloon content is aspirated by the tonocap. The tonocap determines the Pco_2 by infrared detection, after which the analyzed content is sent back to the balloon. Measurements can be performed with intervals of ten minutes. The tonometer and tonocap are manufactured by Datex-Ohmeda Division, Instrumentarium Corporation, Finland. Detection of gastrointestinal ischemia by tonometry may help to diagnose perfusion failure in critically ill patients at an early stage and may aid in the prevention of irreversible organ damage. Tonometry is easy and a minimally invasive procedure.

At the Medical Spectrum Twente hospital, two measurement protocols are used with tonometry. During 24h tonometry the gastric and small bowel Pco_2 of a patient is monitored for 24 hours. An example is given in figure 1.5. Note the pain signals and increased Pco_2 after eating.

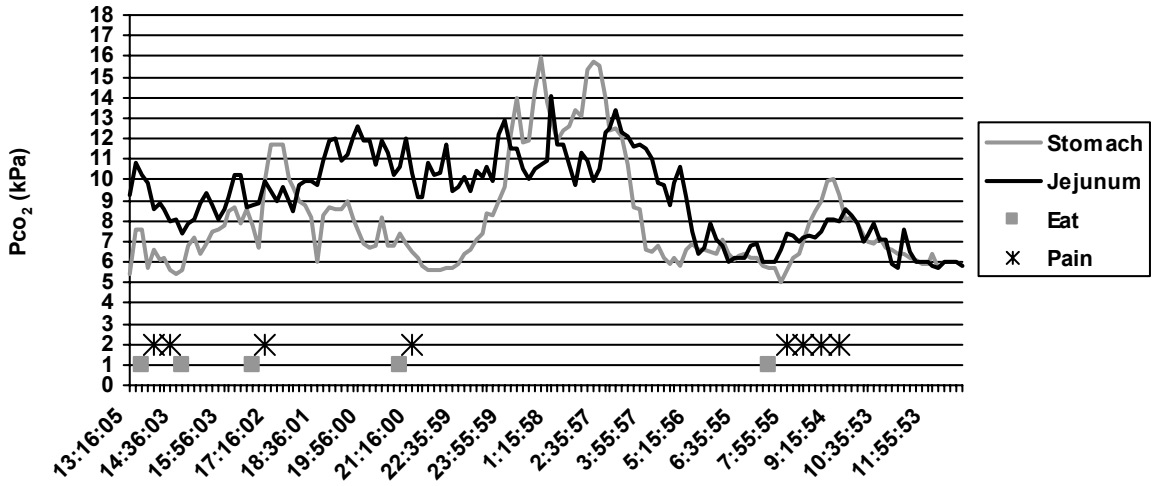

Figure 1.5. Result of a 24h tonometry (figure courtesy of J.J. Kolkman, dept gastroenterology MST Enschede).

The other tonometry measurement protocol is a gastric Pco_2 measurement during a cycle exercise[7]. In figure 1.6 a measurement result is given. During an exercise, more oxygen is delivered to the muscles at the cost of oxygen supply to the stomach and intestines. The result is an obviously increased partial pressure of carbon dioxide in the stomach and

jejunum. An increase of more than 0.8 kPa CO_2 during the exercise is an indication for ischemia. In a prospective study the sensitivity and specificity of the latter test were 78% and 92%, respectively.

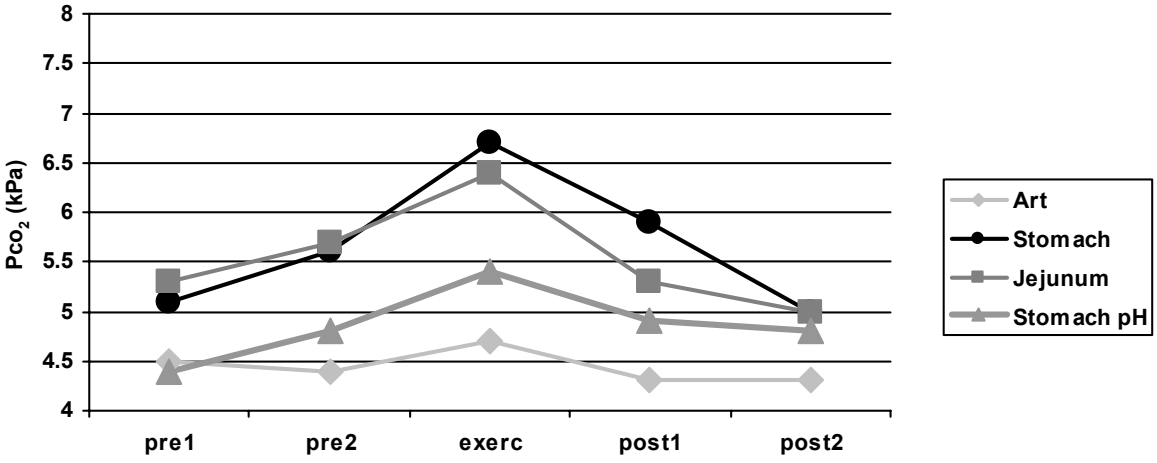

Figure 1.6. Result of an exercise tonometry (figure courtesy of J.J. Kolkman, dept gastroenterology MST Enschede).

1.2.5 Therapy

Several treatments are used, dependent on the type of gastrointestinal ischemia. Treatment of acute gastrointestinal ischemia has two aims. First, the blood flow needs to be restored, which can be achieved by embolectomy (removal of an embolus) or surgical revascularization. Second, all necrotic bowel should be removed to prevent peritonitis.

Chronic gastrointestinal ischemia treatment is aimed at relief of symptoms and avoidance of acute gastrointestinal ischemia (or bowel infarction). Two types of chronic ischemia are recognized. The first type is characterized by a stenosis in only one of the three main vessels. Approximately 50% of these patients have abdominal complaints caused by ischemia, and treatment results in disappearance of symptoms in 80-90%. No complications, bowel infarction or death were seen in over 80 patients. Patients with stenosis in two or three main gastrointestinal vessels have ischemic complaints in over 95%. Complications are frequent and bowel infarction occurred in up to 35% of patients within a year after diagnosis[8]. Treatment can be aimed at life-style measures (avoidance of large meals, reduction of long chain fat content, termination of smoking), medication

(acid suppression, anticoagulants) or surgical or radiological revascularization with an intravascular stent placement.

Colonic ischemia is mostly treated by intravenous fluids to restore the blood flow. Sometimes, segmental colon (fig 1.1) resection is necessary.

1.3 Research goal

Tonometry as diagnostic procedure for gastrointestinal ischemia is extensively and successfully used at the Medical Spectrum Twente hospital, the Netherlands. This hospital has a nationwide referral center for patients of gastrointestinal ischemia. However, the current tonometer has some crucial drawbacks. The largest disadvantage is the interval of ten minutes between two measurements, which makes tonometry especially unsuitable for short term trend monitoring during a cycling exercise. Furthermore, the tonometer measures extracorporeal which increases the risk of systematical errors due to the transportation of the gastric gaseous content to the external measurement apparatus. Therefore there is demand for an improved gastric CO_2 sensor which can measure with intervals below ten minutes. The sensor should be able to measure locally in the stomach. Since measurements should take place intracorporeal, a miniature sensor is desired which can be integrated in a nasogastric catheter and can resist stomach content. The desired measurement range of the sensor is 3 to 20 kPa CO_2. A gradient of 0.8 kPa CO_2 or more is used as indication for ischemia during exercise tonometry. Therefore a detection limit of the sensor of 0.1 kPa CO_2 is assumed to be sufficient. All requirements for the new sensor and the specifications of the current tonometer are given in table 1.1.

Table 1.1 Current specifications of the Tonometer and the required specifications.

	Range (kPa)	Detection limit	Measurement interval	Measurement method	Size catheter (mm)
Tonometer	0…14*	**	10 min	extracorporeal	Ø 2.8
Required	3…20	0.1 kPa	<10 min	intracorporeal	≤Ø 4.5

* it is possible to measure >14 kPa CO_2 but accuracy is not guaranteed

** unspecified

1.4 Carbon dioxide sensors

In this section the main application areas of present carbon dioxide sensors are discussed, apart from the proposed medical application, in order to demonstrate the need for measuring CO_2. Furthermore, the present carbon dioxide measurement principles are reviewed to evaluate options for designing and constructing a suitable gastric CO_2 sensor.

1.4.1 Application areas

It is recognized that carbon dioxide is one of the gases that causes global warming, the so-called greenhouse effect[9]. Atmospheric CO_2 levels have increased substantially since the Industrial Revolution, and are expected to continue doing so[10]. The Earth emits energy in the form of so-called thermal infrared. Some gases, like CO_2, can temporarily absorb thermal infrared and shortly afterwards re-emit in all directions[9]. Some of the thermal infrared is redirected back to the Earth's surface and is absorbed. Consequently, this further heats the surface and air. Due to increasing CO_2 concentrations more and more infrared is redirected back to the surface resulting in global warming. Because of the greenhouse effect the detection of atmospheric CO_2 has become increasingly important.

Measuring CO_2 is also essential for indoor climate control. The primary source of CO_2 in buildings is respiration of occupants. When CO_2 levels become too high by improper ventilation, residents may suffer the sick building syndrome which is generally used as a description for a set of symptoms with unidentified etiology[11]. Symptoms include headache, drowsiness, sore throat, irritated nose and tight chest. By combining a CO_2 sensor with a ventilation system, the carbon dioxide concentration can be regulated to a convenient level.

Carbon dioxide enrichment is a technique applied in horticulture[12]. The technique is to introduce CO_2 into the greenhouse in order to increase photosynthesis and therefore plant growth. Control equipment in combination with CO_2 sensors are used to measure the carbon dioxide levels and adjust the levels by means of CO_2 burners.

In the automotive industry various gasses, under which CO_2, have to be monitored for injection engine control. Furthermore there is interest to install CO_2 sensors in cars that use CO_2-based air conditioning systems.

Due to failure these systems may leak carbon dioxide into the passenger space which has to be detected by the installed sensor in order to warn the driver and passengers, and take precautions like venting.

The request of the medical field for small cheap reliable carbon dioxide sensors is a great drive for researchers to seek for new CO_2 sensing principles. One of the major applications is measuring the partial pressure of CO_2 (Pco_2) in blood. Together with oxygen and blood pH these form the three parameters which determine the metabolic and respiratory activity of the living body[13]. The parameters are closely monitored of patients that are critically ill or undergo a surgical operation. Apart from the medical application, as described in section 1.2, it is furthermore interesting to quantify the concentration of carbon dioxide in exhaled breath in order to record a capnogram. A capnogram is a continuous record of the carbon dioxide content of expired air. This is considered to be essential during anesthesia to ensure patient safety[14]. Another not yet explored medical application is measuring CO_2 levels in the brain to monitor the status of patients. Studies of Dr James R Petite Jr suggest that CO_2 measurements in the brain were a more sensitive indicator of adverse changes in cerebral metabolism than measurements of oxygen. At this moment there are no CO_2 sensors available that can be used in neuro-monitoring. Despite the fact that such a sensor can have clinical value in providing timely information that might assist in the management of patients who have brain injury or cerebrovascular disease.

1.4.2 Carbon dioxide measurement principles

Optical sensors

Many principles for CO_2 measurements have been presented in literature. A popular method for detection of CO_2 is based on its strong absorption in the infrared region at 2.4 μm[15,16]. This kind of sensor comprises an infrared source, such as a hot metal filament, and an infrared detector. The infrared detector measures how much radiation gets through the sample which depends on the concentration of carbon dioxide. At higher concentrations more infrared is absorbed by the CO_2 and consequently less radiation is measured by the detector. The infrared principle is commercially available and used for quantification of a wide range (0…0.5

to 0…60 kPa) concentration of gaseous CO_2 with response times in minutes and a lower detection limit from 0.3 Pa to 0.1 kPa depending on the measurement range. Infrared-based CO_2 sensors are subject to interference from water vapor and carbon monoxide[17,18].

Fiber-optics is another optical technique to measure carbon dioxide. This kind of devices, or optodes, contain a chemical-sensitive layer at the tip of a fiber, which changes the optical properties in response to CO_2. Bondi *et al.*[17,19] used dyes at the end of the tip which change fluorescence as result of changes in CO_2 concentrations. It is also possible to use dyes that change color in response to CO_2 as proven by Choi *et al.*[18] and Baldini *et al.*[20] Weigi and Wolfbeis showed a similar type of optical CO_2 sensor with a color changing dye[21]. They coated the inside of a capillary with the dye. Gas or liquid sample can flow through the same capillary. The change in color due to CO_2 is measured by a detector mounted on the side of the capillary. Opposite to the detector a light source is present.

Optodes have been used to measure various ranges CO_2 from 0 to 100 kPa. Typical response times vary between 0.7 and 7 minutes and the lower detection limit can be as small as 0.25 kPa. Some optodes suffer cross-sensitivity for humidity, temperature or other gasses like oxygen. There are also fiber-optical sensors based on the Severinghaus concept. These sensors are discussed in the Severinghaus section below. In general the above described optical methods are relatively expensive due to necessary advanced readout equipment.

Surface acoustic wave sensors

Basically, a surface acoustic wave (SAW) device consists of a solid substrate with an input and output transducer[22]. The input transducer converts the incoming signal by the inverse piezoelectric effect into acoustic waves that propagate along the planar surface of the solid. At the output transducer, the surface acoustic waves are reconverted into an electrical signal. Hoyt *et al.* modified the surface of two SAW devices with two types of polymers[23]. One polymer was sensitive to CO_2 and humidity and the other polymer primarily to humidity. Upon adsorbtion of the CO_2-sensitive polymer with CO_2, the surface mass is changed and consequently the acoustic waves travel more slowly (resulting in a decreased frequency). By analyzing and

comparing both SAW signals it is possible to simultaneously measure CO_2 and humidity.

Although laboratory experiments show reasonably good results with a measurement range of 0 to 100 kPa CO_2 and a response time below one minute, the authors state that the device is not suitable for real-world measurements due to uncertainties present in the measurements. Furthermore, robust quantification of CO_2 is possible only at low humidity.

Electrochemical sensors

The field of electrochemical carbon dioxide sensors is reasonably broad. One type of electrochemical sensor is the intensively explored potentiometric sensor which consists of a sensing electrode, a solid electrolyte and a reference electrode[24]. The advantages of this kind of device are the high sensitivity, selectivity and long-term stability to CO_2 gas. The selectivity is caused by the fact that the ion that migrates in the electrolyte is only one species and is closely related to the gas sensing mechanism[25]. As sensing material carbonates are generally used such as Li_2CO_3 [24-29], Na_2CO_3 [30], $CaCO_3$ or $BaCO_2$. The solid electrode should have a structure into which ions can migrate. Examples of materials that can be used are Nasicon[26,30,31,32], β–alumina[33], lithium ion conductor[34] and stabilized zirconia[27,28,29] with mobile ions of alkali or oxygen. Reference electrodes have been made with Na_xCoO_2,[31] Ln_2O_3 [30], $LiMn_2O_4$ [24]. All sensors based on solid ionic conductors are galvanic cell arrangements[31]. Chemical energy is converted into electrical energy by the electrochemical reaction. Below, an example is given of such a reaction, presented by Kim *et al.*[24] A schematic diagram of their device is given in figure 1.7.

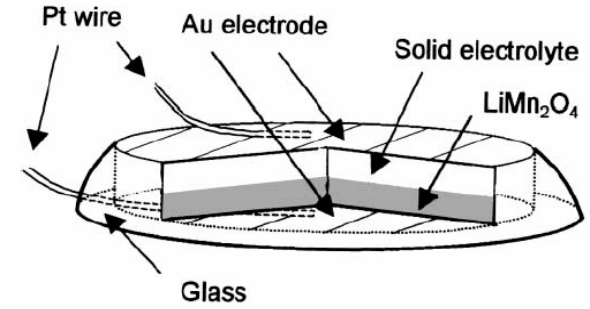

Figure 1.7. Schematic representation of the electrochemical CO_2 sensor of Kim et al.[24]

The electrochemical cell consists of a reference electrode, a solid electrolyte and a sensing electrode. The used materials are

$$\underset{\text{Reference electrode}}{\text{Au, } LiMn_2O_4} \,|\, \underset{\text{Solid electrolyte}}{Li_2CO_3\text{-}Li_3PO_4\text{-}Al_2O_3} \,|\, \underset{\text{Sensing electrode}}{\text{Au, } CO_2, O_2}. \qquad (1.1)$$

The cell reactions at both the sensing and reference electrode can be described by

$$2xLi^+ + 2xe^- + xCO_2 + \tfrac{1}{2}xO_2 = xLi_2CO_3 \text{ (sens)} \qquad (1.2)$$

$$2LiMn_2O_4 = 2Li_{1-x}Mn_2O_4 + 2xLi^+ + 2xe^- \text{ (ref)}. \qquad (1.3)$$

During CO_2 sensing, lithium ions react with carbon dioxide into lithium carbonates on the surface of the sensing electrode with consumption of oxygen (equation 1.2). The lithium ions, necessary for this reaction, are released from the reference electrode to the solid electrolyte as a product of the partial transformation of $LiMn_2O_4$ into $Li_{1-x}Mn_2O_4$ (equation 1.3). Combining equations 1.2 and 1.3 results in the following total cell reaction

$$2LiMn_2O_4 + xCO_2 + \tfrac{1}{2}xO_2 \rightarrow xLi_2CO_3 + 2\ Li_{1-x}Mn_2O_4. \qquad (1.4)$$

Devices using solid electrolyte are mostly potentiometric at operating temperatures above 400 ^oC. Shimanoe *et al.* recently developed a FET-type sensor that operates at room temperature[35]. Their sensor, like all potentiometric electrochemical sensors, is only suitable for detection of CO_2 of low concentrations. Drawback for these potentiometric devices is that they can suffer disturbance by humidity.

Another measurement method of electrochemical gas sensors is based on amperometry[36]. Fasching *et al.* constructed a miniaturized sensor for carbon dioxide dissolved in liquids[37]. Their sensor consists of a working, counter and reference electrode. When the rhodium working electrode is biased cathodically, carbon dioxide is chemisorbed as a reduction product. After 60 seconds of adsorption period, the working electrode is biased anodically. The chemisorbed product is oxidized and desorption takes place from the working electrode. The resulting current is integrated in a small

interval, giving charge Q_1. After a further cathodic bias the oxide is again reduced. Then the potential is increased again and a second integration is performed resulting in charge Q_2. The operating potential is related to the Ag/AgCl reference electrode. The difference of the two charges is a measure for the partial CO_2 pressure. The differential measuring method eliminates small interference by the underlying OH adsorption (the chemisorption of CO_2 takes place at the rhodium surface only in the potential range of hydrogen adsorption) and the beginning of oxide building processes. The sensor has successfully been tested in DI water and blood serum. Unfortunately the sensor has a life time little over three days and shows a drift of 1% per hour.

A different type of an amperometric CO_2 sensor has been presented by Zhou *et al.*[38] Their device consists of a gold microdisc as working electrode, a gold ring counter/reference electrode and a solid polymer electrolyte. The sensor shows a good linearity over the range 0 to 100 kPa CO_2 but the lifetime is limited to three days and frequent recalibrations are necessary.

Conductometry is another measurement principle for electrochemical CO_2 sensors. Haeusler and Meyer presented a sensing principle based on changes in conductance of metal oxides in the presence of carbon dioxide[39]. $BaTiO_3$ and various semiconducting oxides were studied. It was found that $CuO\text{-}BaTiO_3\text{-}La_2O_3\text{-}CaCO_3$ was the best composition for a CO_2 sensing material. The measurement range is 0 to 20 kPa CO_2 with a lower detection limit of 0.5 kPa CO_2. Drawback of this device is the high operating temperature (±600 ^oC) at which the sensor gives maximum response.

Although also an electrochemical sensor, the Severinghaus electrode is such a special sensor that a separate section is devoted to this type of CO_2 sensor.

Severinghaus-based sensors

The most widely-used carbon dioxide sensor is based on the Severinghaus concept[40]. A lot of research has been performed on the principle and resulted in various types of sensors. The principle is as follows: CO_2 diffuses through a gas permeable membrane into an electrolyte solution resulting in

a change in pH which is measured. Detailed information on the principle can be found in chapter 3. Several methods have been explored to measure the change in pH. Severinghaus and Bradley used an ordinary glass electrode which results in a sensor for detection of CO_2 between 0 and 100 kPa with a detection limit of 0.25 kPa and a response time around 4 minutes. The disadvantage of the glass electrode is that it is not suitable for miniaturization and suffers from drift[40]. Therefore alternative pH measurement methods have been explored.

One of these methods is measuring the acidity with a pH-sensitive metal/metaloxide, such as iridium oxide[41-43]. With use of a silver/silverchloride (Ag/AgCl) reference electrode the pH is determined potentiometrically. In literature, sensors based on this principle are found with a measurement range of 1 to 10 kPa and a response time slightly above 3 minutes.

Another more sophisticated possibility is measuring the pH with an ion sensitive field effect transistor (ISFET)[44-46]. The ISFET is basically a potentiometric sensor where the output potential, measured with respect to a reference electrode, is a function of the pH of the solution[47]. ISFET CO_2 sensors have been presented that measure between 0 and 20 kPa CO_2 with 0.13 kPa detection limit and a response time around 2 minutes. Based on the ISFET, a sensor actuator system has been developed for coulometric detection of CO_2 by Van der Schoot *et al.*[48] The carbon dioxide concentration is determined by means of coulometric titration of CO_2 in the internal electrolyte which is equilibrated with the environment. During a measurement, the pH of the electrolyte is increased rapidly by coulometric generation of hydroxyl ions. These ions react with the present CO_2 to bicarbonate ions within seconds. The remaining hydroxyl ions are subsequently titrated by generating hydrogen ions at sufficiently high speed through which the original CO_2 concentration can be determined.

As already mentioned before, there are also optical CO_2 sensors that use the Severinghaus concept. In literature examples can be found where a bicarbonate electrolyte solution was mixed with a pH-sensitive fluorescence indicator and entrapped in a gas permeable polymer matrix attached to the end of a fiber[49-51]. The degree of fluorescence depends on the pH and thus indirectly on the CO_2 concentration.

The Severinghaus concept has also been exploited where the pH is measured with polymeric membrane electrodes[52-54] or copper complexes which dissociate pH-dependent[55]. Varlan and Sansen presented a sensor principle that slightly differs from the Severinghaus concept[56]. Instead of measuring pH variations they measured changes in conductivity as a result of the reaction of carbon dioxide and bicarbonate solution inside a cavity covered with a gas permeable membrane. They were able to measure CO_2 between 0 and 11 kPa with a very fast response time around 5 seconds. The strength of the device is the absence of a reference electrode. Unfortunately, problems were experienced in keeping the cavities clean, with drift as result.

1.4.3 Conclusions

The main application areas of carbon dioxide sensors have been presented together with CO_2 sensing principles. The most relevant parameters of the various CO_2 sensors, if available in literature, are given in table 1.2.

Table 1.2. Most relevant parameters of CO_2 sensors found in literature.

		range (kPa)	resp. time (min)	detect. limit (kPa)	T_{oper} (^oC)	ref. elec-trode	suitable for intra. use	Ref. #
Optical	Infrared	0…60	< 2		room	no	no	14,15
	Optodes	0…100	0.7…7	0.25	room	no	yes	16-20
Acoustical	SAW	0…100	< 1	0.3	room	no	yes	22
Electro-chemical	Potentiom.	0…0.3	1-2	0.1 x10^{-3}	400$^+$	no	yes	23-34
	Amperom.	0…100	< 2		room	some	yes	36,37
	Conductom.	0…20		0.5	600	yes	yes	38
Severing-haus	Glass	0…100	4	2.5	room	yes	no	39
	Iridium ox.	1…10	> 3		room	yes	yes	40-42
	ISFET	0…20	2	0.13	room	yes	yes	43-45,47
	Optical	0…20	5	0.13	room	no	yes	48-50
	Polym.mem.	2…20	< 2		room	yes	yes	51-53
	Copp.compl	0…100	< 2		room	no	yes	54
	Conductom.	0…11	0.08		room	no	yes	55

Regarding the medical requirements of gastric CO_2 detection, most available principles are not suitable. Optical sensors are large and expensive, have a high lower detection limit and require advanced readout equipment. Most electrochemical CO_2 sensors work at high operating temperatures, are cross-sensitive (other gases or humidity) and are only suitable for measuring low concentrations of CO_2. The Severinghaus concept has proven to be beneficial: it operates at room temperature, is well predictable and is fully reversible. The principle is based on converting the partial pressure of CO_2 into a certain pH. Severinghaus used a pH glass electrode to measure this pH, but this electrode is difficult to miniaturize. Although the micro-sized ISFET may be a good alternative, a reference electrode is needed, as for most other presented alternatives like iridium oxide or polymeric membrane electrodes. The reference electrode is known to suffer from drift and is difficult to miniaturize and maintain.

As already mentioned, the Severinghaus concept has some nice advantages, which makes it suitable for gastric Pco_2 measurements. However, no suitable pH measurement method can be found in literature that meets the medical requirements and/or does not require a reference electrode. One possible method, never explored for this purpose, is determining the pH by means of a pH-sensitive hydrogel. In the medical field a lot of experience exists with catheter-tip pressure sensors. When such an existing pressure sensor would be modified with a hydrogel, a new type of CO_2 sensor can be created which would be accepted easily in the medical field. In the following chapters is described how such a sensor has been realized.

1.5 Outline of this thesis

A medical background on gastrointestinal ischemia is provided in chapter one. This form of ischemia can be diagnosed by measuring gastric/intestinal carbon dioxide levels for which an improved intracorporeal CO_2 sensor is requested. In the second part of this chapter an overview of CO_2 measurement methods is given.

In chapter two, hydrogels, which potentially can be used for pH sensing, are discussed. The chapter is started with explaining the chemistry and physics behind stimulus-sensitive hydrogels. Subsequently, applications of hydrogels in sensors, actuators and μTAS are discussed.

In chapter three the sensor is presented which is nominated for gastric CO_2 measurements. The sensor is based on the swelling abilities of hydrogels and makes use of the Severinghaus concept.

In chapter four the study is described of pressure generation of hydrogels under isochoric conditions. The theory behind hydrogel swelling is extensively discussed and verified with a number of experiments.

With the results of chapter four the optimal design parameters of the hydrogel-based carbon dioxide sensor can be determined, which are presented in chapter five. Also the design of the porous cover and gas permeable membrane are described.

In chapter six the technological aspects of the sensor are discussed. The recipes for the electrolyte solution and hydrogel are provided as well as the realization of the porous cover and the gas permeable membrane. Furthermore the assembly of the complete sensor is provided.

The results of measurements with the hydrogel-based carbon dioxide sensor are presented in chapter seven. The results include first time hydration, CO_2 response and temperature sensitivity. Furthermore, the response time limiting factor is determined.

This thesis ends with chapter eight where a reiteration is given of the conclusions per chapter. Furthermore recommendations for further research are provided.

1.6 References

1 A.B. Groeneveld, J.J. Kolkman, *J. Crit. Care* 1994, **9**, 198.

2 J.J. Kolkman, J.A. Otte, A.B. Groeneveld, *Br. J. Anaesthesia* 2000, **84**,101.

3 J.J. Kolkman, Gastric Pco_2 tonometry: Methodology and clinical potential for detection of ischemia (thesis), 1997, Thesis Free University Amsterdam, Amsterdam, The Netherlands.

4 J.J. Kolkman, M.D. L.J. Zwaarekant, K. Boshuizen, A.B. Groeneveld, S.G. Meuwissen, *J. Clinical Monitoring* 1997, **13**, 115.

5 M.A. Hamiltoon, M.G. Mythen, *Clinical Window* 2000, **2**, 1.

6 B.V. Vallet, *Clinical Window* 2004, **16**, 1.

7 J.A. Otte, E. Oostveen, R.H. Geelkerken, A.B. Groeneveld, J.J. Kolkman, *J. Appl. Physiol.* 2001, **91**, 866.

8 J.J. Kolkman, *Scand J Gastroenterology* 2004, in press.

9 C. Baird, *Environmental Chemistry*, 1st ed., 1995, W.H. Freemand and Company, New York, USA.

10 A.B. Robinson, S.L. Baliunas, W. Soon, Z.W. Robinson, *Med. Sentinal* 1998, **3** (sep), 1.

11 C.A. Erdmann, K.C. Steiner, M.G. Apte, *Proc. Indoor Air Conference* 2002, **3**, 443.

12 C.R. Adams, K.M. Bamford, M.P. Early, Principles of Horticulture, 3rd ed., 1984, Butterworth-Heinemann, Oxford, UK.

13 R.M. Berne, M.N. Levy, *Physiology*, 3th ed., 1993, Mosby – Year Book, Missouri, USA.

14 K. Bhavani-Shankar, H. Moseley, A.Y. Kumar, Y. Delph, *Can. J. Anesth.* 1992, **39** (6), 617.

15 B.D. Schurin, R.E. Ellis, *Appl. Opt.* 1968, **7**, 467.

16 R.E. Ellis, B.D. Schurin, *Appl. Opt.* 1969, **8**, 2265.

17 M.D. Marazuela, M.C. Moreno Bondi, G. Orellana, *Sens. Actuators B* 1995, **29**, 126.

18 M.F. Choi, P. Hawkins, *Anal. Chem.* 1995, **67**, 3897.

19 M.C. Moreno Bondi, E. Segovia, M.D. Marazuela, *Anal. Chem.* 1992, **64**, 2210.

20 F. Baldini, A. Falai, A.R. De Gaudio, D. Landi, A. Lueger, A. Mencaglia, D. Scherr, W. Trettnak, *Sens. Actuators B* 2003, **90**, 132.

21 B.H. Weigi, O.S. Wolfbeis, *Anal. Chem.* 1994, **66**, 3323.

22 C.C. Ruppel, T.A. Fjedley, *Int. J. High Speed Electronics and Systems* 2000, **70**, 1.

23 A.E. Hoyt A.J. Ricco, J.W. Bartholomew, G.C. Osbourn, *Anal. Chem.* 1998, **70**, 2137.

24 D.H. Kim, J.Y. Yoon, H.C. Park, K.H. Kim, *Sens. Actuators B* 2001, **76**, 594.

25 N. Imanaka, Y. Hirota, G. Adachi, *Sens. Actuators B* 1995, **24-25**, 380.

26 Y. Miyachi, G. Sakai, K. Shimanoe, N.Yamazoe, *Sens. Actuators B* 2003, **93**, 250.

27 N. Imanaka, M. Kamikawa, G.Y. Adachi, *Anal. Chem.* 2002, **74**, 4800.

28 S. Tamura, N. Imanaka, M. Kamikawa, G.Y. Adachi, *Sens. Actuators B* 2001, **73**, 205.

29 N. Imanaka, M. Kamikawa, S. Tamura, G. Adachi, *Sens. Actuators B* 2001, **77**, 301.

30 K. Obata, S. Kumazawa, K. Shimanoe, N. Miura, N. Yamazoe, *Sens. Actuators B* 2001, **76**, 639.

31 E. Stuedel, P. Birke, W. Weppner, *Electrochimica Acta* 1997, **52**, 3147.

32 F. Qiu, L. Sun, X. Li, M. Hirata, H. Suo, B. Xu, *Sens. Actuators B* 2001, **76**, 594.

33 H. Nafe, *Sens. Actuators B* 1994, **21**, 79.

34 N. Imanaka, T. Murata, T. Kawasato, G. Adachi, *Sens. Actuators B* 1993, **13**, 476.

35 K. Shimanoe, K. Goto, K. Obeta, S. Nakata, G. Sakai, N. Yamazoe, *Sens. Actuators* 2004, **102**, 14.

36 S.C. Chang, *Talanta* 1993, **40**, 461.

37 R. Faschinf, F. Keplinger, G. Hanreich, G. Jobst, G. Urban, F. Kohl, R. Chabicovsky, *Sens. Actuators B* 2001, **78**, 291.

38 Z.B. Zhou, L.D. Feng, Y.M. Zhoud, *Sens. Actuators B* 2001, **76**, 600.

39 A. Haeusler, J.U. Meyer, *Sens. Actuators B* 1996, **34**, 388.

40 J.W. Severinghaus, A.F. Bradley, *J. Appl. Physiol.* 1958, **13**, 515.

41 H. Suzuki, H. Arakawa, *Anal. Chem.* 1999, **71**, 1737.

42 H. Beyenal, C.C. Davis, Z. Lewandowski, *Sens. Actuators B* 2004, **97**, 202.

43 M.J. Tierney, H.O. Kim, *Anal. Chem.* 1993, **65**, 3435.

44 T. Sekiguchi,Y. Nagai,T. Makino, K. Ohno, M. Nakamura, H. Hosaka, H. Sakio, S. Ohtsu, H. Takahashi, *Sens. Actuators B* 1998, **49**, 171.

45 Ph. Arquint, A. van den Berg, B.H. van der Schoot, N.F. de Rooij, *Sens. Actuators B* 1993, **13-14**, 340.

46 K. Tsukada, Y. Miyahara, Y. Shibata, H. Miyagi, *Sens. Actuators B* 1990, **2**, 291.

47 P. Bergveld, *Sens. Actuators B* 2003, **88**, 1.

48 B.H. van der Schoot, P. Bergveld, *Sens. Actuators* 1998, **13**, 251.

49 O.S. Wolfbeis, L.J. Weis, *Anal. Chem.* 1988, **60**, 2028.

50 Z. Zhujun, W.R. Seitz, *Anal. Chim. Acta* 1984, **160**, 305.

51 C Munkholm, D.R. Walt, F.P. Milanovich, *Talanta*, 1988, **35**, 109.

52 W.N. Opdycke, M.E. Meyerhoff, *Anal. Chem.* 1986, **58**, 950.

53 P. Zhao, W.J. Cai, *Anal. Chem.* 1997, **69**, 5052.

54 J.H. Shin, J.S. Lee, S.H. Choi, D.K. Lee, H. Nam, G.S. Cha, *Anal. Chem.* 2000, **72**, 4468.

55 R. Fasching, F. Kohl, G. Urban, *Sens. Actuators B* 2003, **93**, 197.

56 A.R. Varlan, W. Sansen, *Sens. Actuators B* 1997, **44**, 309.

Chapter 2

Hydrogels and Their Applications in Sensors and Actuators*

In this chapter the use of stimulus-sensitive hydrogels as sensors and actuators for (micro) analytical applications is discussed. The first part aims at making the reader familiar with stimulus-sensitive hydrogels, their chemical composition and their chemo-physical behavior. The second part focuses on the use of stimulus-sensitive hydrogels for microsensors and microactuators as well as their application in micro total analysis systems. The benefits of stimulus-sensitive hydrogels, their miniaturization and the use of 365 nm UV photolithography as a fast economical manufacturing technique are discussed.

2.1 Introduction

Stimulus-sensitive hydrogels are water-filled polymers which undergo large volume changes in response to small changes in so-called stimuli. Stimuli include pH[1], temperature[1], ion concentration[2], electrical field[3], solvent composition[1] and light[4]. The unique behavior of these hydrogels has been explored intensively and used for a large number of applications. Stimulus-sensitive hydrogels have been tested for: bioseparation[5,6], drug delivery[7-10], biomedical applications[11], sensors and actuators.

* This chapter is based on H. van der Linden, S. Herber, W. Olthuis, P. Bergveld, *The Analyst* 2003, **128**, 325.

This chapter is limited to the use of stimulus-sensitive hydrogels for sensor and actuator purposes. Furthermore the use of these hydrogels in the microanalysis field is emphasized. For information on the other subjects the reader is referred to the articles mentioned above.

Gel-based sensors include ion-sensitive sensors for dissolved ions like Ba^{2+} and Na^{+} [12], antigen sensitive sensors[13], enzyme sensors[12], pH sensors[14] and gas sensors. Gel-based actuators have been used for artificial muscles[15], microvalves[16,17], pH controllers[18] and blood microsamplers[19].

It is the aim of this chapter to give basic understanding of stimulus-sensitive hydrogels and explain why these gels can be used as sensors and actuators. Special attention is given to the use of these hydrogels in the field of micro total analysis systems (μTAS).

2.2 The chemistry and physics behind stimulus-sensitive hydrogels

A hydrogel consists of a three-dimensional polymer matrix containing water. The amount of water in the polymer matrix can be very large up to values of 99% by weight[20]. The polymer matrix is made up of a very large number of long molecular chains, also called backbones, which are held together by interconnections between these chains, called crosslinks. The crosslinks keep the chains in the polymer matrix together, thus circumventing the dissolution of the long molecular chains and increase the mechanical stability of the hydrogel. The physics behind the effect of the gel network composition on the mechanical properties of the network have been investigated intensively by Flory and Rehner[21,22]. The long molecular chains in turn are composed of small molecular units called monomers and comonomers which have been attached to each other during the chemical synthesis of the polymer network. For a visual representation of a hydrogel matrix see figure 2.1.

The family of stimulus-sensitive hydrogels can largely be subdivided into two types of gels: pH-sensitive hydrogels and temperature-sensitive hydrogels. Other types of gels exist and some examples will be given below. Temperature- and pH-sensitive hydrogels are very different in their physical behavior and swelling mechanism. The properties of these kinds of gels will be discussed independently in detail in the next section.

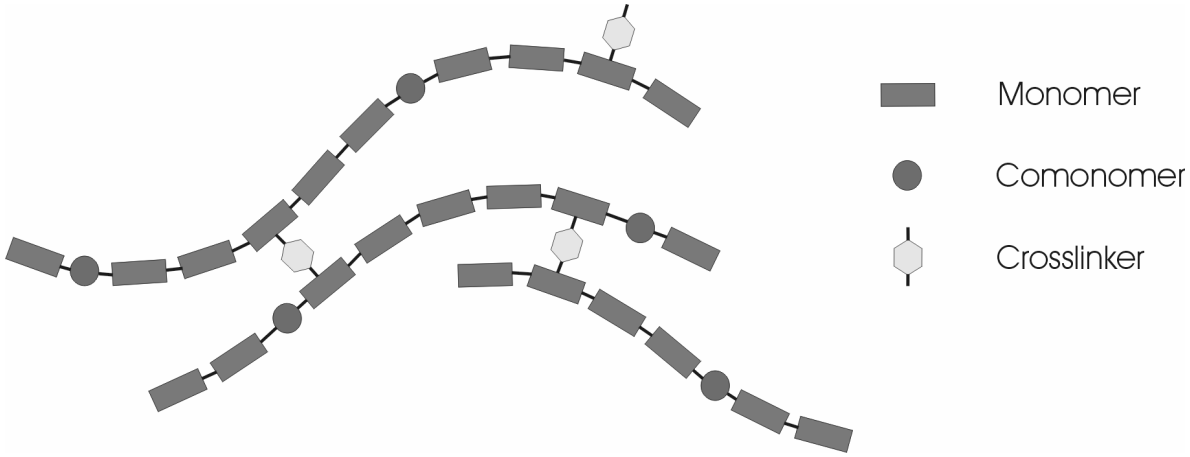

Figure 2.1. The chemical structure of a hydrogel matrix.

2.2.1 Temperature-sensitive hydrogels

A common group of monomers, used in the synthesis of temperature-sensitive hydrogels, are the N-alkyl acrylamides. A well-known monomer from this group is N-isopropyl acrylamide (NIPAAm). This monomer has side-chains which have favorable interactions with water in the form of hydrogen bonds. This causes a hydrogel made from this monomer, called a poly-NIPAAm hydrogel, to attract water molecules and swell around room temperature.

The efficiency of the hydrogen bonding process has a negative temperature dependency and above a certain temperature, called the lower critical solution temperature (LCST), the hydrogen bonds between the monomer side-groups and water molecules will increasingly be disrupted with increasing temperature.

The backbones of the polymer, the long chains of C-C bonds to which the side-chains are attached, are hydrophobic and wish to reduce their surface area exposed to the highly polar water molecules. They can do so by forming aggregates, as shown in figure 2.2. Normally, when the hydrogen bonds between the side-groups and the water are present, the aggregation of the backbones is prevented because the hydrogen bond interactions with the water molecules are stronger than the backbone interactions. When the hydrogen bonds are broken, due to increasing thermal agitation, the aggregation process takes place. This results in the shrinkage of the temperature-sensitive hydrogel with increasing temperature.

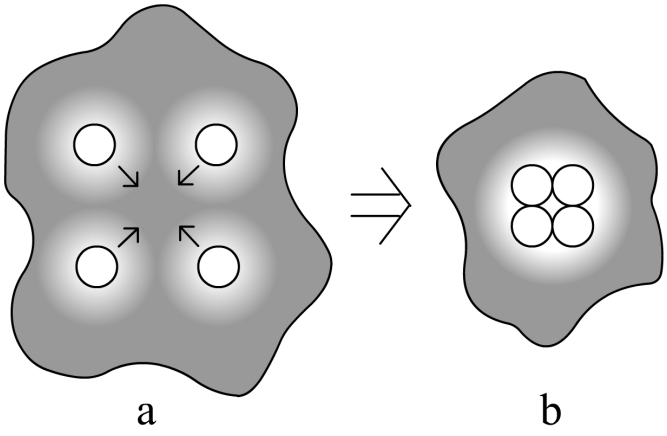

Figure 2.2. (a) Backbones of the temperature-sensitive hydrogel in the swollen condition. (b) The backbones in the aggregated condition. Note the reduction of the surface area exposed to water.

The temperature behavior of a poly-NIPAAm hydrogel is shown in figure 2.3. This kind of graph is used commonly to depict the swelling behavior of stimulus-sensitive gels as function of a stimulus and is called a swell curve.

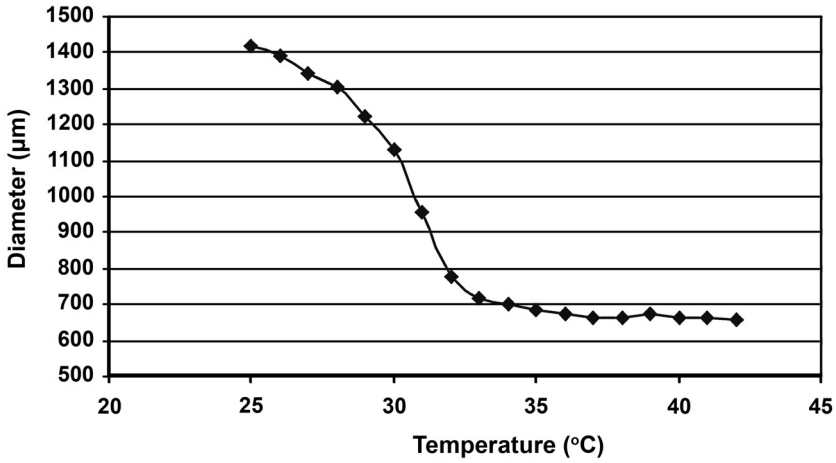

Figure 2.3. Swell curve of a disc-shaped poly-NIPAAm hydrogel.

2.2.2 pH-sensitive hydrogels

Hydrogels that respond to pH (and ion concentration, as explained below) contain (co)monomers with weak acidic or weak basic side-groups. These side-groups are ionizable and their charge will be a function of the pH.

Structure examples of pH-dependent monomers and their ionization behavior are shown in figure 2.4. On the left the ionization versus pH is shown for the weak acidic monomer acrylic acid (AAc) and on the right this is shown for the weak basic monomer dimethylamino ethylmethacrylate (DMAEMA).

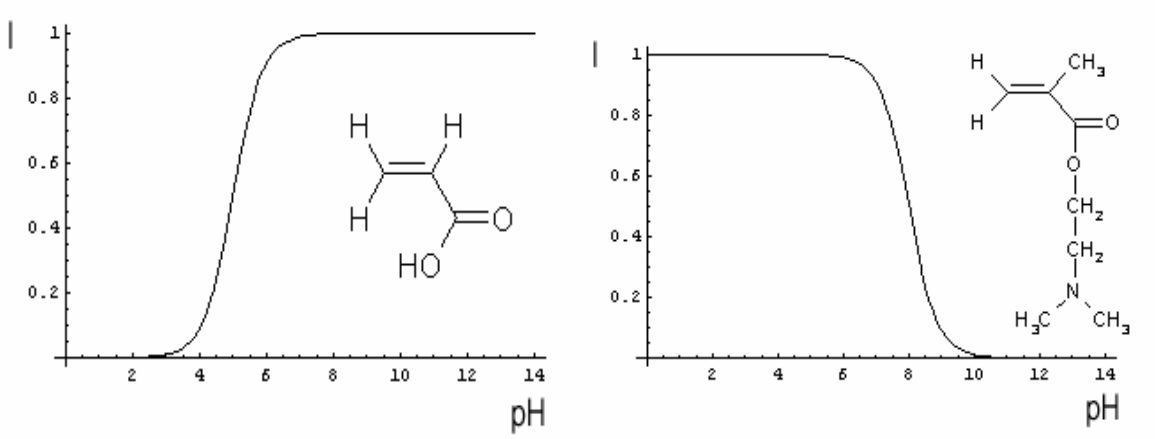

Figure 2.4. Ionization behavior of acrylic acid and dimethyl aminomethacrylate. The degree of ionization (I) is plotted versus the pH. Acrylic acid is ionized at high pH and dimethyl aminomethacrylate at low pH.

The swelling of a pH-sensitive hydrogel is the result of the interplay of the pH and the ionic strength of the solution which the hydrogel is exposed to. The ionizable monomers inside the hydrogel will dissociate as a function of the pH and the resulting free counterions in the hydrogel exchange with salt ions from the solution. Inside the hydrogel a certain counterion concentration will develop, that causes an osmotic pressure difference to develop between the gel and the solution. Consequently the hydrogel will swell until the elastic forces inside the hydrogel are in equilibrium with the osmotic force. An important condition in the swelling of a pH-sensitive hydrogel is the fact that the hydrogel has to maintain global charge neutrality inside itself. A hydrogel cannot give off an ion to the surrounding solution without receiving a suitable counterion in return.

The ionic strength of the surrounding solution has a large influence on the degree of swelling of the hydrogel, as shown in figure 2.5 and discussed below.

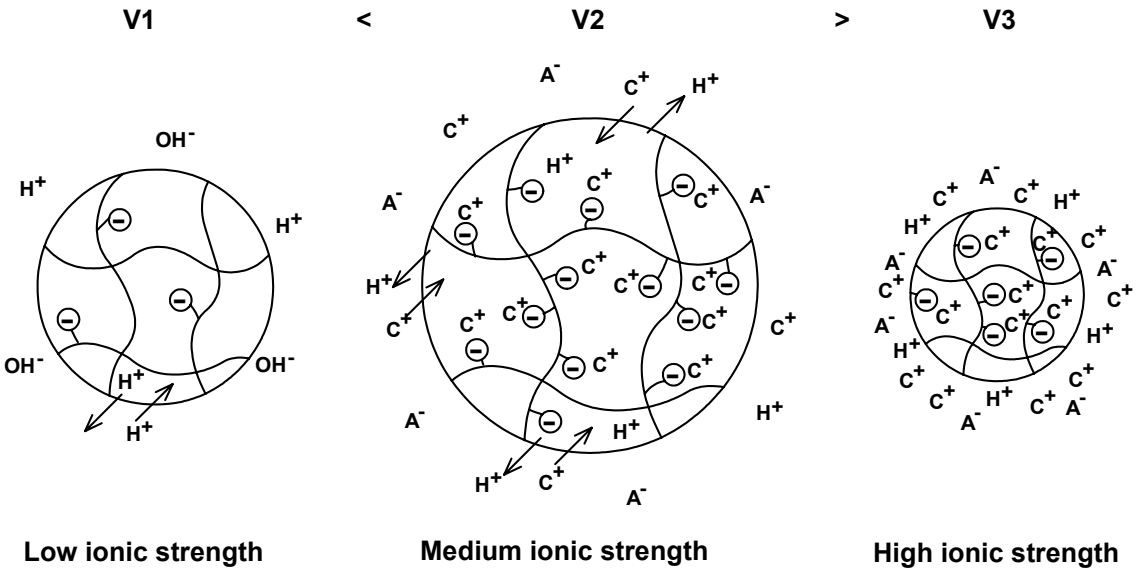

Figure 2.5. The swelling of a pH-sensitive hydrogel as a function of the ionic strength. (A^-, C^+ mean anion and cation respectively).

When a hydrogel with an acidic comonomer, e.g. poly-hydroxy ethylmethacrylate-co-acrylic acid (poly-HEMA-co-AAc), is exposed to pure water (at pH 7) no osmotic swelling will take place in the gel, although the pH of the solution is higher than the pK_a of the acrylic acid comonomers (the pK_a of acrylic acid comonomers is around 5). The hydrogel can give off protons to the solution, but to maintain electroneutrality the hydrogel also has to take up counterions from the solution. At neutral pH and low ionic strength, the only counterions available are protons resulting from the autoprotolysis of water. As a result, the pH inside the hydrogel will be low and all the acrylic acid groups in the hydrogel will be in the protonated and uncharged state. Consequently, there will be no free counterion concentration inside the hydrogel which would cause osmotic swelling. When the ionic strength of the solution is increased, the hydrogel can exchange ions with the solution. By doing so, the hydrogel maintains charge neutrality and the concentration of free counterions inside the hydrogel increases. An osmotic pressure difference between the hydrogel and the solution arises which causes the gel to swell. When the ionic strength is increased to high levels (1 M – 10 M) the hydrogels will shrink. This is due to the loss of the osmotic pressure difference between the gel and the solution (the solution now has osmotic pressures in the range of the osmotic pressure inside the gel).

2.3 Hydrogel sensors

Roughly, all hydrogel sensors consist of two main parts: a hydrogel element and a transducer. The transducer converts the swelling signal of the hydrogel to the electrical or optical domain. A number of different hydrogels has been used to function as the sensing element:

- pH-sensitive hydrogels;
- ion-sensitive hydrogels;
- antigen-sensitive hydrogels;
- glucose-sensitive hydrogels.

These hydrogels will be discussed first and subsequently, the applied hydrogel transduction methods are presented.

2.3.1 Hydrogels used as sensing element

pH-sensitive hydrogels

pH-sensitive hydrogels with one kind of monobasic or monoacidic side-groups will respond to the pH in a restricted operating window around the pK_a of the side-groups. With these gels a pH sensor for a specific pH range can be created[14,23-26]. To enlarge the operating window, a hydrogel containing two or more different ionizable monomers, with different pK_a values, or a monomer with two pK_a values could be used. The applicability of a pH-sensitive hydrogel for sensors can be extended greatly by adding an intermediate step where an analyte is converted to pH.

Ion-sensitive hydrogels

To make a hydrogel sensitive to a specific dissolved ion it is necessary to attach groups to the hydrogel which selectively bind to the ion. One such approach is to incorporate crown ethers into the gel. The crown ethers selectively form charged complexes with the ion. This brings free charges into the gel network which consequently causes hydration and thus gel swelling. Sensors of this kind have been reported for the detection of Na^+ [27], Pb^{2+} [2,12], Ba^{2+} [12] and K^+ [12,27].

Antigen-sensitive hydrogels

Antigen-sensitive hydrogels change volume in response to a specific antigen. Miyata *et al.* have reported an antigen sensor, that uses a neutral hydrogel with an antigen and its corresponding antibody immobilized in the gel.[13] Binding between the antigen and the antibody introduces reversible crosslinks in the gel network. A change in volume is evoked by exposing the hydrogel to a solution containing the free antigen. Competitive binding of the free antigen with the antibody results in a decrease in the amount of reversible crosslinks. The resulting gel network allows more expansion which results in the swelling of the gel.

Glucose-sensitive hydrogels

Phenylboronic acid has been used to make glucose-sensitive hydrogels. The phenylboronic acid forms a complex with glucose and releases a proton during this process. Arnold *et al.*[28] have immobilized phenyl boronic acid inside a hydrogel and used conductimetry to measure the conductance increase due to the release of protons after glucose reacted with the phenylboronic acid groups inside the hydrogel.

2.3.2 Transduction methods

Different types of transduction methods have been explored to measure the volume change of a hydrogel. These include optical, conductometric, amperometric and mechanical methods.

Optical methods

The optical methods have been widely explored with different techniques. The change of fluorescence intensity in relation to the swelling of a fluorophore-labeled hydrogel has been presented[29]. Also an interferometric method has been explored for measuring hydrogel swelling[30,31]. Here, the sensor material is part of an optical thin-film system which transforms the variation in volume into spectral information.

Another optical method makes use of the diffraction of light from a hydrogel containing a crystalline colloidal array (CCA). The group of Asher polymerized a CCA of spherical polystyrene colloid particles in a thin hydrogel film[2,12]. The particles in the CCA are regularly spaced and cause

the gel to display Bragg diffraction. Because of this, the CCA gels are brightly colored. When the hydrogel changes volume, the spacing of the particles in the CCA is changed, causing a change in the diffraction process and the color of the gel.

Hydrogel swelling has also been detected by refractometry; the refractive index of a gel changes during swelling[32-35]. Lowe *et al.* used a reflection hologram to characterize polymer swelling[27]. Holographic diffraction gratings which act as a reflector of light were realized in a hydrogel. The reflection spectrum of the hologram changes with changing hydrogel volume. Another technique is based on the reflectance of hydrogels; the intensity of light reflected from a hydrogel depends on the volume of the polymer[36,37].

Conductometric and amperometric methods

A conductometric method for detection was developed by Sheppard *et al.*[14,24] and further explored by Arnold *et al.*[28] A thin hydrogel layer was deposited on a planar interdigitated conductivity electrode array. The hydrogel changes volume in response to pH leading to a corresponding increase or decrease in ion mobility inside the hydrogel layer and a change in conductivity.

Another method of detection is amperometry[38]. A glucose sensor has been constructed where the swelling of the gel leads to increased diffusion of ion species and thus to measurable current increases.

Mechanical methods

Mechanical detection of polymer swelling can be done in different ways. Strong *et al.* used a capacitive transducer[23]. By swelling, a hydrogel deflects one of the two capacitor plates resulting in a change in capacity. Another method is attaching a hydrogel to a magnetoelastic element[25,26]. The magnetoelastic element mechanically vibrates at a resonant frequency which depends upon the hydrogel mass. The resonant frequency changes when the mass of the hydrogel changes. Another mechanical detection method is used by Seitz *et al.*[39] They have used a strain gauge to measure the swelling of a very small spherical hydrogel bead.

Although stimulus-sensitive hydrogel-based sensors seem to be promising for the future, they suffer a common problem. Stimulus-sensitive

hydrogels such as for instance pH-sensitive hydrogels have a low selectivity, resulting in cross-sensitivity. These gels do not only respond to pH but also to ion concentration, as already discussed above. In the literature different tactics are used to eliminate the cross-sensitivity. Grimes *et al.*[25] used a reference hydrogel. They constructed a salt-independent pH sensor which makes use of two types of hydrogel. One is a pH and ion concentration sensitive polymer and the other a hydrogel responsive only to the ion concentration. Differential measuring between the two hydrogels eliminates the effect of salt on pH measurements.

Arnold *et al.* used a different technique for their glucose sensor[28]. Their hydrogel is encapsulated within a bipolar ion exchange membrane impermeable for ions, but freely permeable for glucose. This way the hydrogel response to glucose can be measured without the interference of ions. Other methods, discussed above, are based on making the hydrogel selective for the analyte by incorporating antibodies or crown ethers into the polymer. An overview of the discussed stimulus-sensitive hydrogel sensors is given in figure 2.6.

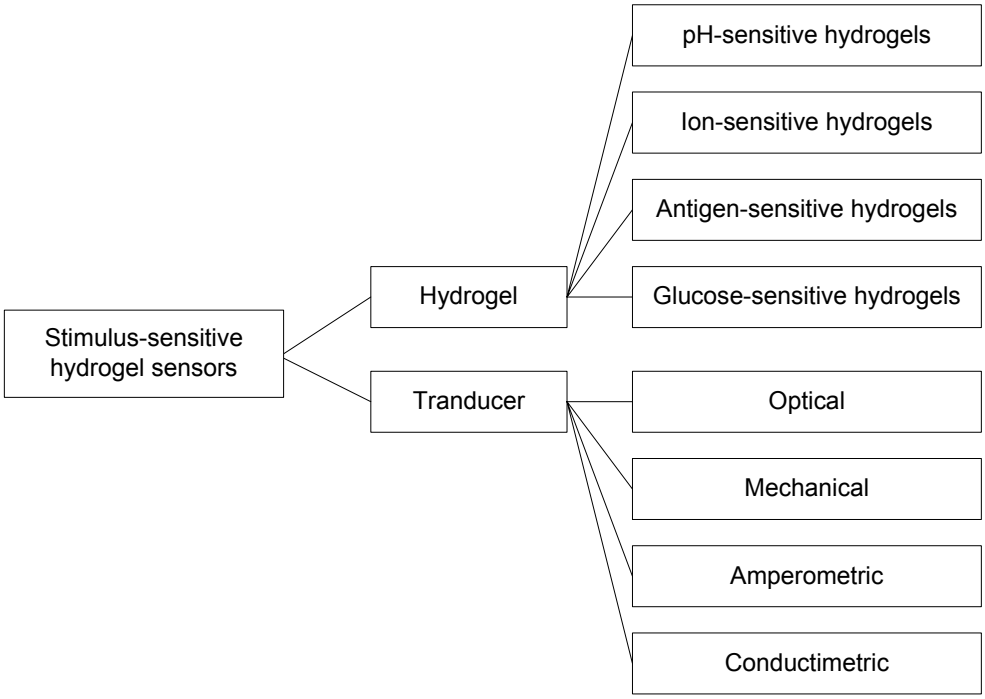

Figure 2.6. Overview of the types of hydrogels and transducers used in stimulus-sensitive hydrogel sensors.

2.4 Stimulus-sensitive hydrogel actuators

Stimulus-sensitive hydrogels have been tested for a number of actuator applications. In most cases a chemical signal in the form of a pH change was directly converted to mechanical work. The main reasons for the development of hydrogel actuators are:

- their considerable power density which is close to that of a human muscle;
- the large displacements that are obtained with these actuators;
- the high resilience of the actuators because of the high water content of the polymer matrices which makes them suitable to handle fragile substrates.

Examples of actuator research include: artificial muscles[40], a gel looper[41] (a worm-like device that moves by repeatedly curling and straightening itself), and a gel eel which could propel itself under the influence of an electrical field[42]. Recently a number of actuators based on miniaturized stimulus-sensitive hydrogels has been shown[16,18].

Important parameters of any actuator are the type of input needed to control the actuator, for instance electric or magnetic input, and the operation speed of the actuator. These parameters will set the limits for the applicability of the actuator. The two parameters for stimulus-sensitive hydrogel actuators are discussed below.

2.4.1 Hydrogel actuator control

The control parameters for a hydrogel actuator depend on the type of hydrogel used in the actuator, i.e. temperature-sensitive or pH-sensitive type. When a temperature-sensitive hydrogel is used, the actuator can be controlled by changing the temperature of the actuator. The temperature change can be generated by heaters, hot fluids, IR light and endo- or exothermic chemical reactions.

When the hydrogel is composed of a pH-sensitive hydrogel different control strategies are needed. These include the use of solutions with different pH values, electrolysis of water which generates pH changes at the electrodes, the use of a compound that releases protons under irradiation

with light, such as pyridine[4] and the use of electrical fields[3]. The diversity of the control parameters opens up a lot of possibilities to make hydrogel actuator systems.

2.4.2 Operation speed of hydrogel actuators

Because the volume changes in a hydrogel actuator are caused by a diffusion process, hydrogel actuators are intrinsically slow. The gel swelling kinetics have been studied by Tanaka and Fillmore which resulted in the discovery of a simple relation between the swelling kinetics and the dimensions of a hydrogel[43]. For instance the kinetics of a hydrogel sphere are a function of the diameter of the sphere and the apparent diffusion coefficient of the polymer network into the water phase, as expressed in the following equation,

$$time = \frac{r^2}{D_{gel}}. \qquad (2.1)$$

The radius of the hydrogel sphere is given by r and the apparent diffusion coefficient of the hydrogel network into the water phase is given by D_{gel}. Calculations using this equation reveal that the swelling of large hydrogels is prohibitively slow and the best way to increase the operation speed of hydrogel actuators is to make their dimensions very small. To give an idea of the influence of the dimensions on the swelling time of a hydrogel actuator see table 1.

Table 1. The effect of the radius of a spherical on the swell time of the hydrogel. For D a value of $3.2*10^{-7}$ $cm^2/sec.$ has been used[8].

Gel Radius	10 cm	1 cm	100 µm	10 µm	1 µm
Time Constant	10 years	36 days	9 hours	5 minutes	3 seconds

As can be seen from this table the hydrogels need to have dimensions in the micrometer range or a higher value of the apparent diffusion coefficient to have reasonable operation frequencies. This can be done by making the polymers smaller or by changing the polymer morphology to

make the gels more porous. Both these methods are done by changing the chemistry used to synthesize the polymers.

By using a special synthesis technique called emulsion inversion polymerization, it is possible to synthesize micrometer scale polymer spheres called hydrogel microspheres[44]. During the synthesis the formed polymer precipitates from the solvent and induces the formation of the microspheres. These spheres have a very rapid response to pH changes which lies in the millisecond range.

Another method, called photopatterning, uses UV light and a photo-initiator to locally control the polymerization reaction. When UV light strikes a photo-initiator molecule in the solution from which the hydrogel is to be synthesized, it forms a free radical that initiates the polymerization reaction. By using masking techniques commonly found in photolithographic techniques to control the topography of the UV light, it is possible to control the formation of the hydrogel network on the micrometer scale and make hydrogels with small time constants.

Finally by using a method similar to the synthesis of the microspheres it is possible to make hydrogels that contain large pores in the polymer matrix. During the synthesis reaction the formed polymer also precipitates but instead of forming microspheres it forms larger aggregates resulting in a very porous hydrogel. Because of the porous nature of the network the diffusion time of the network is greatly reduced and fast actuators are possible.

As described in the above paragraph it is necessary to make hydrogel actuators as small as possible. This together with the advantages of hydrogels such as the high power density and high resilience have led to a large interest from the micro total analysis field (μTAS field) as will be discussed below.

2.5 Micro total analysis systems

The μTAS field is focused on the development of very small total analysis systems for performing for instance blood analyses. The keywords in the μTAS field are miniaturization and mass-fabrication. By miniaturizing standard analysis equipment, a number of advantages is achieved. For instance the volume needed for a blood analysis is greatly reduced from the

mL range to the nL range. With nanoliter volumes needed for blood analyses it is possible to perform a large number of point-of-care measurements without endangering the patient. Another advantage is the drastic increase in speed when operations are performed on a small scale.

The μTAS field relies heavily on the miniaturization techniques that have been developed in the microelectronics industry. By using the same techniques and substrates as in the micro electronics industry, like silicon, it has been possible to fabricate miniature sensors and actuators with very fast response times and very small volumes. As in the microelectronics industry the application of mass-production techniques is expected to greatly lower the unit cost of micro total analysis devices which could lead to very wide-spread application of these devices. For more information readers are referred to van den Berg[45] and Feynman[46].

2.5.1 Hydrogels and their applications in μTAS

Hydrogels have become a focus of attention in the μTAS field because of a number of reasons: they are powerful actuators but at the same time they are soft because of their high water content. This makes them suitable for μTAS systems where living substrates like cells or embryos are handled.

The use of (365 nm) UV-photolithography is ubiquitous in the cleanroom laboratories where ICs and μTAS systems are made. The photopatterning technique described above can be used in conjunction with the UV-photolithography equipment to make a large number, i.e. 100-1000, of stimulus sensitive hydrogels, with micrometer dimensional precision, at the same time. This process is fast, with exposure times from 10 to 100 seconds, and very suited for the mass-production of stimulus-sensitive hydrogel sensors and actuators or μTAS systems containing these.

Finally the simplicity of the systems needed to control the hydrogel actuators make them superior over a large number of other actuators used in μTAS systems.

2.5.2 Hydrogel microsensors

In spite of the advantages not many hydrogel microsensors have been developed up to now, though miniaturization is crucial to make sensors based on polymer swelling with fast response times. Some of the sensors discussed in the stimulus-sensitive hydrogel sensors section are actually

microsensors. An example is the salt-independent pH sensor by Grimes *et al.*[25,26] They coated a 8 µm thick hydrogel layer on small magnetoelastic elements. Sheppard *et al.* made a microfabricated conductometric pH sensor[14,24]. Their hydrogel layer was photolithographically patterned on the electrodes and also had a thickness of 8 µm. They varied the pH with steps of 0.2 pH units and found a response time of 350 seconds.

2.5.3 Hydrogel microactuators

Although this field is very young, already a number of research groups across the world have shown examples of stimulus-sensitive hydrogel actuators. Kobayashi *et al.* have shown a blood sampling system called the µmosquito that uses a temperature sensitive hydrogel to obtain a blood sample from a patient[19].

Beebe *et al.*[16] showed the use of pH-sensitive hydrogel as valves for the control of liquid flow through microchannels. By changing the pH of the solution that was run through the microchannels, the hydrogel valves were closed or opened. The hydrogel microvalves were fabricated with UV-photolithography and showed promising results for µTAS applications. An important aspect of these valves is their high resilience due to their high water content. Dust contamination is a major source of malfunction in µTAS systems. Because dust is on the order of micrometers it can interfere with the function of the conventional hard mechanical microfluidic actuators in a µTAS system. Because the dust particles get caught in the moving parts of the actuators, which are almost always made out of rigid materials like silicon or glass, they cause such a high friction that the actuator function is compromised. Because hydrogel actuators are soft, dust particles will not get caught as the hydrogel actuator will shape itself around the dust particle. This resilience also makes it possible to use hydrogels to handle soft substrates like cells and embryos which would normally get damaged by the contact with actuators made out of hard materials.

Another example of hydrogel actuator work is the pH regulator for microflow applications shown by Eddington *et al.*[18] By using a pH-sensitive hydrogel throttle valve in a pH-regulated feedback system it was possible to adjust the pH of a solution coming into the regulator by mixing with a

buffer of known pH. The pH of the solution coming out of the regulator was kept constant over a range of pH values for the input stream.

Madou *et al.* have fabricated very small pH responsive valves for drug dosing applications. These pH sphincter valves were used to regulate the amount of drug flowing out of a drug reservoir. A valve of this kind could be used to fabricate smart drug-dosing systems.

The German company Gesim Gmbh. has shown a microvalve that uses a temperature-sensitive hydrogel, controlled by a microheater[17]. The temperatures needed to control the valves are around physiological temperature which makes the valves interesting for biomedical and cell-handling applications. The voltage needed to control the microvalves was in the order of a few volts which again shows the advantage of hydrogel actuators.

Another method to control hydrogel micro actuators is the use of an electrical field over a pH-sensitive hydrogel in a 50/50 percent water/acetone mixture. The electrical field causes a stress to develop across the gel and leads to shrinking of the gel[3].

2.6 Conclusions

Stimulus-sensitive hydrogels are very interesting materials for the fabrication of sensors and actuators. Because the kinetics of the swelling process is dictated by diffusion, miniaturization is indispensable to make sensors and actuators with good characteristics.

It has been shown that with the chemical modification of hydrogels a large number of different sensors can be made. These include sensors for dissolved ions, gases, enzyme substrates and antigens. To convert the swelling signal to an electrical signal a number of possibilities exist like conductometry and light transmission.

Stimulus-sensitive hydrogel actuators have a number of advantages over existing μTAS actuators. Their high resilience gives them superior dust tolerance over actuators made from hard materials and it makes them suitable for cell-handling applications. The fact that hydrogel actuators can be controlled with small voltages and currents gives them an extra benefit over conventional μTAS actuators. In contrast with these conventional actuators no elaborate interfacing electronics is needed to control hydrogel

actuators and direct interfacing with microcontrollers is possible. By integrating the microelectronic circuits needed for the operation of the μTAS system on the same chip surface, a further degree of miniaturization is achieved. This could lead to the development of extremely small total analysis systems that can operate for very long time periods and need only a small energy source.

The fabrication of gel sensors and actuators with UV photolithography makes them compatible with the conventional fabrication techniques used in μTAS system fabrication and opens up the opportunity of mass production.

2.7 References

1 T. Tanaka, Experimental methods in polymer science, 1st ed., 2000, Academic Press, San Diego, USA.

2 J. H. Holtz, J. S. Holtz, C. H. Munro, S. A. Asher, *Anal. Chem.* 1998, **70**, 780.

3 T. Tanaka, I. Nishio, S.T. Sun, S. Ueno-Nishio, *Science* 1982, **218**, 467.

4 A. Suzuki and T. Tanaka, *Nature* 1990, **346**, 345.

5 J.J. Kim and K. Park, *Bioseparation* 1999, **7**, 177.

6 Y. Galaev and B. Mattiasson, *Trends in Biotechnology* 1999, **17**, 335.

7 P. Gupta, K. Vermani, S. Garg, *Drug Discovery Today* 2002, **7**, 569.

8 Y. Qiu and K. Park, *Advanced Drug Delivery Reviews* 2001, **53**, 321.

9 N.A. Peppas, P. Bures, W. Leobandung, H. Ichikawa, *European Journal of Pharmaceutics and Biopharmaceutics* 2000, **50**, 27.

10 Kost and R. Langer, *Advanced Drug Delivery Reviews* 2001, **46**, 125.

11 S. Hoffman, *Advanced Drug Delivery Reviews* 2002, **43**, 3.

12 H. Holtz and S.A. Asher, *Nature* 1997, **389**, 829.

13 T. Miyata, N. Asami, T. Uragami, *Nature* 1999, **399**, 766.

14 N.F. Sheppard Jr., M.J. Lesho, P. McNally, A. S. Francomacaro, *Sens. Actuators B* 1995, **28**, 95.

15 Q.M. Zhang, T. Furukawa, Y. Bar-Cohen, J. Scheinbeim, *Materials research society symposium proceedings* 2000, 600.

16 D.J. Beebe, J.S. Moore, J.M. Bauer, Q. Yu, R.H. Liu, C. Devadoss, B.-H. Jo, *Nature*, **404**, 588.

17 S. Howitz, T. Gehring, L. Rebenklau, A. Richter, Nanotech conference proceedings, Montreux, 2001.

18 D.T. Eddington, R.H. Liu, J. S. Moore, D.J. Beebe, *Lab on a Chip* 2001, **1**, 96.

19 Kobayashi and H. Suzuki, *Sens. Actuators B* 2001, **80**, 1.

20 V.Kudela, Encyclopedia of polymer science and engineering, 1987, Wiley, New York, USA.

21 P.J. Flory and J. Rehner, *J. Chem. Phys.* 1943, **11**, 511.

22 P.J. Flory and J. Rehner, *J. Chem. Phys.* 1943, **11**, 521.

23 Z.A. Strong, A.W. Wang, C. F. McConaghy, *Biomedical Microdevices* 2002, **4:2**, 97.

24 J. Lesho and N.F. Sheppard Jr., *Sens. Actuators B* 1996, **37**, 61.

25 Y.C. Qing and C.A. Grimes, *Sens. Actuators B* 2001, **79**, 144.

26 Y.C. Qing and C.A. Grimes, *Sens. Actuators B* 2000, **71**, 112.

27 G. Mayes, J. Blyth, R.B. Millington, C.R. Lowe, *Anal. Chem.* 2002, **74**, 3649.

28 F.H. Arnold, W. Zheng, A.S. Michaels, *J. Membr. Sci.* 2000, **167**, 227.

29 F. McCurley, *Biosens. & Bioelectron.* 1994, **9**, 527.

30 F. R. Aussenegg, H. Brunner, A. Leitner, C. Lobmaier, T. Schalkhammer, F. Pittner, *Sens. Actuators B* 1995, **29**, 204.

31 T. Schalkhammer, C. Lobmaier, F. Pittner, A. Leitner, H. Brunner, F.R. Aussenegg, *Sens. Actuators B* 1995, **24-25**, 166.

32 J. Dubendorfer, R. E. Kunz, G. Jobst, I. Moser, G. Urban, *Sens. Actuators, B* 1998, **50**, 210.

33 H. Wang and W.R. Seitz, *Spie conference on internal standardization and calibration architectures for chemical sensors* 1999, **3856**, 224.

34 W.R. Seitz, M.T.V. Rooney, E.W. Miele, H. Wang, N. Kaval, L. Zhang, S. Doherty, S. Milde, J. Lenda, *Anal. Chim. Acta* 1999, **400**, 55.

35 M.T.V. Rooney and W.R. Seitz, *Anal. Commun.* 1999, **36**, 267.

36 Z. Shakhsher, W.R. Seitz, K.D. Legg, *Anal. Chem.* 1994, **66**, 1731.

37 L. Zhang, M.E. Langmuir, M. Bai, W.R. Seitz, *Talanta* 1997, **44**, 1691.

38 Kikuchi, K. Suzuki, O. Okabayashi, H. Hoshino, K. Kataoka, Y. Sakurai, T. Okano, *Anal. Chem.* 1996, **68**, 823.

39 L. Zhang and W.R. Seitz, Personal Communication, 2002.

40 S. P. Marra, K.T. Ramesh, A.S. Douglas, *Mater. Sci. Eng. C* 2001, **14**, 25.

41 Y. Osada and S.B. Ross-Murphy, *Scientific American* 1993, 42.

42 Y. Osada and J.P. Gong, *Adv. Mater.* 1998, **10**, 827.

43 T. Tanaka and D.J. Fillmore, *J. Chem. Phys.* 1979, **70**, 1214.

44 G.M. Eichenbaum, P.F. Kiser, S.A. Simon and D. Needham, *Macromolecules* 1998, **31**, 5084.

45 A. van den Berg and T.S.J. Lammerink, *Topics in Current Chemistry* 1998, **194**, 22.

46 R.P. Feynman, *J. Microelectromech. Syst.*, 1992, **1**, 60.

Chapter 3

The Hydrogel-based Carbon Dioxide Sensor*

The hydrogel-based carbon dioxide sensor is based on the Severinghaus concept: the partial pressure of CO_2 is determined by measuring the pH of a bicarbonate electrolyte. Here, the pH is measured by means of a pH-sensitive hydrogel which is confined between a pressure sensor and a porous cover. A gas permeable membrane in mounted on top of the cover to retain the electrolyte in the so-formed reservoir. The electrolyte is in contact with the hydrogel through the pores of the cover. CO_2 can diffuse through the membrane into the bicarbonate electrolyte resulting in a certain pH. Since the pH-sensitive hydrogel is confined, it generates a pressure related to the pH. This pressure is measured by the pressure sensor. The principle is put to the proof by exploring two hydrogel configurations: microspheres and a thin disk. Although it is possible to detect CO_2 with both configurations, the hydrogel disk appears to be the best option for the final CO_2 sensor.

* Parts of this chapter are based on S. Herber, W. Olthuis, P. Bergveld, Sens. Actuators B 2003, 91, 378 & S. Herber, W. Olthuis, P. Bergveld, A. van den Berg, Sens. Actuators B 2004, 103, 284.

3.1 Introduction

This chapter starts with an explanation of the Severinghaus concept after which the operational principle of the hydrogel-based CO_2 sensor is demonstrated. In the last section preliminary research towards the final design of the sensor is presented. Here, two hydrogel configurations are explored in order to put the sensor principle to the proof and to find the most suitable design for the final hydrogel-based CO_2 sensor.

3.2 The Severinghaus concept

3.2.1 The electrode and its operational principle

The liquid electrolyte CO_2 sensor was introduced by Stow *et al.*[1] in 1957. Considerable improvements were made by Severinghaus and Bradley[2] in 1958. At present, the Severinghaus electrode is one of the most widely used devices for continuous CO_2 measurements. The original Severinghaus electrode consists of a pH glass electrode, a reference electrode, two electrolyte solutions and a hydrophobic gas permeable membrane. A cross section of the Severinghaus electrode is given in figure 3.1.

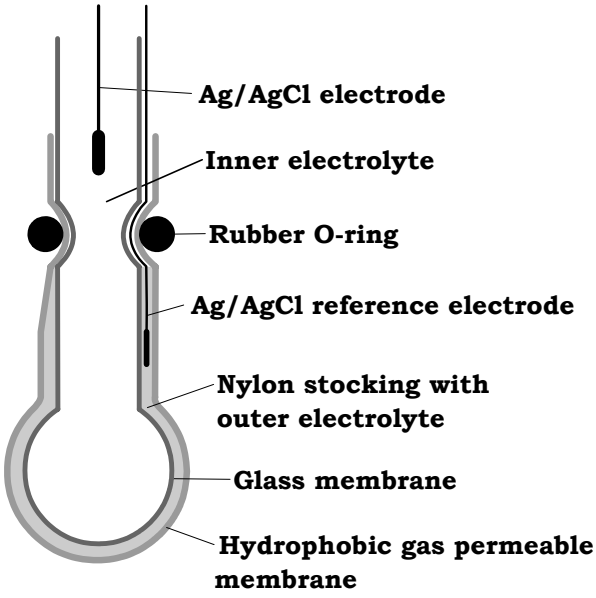

Figure 3.1. Cross section of the classical Severinghaus electrode.

The gas permeable membrane minimizes interference by other nonvolatile species resulting in good selectivity of the device[3]. The basic working principle is as follows: CO_2 diffuses through the hydrophobic membrane into the outer electrolyte. A reaction takes place resulting in a pH change, which is extensively discussed below. The pH is measured by the glass membrane electrode, which has an inner electrolyte contacted by an Ag/AgCl electrode. Thus, the measured pH is in relation with the partial pressure of carbon dioxide (Pco_2).

3.2.2 The CO_2-pH relation

The conversion of CO_2 into H^+ and HCO_3^- in aqueous solutions is an important chemical reaction in many geological and biological processes. The overall reaction is given by

$$Pco_2 + H_2O \Leftrightarrow H_2CO_3 \Leftrightarrow H^+ + HCO_3^- \Leftrightarrow 2H^+ + CO_3^{2-} . \tag{3.1}$$

The relation between Pco_2 and the concentration of dissolved carbon dioxide in an electrolyte is given by Henry's law,

$$[CO_2] = s \cdot Pco_2 , \tag{3.2}$$

where s is Henry's coefficient which represents the solubility of CO_2 in the electrolyte. The dissolved CO_2 reacts with water as follows

$$CO_2(aq) + H_2O \overset{K_h}{\Leftrightarrow} H_2CO_3 . \tag{3.3}$$

Though very little H_2CO_3 can be found in the solution since it dissociates by the following reaction

$$H_2CO_3 \overset{K_1}{\Leftrightarrow} H^+ + HCO_3^- . \tag{3.4}$$

The bicarbonate ion can further dissociate into a carbonate ion,

$$HCO_3^- \overset{K_2}{\Leftrightarrow} H^+ + CO_3^{2-} . \tag{3.5}$$

For low concentrations around pH 7 the autoprotolysis of water is also relevant. The autoprotolysis reaction is

$$2H_2O \overset{K_W}{\Leftrightarrow} H_3O^+ + OH^- . \tag{3.6}$$

Severinghaus used sodium bicarbonate ($NaHCO_3$) as outer electrolyte of the sensor. At low concentrations the bicarbonate doubles the pH response to CO_2, which is explained further in this section. Sodium bicarbonate completely dissolves in water as follows

$$NaHCO_3 \rightarrow Na^+ + HCO_3^- . \tag{3.7}$$

To find the relation between CO_2 and pH, it is necessary to apply the electroneutrality equation. The electroneutrality equation expresses the balance of positive and negative charges in the solution,

$$\sum z_i \cdot m_i = 0 , \tag{3.8}$$

with z_i the charge of the ion i and m_i the concentration. The electroneutrality equation must include all charged species in the system. In the Severinghaus electrolyte the following ions are present: H^+, Na^+, HCO_3^-, CO_3^{2-} and OH^- (equations 3.4-3.7). Applying the electroneutrality equation gives

$$[H^+] + [Na^+] - [HCO_3^-] - 2 \cdot [CO_3^{2-}] - [OH^-] = 0 . \tag{3.9}$$

The electroneutrality equation can be solved in order to get the CO_2-pH relation by rewriting equations 3.2-3.7, and substituting them in equation 3.9. Equation 3.3 can be rewritten to

$$K_h = \frac{[H_2CO_3]}{[CO_2]} \rightarrow [H_2CO_3] = [CO_2] \cdot K_h .$$

Combining this with equation 3.2 gives

$$[H_2CO_3] = s \cdot Pco_2 \cdot K_h . \tag{3.10}$$

Equation 3.4 can be rewritten to

$$K_1 = \frac{[H^+] \cdot [HCO_3^-]}{[H_2CO_3]} \rightarrow [HCO_3^-] = \frac{K_1 \cdot [H_2CO_3]}{[H^+]} .$$

Combined with equation 3.10 gives

$$[HCO_3^-] = \frac{K_1 \cdot s \cdot Pco_2 \cdot K_h}{[H^+]} . \tag{3.11}$$

Rewriting equation 3.5 and 3.6 results in

$$[CO_3^{2-}] = \frac{K_2 \cdot [HCO_3^-]}{[H^+]} , \tag{3.12}$$

$$[OH^-] = \frac{K_w}{H^+} . \tag{3.13}$$

Taking equation 3.11, 3.12 and 3.13 together with the electroneutrality equation 3.9 gives the general formula describing Severinghaus-based CO_2 sensors,

$$\begin{aligned} [H^+]^3 + [Na^+] \cdot [H^+]^2 - (K_1 \cdot K_h \cdot s \cdot Pco_2 + K_w) \cdot [H^+] \\ - 2 \cdot K_1 \cdot K_2 \cdot K_h \cdot s \cdot Pco_2 = 0 . \end{aligned} \tag{3.14}$$

The concentration of sodium ions equals the concentration of added sodium bicarbonate. Equation 3.14 can be rewritten to

$$Pco_2 = \frac{[H^+]^2 + [NaHCO_3] \cdot [H^+] - K_w}{s \cdot K_1 \cdot K_h \cdot (1 + \frac{2 \cdot K_2}{[H^+]})} . \tag{3.15}$$

With equation 3.15, the partial pressure of CO_2 can be determined when the pH, being $-^{10}\log[H^+]$, and the bicarbonate concentration are known. In literature, dissociation constants K_1 and K_h are often multiplied and displayed as a single constant. In table 3.1 values are given of the above presented constants at a temperature of 25 °C.

Table 3.1. Values for the constants of equation 3.15 at 25 °C.

$K_1.K_h$ [ref[4]]	K_2 [ref[4]]	K_w [ref[5]]	s (mol/m^3·kPa) [ref[6]]
4.30×10^{-7}	5.61×10^{-11}	1.01×10^{-14}	4.49×10^{-5}

A plot is made using equation 3.15 and the values of table 3.1 which represents the relation between the partial pressure of carbon dioxide and the pH for various bicarbonate concentrations, shown in figure 3.2. The limits of the medically relevant Pco_2 range are also indicated. With this plot it is possible to predict the range in which the pH will vary within the medically relevant Pco_2 range when a certain bicarbonate concentration is used.

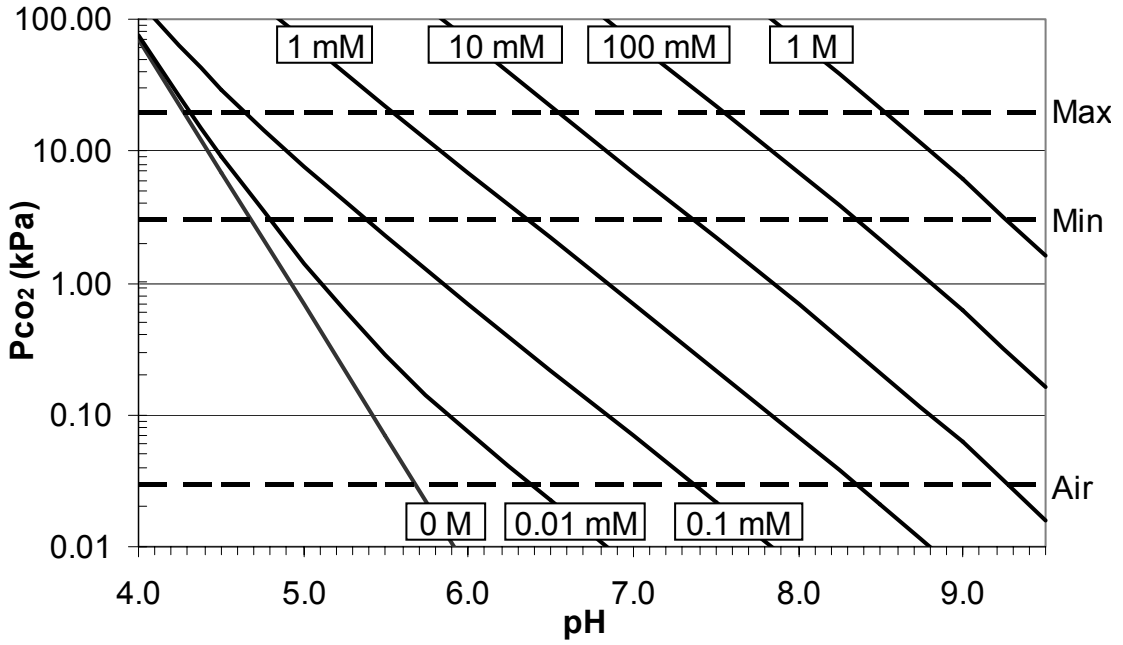

Figure 3.2. The relation between Pco_2 and pH for various bicarbonate concentrations.

As already mentioned before, bicarbonate doubles the pH change to Pco_2 which will be explained below. Severinghaus defined the sensitivity of his electrode, *S*, as

$$S = \frac{\partial pH}{\partial \log Pco_2}. \tag{3.16}$$

In water without bicarbonate, equation 3.15 can be approximated by

$$Pco_2 = \frac{[H^+]^2}{s.K_1}. \tag{3.17}$$

Taking the logarithm of the above equation gives

$$\log Pco_2 = \log\left(\frac{[H^+]^2}{s.K_1}\right),$$

which can be rewritten to pH as follows

$$\log Pco_2 = 2\log[H^+] - \log(s.K_1) \rightarrow$$

$$\log Pco_2 = -2pH - \log(s.K_1) \rightarrow$$

$$pH = -1/2\log(s.K_1) - 1/2\log Pco_2. \tag{3.18}$$

Since ($s.K_1$) is a constant, it does not contribute to the sensitivity. Combining equation 3.18 and 3.16 gives the sensitivity without adding sodium bicarbonate,

$$S = \frac{\partial pH}{\partial \log Pco_2} = -\frac{1}{2}. \tag{3.19}$$

The sensitivity is negative as expected: an increase in Pco_2 results in a decrease in pH. When sodium bicarbonate is added, the second term in equation 3.15 becomes dominant and the equation can be approximated by

$$Pco_2 = \frac{[H^+] \cdot [NaHCO_3]}{s.K_1}. \tag{3.20}$$

By applying the same calculation method as above, the sensitivity, *S*, can be determined as follows

$$\log Pco_2 = \log\left(\frac{[H^+] \cdot [NaHCO_3]}{s.K_1}\right) \rightarrow$$

$$\log Pco_2 = -pH + \log[NaHCO_3] - \log(s.K_1) \rightarrow$$

$$pH = \log[NaHCO_3] - \log(s.K_1) - \log Pco_2 \rightarrow$$

log[$NaHCO_3$] and log(s.K_1) are constants thus:

$$S = \frac{\partial pH}{\partial \log Pco_2} = -1. \tag{3.21}$$

Thus, adding bicarbonate to water doubles the pH change and so the sensitivity. Figure 3.3 shows the relation between the sensitivity and various bicarbonate concentrations. As can be seen, the sensitivity is doubled when 1.0x10^{-3} M bicarbonate or higher is used.

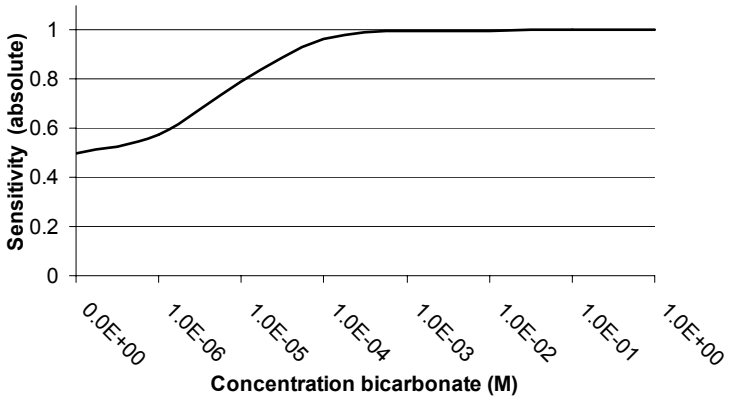

Figure 3.3. Plot of the relation between the absolute sensitivity and various bicarbonate concentrations

3.3 Sensor operational principle

The sensor presented here exploits a pH-sensitive hydrogel to measure pH changes induced by CO_2, according to the Severinghaus concept. A schematic representation of the sensor is given in figure 3.4.

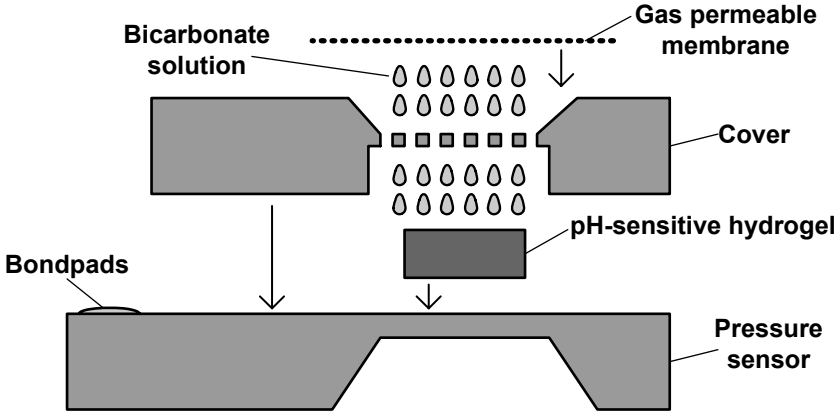

Figure 3.4. Schematic representation of the hydrogel-based CO_2 sensor.

The sensor consists of a pressure sensor and a porous cover between which a pH-sensitive hydrogel is confined. The porous cover comprises a reservoir filled with a bicarbonate electrolyte in contact with the hydrogel. A gas permeable membrane is mounted on top of the porous cover. The membrane has two functions: it retains the electrolyte in the reservoir and it prevents external solutions to enter the sensor, which can potentially influence the CO_2-pH relation or ionic strength of the electrolyte. A block diagram of the sensor principle is given in figure 3.5.

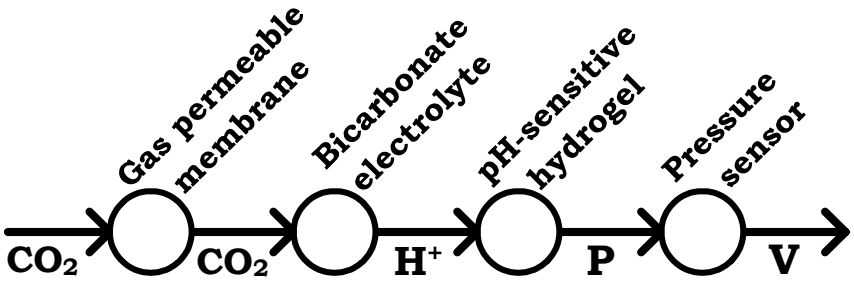

Figure 3.5. Block diagram of the working principle of the hydrogel-based CO_2 sensor.

The working principle is as follows: CO_2 diffuses through the gas permeable membrane into the electrolyte. A reaction takes place resulting in a change in pH according to the Severinghaus concept. Since the pH-sensitive hydrogel is enclosed, it can not swell and will, instead, generate a pressure in response to the pH change. This pressure is measured by the pressure sensor and translated into an electrical signal. Thus, the measured pressure is in relation with the partial pressure of carbon dioxide. Note that the stiffness of the porous cover exceeds the stiffness of the pressure sensor membrane many times so that when the hydrogel attempts to swell, it will deflect the pressure sensor membrane and not the porous cover. Detailed information on the deflection can be found in chapter 5.

3.4 Explorative experiments

In preliminary research towards the final design of the hydrogel-based sensor, two hydrogel configurations were explored in order to proof the sensor principle and to find the optimal configuration. The two investigated hydrogel configurations were microspheres and a thin disk. Hydrogel microspheres were explored for their fast swelling time. The characteristic time of hydrogel swelling is proportional to the square of the size of the gel[7]. Since a hydrogel microsphere has a size in the order of a few micrometers, it swells relatively fast. Additionally, there are pathways between the microspheres through which fast diffusion of ions to every single microsphere can take place without the restriction of a polymer network, as in the case of a solid hydrogel. Therefore, theoretically a multitude of microspheres should equilibrate faster than a solid hydrogel with the same volume. In section 3.4.1 the result with hydrogel microspheres is shown and in section 3.4.2 with a thin hydrogel disk. The presented experimental data represents the best feasible at that moment.

3.4.1 Hydrogel microspheres

Hydrogel microspheres were enclosed between a pressure sensor and a porous cover and the CO_2 response was examined[8]. The microspheres, with a diameter of a few μm, were prepared by precipitation polymerization. This is a polymerization reaction in which the polymer being formed is insoluble

in its own monomer or in a particular monomer-solvent combination and thus precipitates out as it is formed[9]. The monomers Methylenebis(acrylamide) (0.1928 g), 4-nitrophenyl methacrylate (NPMA, 0.5175 g) and methacrylic acid (MAA, 0.2153 g) were dissolved in 10 mL ethanol, which was degassed at room temperature with nitrogen for 20 minutes. The solution was heated to 60 ^{o}C under nitrogen atmosphere after which solid azobis(isobutyronitrile) was added. The solution was briefly stirred for 5 minutes which resulted in a cloudy dispersion of particles. The reaction was continued for 3 hours without stirring after which the product was cleaned by centrifugation and resuspended in ethanol five times. To make the hydrogel microspheres reactive in the alkaline pH range, the nitrophenol groups were replaced by means of an amphoterization reaction. The spheres were resuspended in diethylenetriamide (DETA) (6.1598 mL) resulting in a yellow solution caused by the replaced nitrophenol. The mole amount of DETA was set 100 times the mole amount of the reactive nitrophenol groups to prevent DETA to act as a cross-linker between the groups. The reaction was run for 12 hours with constant stirring. The MAA-co-DETA microspheres were washed by centrifugation and resuspension in four steps. The first time in 100% ethanol, then 66% ethanol and 34% water, the third time in 34% ethanol and 66% water and finally in 100% water. MAA-co-DETA has three dissociation constants. The first, pK_{a1}, is 4.7 from the methacrylic acid. The second and third, pK_{a2} and pK_{a3}, are 7.7 and 9.1 from the diethylenetriamide. This makes that the DETA-coupled hydrogel swells gradually over a wide pH range. An increase in pH, at pH 5 and higher, results in swelling[10] and, in the case of confinement, in an increased pressure.

A Baxter disposable Truwave pressure sensor, normally used for medical purposes, was modified. The device consists of a silicon pressure sensor with on top of the membrane a protective silicone layer and the whole is molded in plastic. To make the sensor suitable for the CO_2 application, the top of the plastic housing was milled off to obtain access to the silicone layer of which a thin layer is removed. An amount of a highly concentrated hydrogel microspheres solution was pipetted on top of the remaining rubber layer. After two hours of drying at room temperature a dense, homogeneous layer of hydrogel microspheres was created with a thickness of approximately 0.5 mm. Then, the sensor was placed in a

specially manufactured holder, which fixed the volume and position of the microspheres between the pressure sensor membrane and a combined metal screen/microporous membrane. The metal screen was used for its stiffness and the microporous (1 µm) membrane to retain the microspheres. The manufactured holder with sensor is shown in figure 3.6. Note that in this stage no gas permeable membrane was added to the sensor configuration.

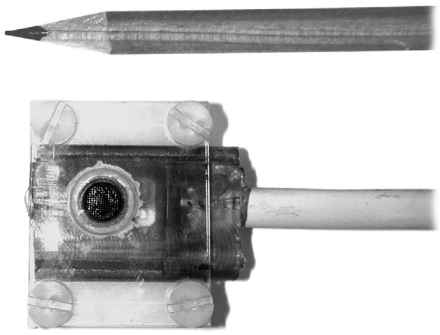

Figure 3.6. Photo of the constructed CO_2 sensor based on hydrogel microspheres.

For provisional test measurements, the holder with sensor and a pH glass membrane electrode (PHM 83, Radiometer Copenhagen) were placed in a beaker with 50 mM bicarbonate solution*. A Delta Elektronika voltage supply (E 015-2) was used to provide voltage to the pressure sensor. Both hydrogel-based sensor and pH glass membrane electrode were connected to a computer via a LabVIEW data acquisition card (National Instruments). A LabVIEW software program was written to log the pressure and pH versus time.

CO_2 gas was led through the bicarbonate solution to change the pH and consequently provoke response of the hydrogel in the form of pressure generation. In figure 3.7 the result of a CO_2 measurement is shown.

* At the moment of the experiment, no optimum in bicarbonate concentration had yet been determined and a certain value was chosen.

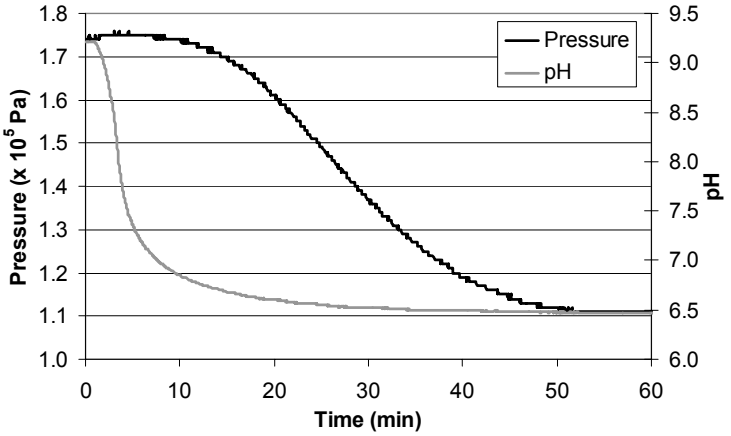

Figure 3.7. Plot of the pH change of a 50 mM sodium bicarbonate solution and the pressure change of the hydrogel based sensor as result of a Pco_2 change from 0.03 kPa (air) to 100 kPa (MAA-co-DETA hydrogel).

The starting pressure of the sensor was approximately $1.75x10^5$ Pa and is the result of hydratation of the hydrogel, discussed more in detail in chapter 7. At t = 0 minutes, the pH of the sodium bicarbonate solution was in equilibrium with air, which has a Pco_2 of 0.03 kPa*. Then, 100 kPa CO_2 was led through the gas chamber. As a result, the pH of the bicarbonate changed from 9.2 to 6.5. The hydrogel microspheres reacted to this pH lowering, reflected by a pressure drop from $1.75 x10^5$ to $1.10x10^5$ Pa in 51 minutes. This long response time was not expected and might be caused by two factors. In the sensor configuration an additional microporous membrane is used to enclose the spheres. Diffusion of ions to the hydrogel is slowed down by this membrane and it is possible that this is responsible for the long response time. Another cause might be the amount of hydrogel microspheres in the sensor. Since the microspheres were dosed manually, it was difficult to add a very small amount. The thickness of the used microspheres layer was estimated to be approximately 0.5 mm, which is reasonable thick and consequently results in a long response time.

During these experiments, problems were experienced with the hydrogel microspheres. One of the problems is of technological kind: the spheres were difficult to handle, hard to dose and difficult to confine, all due to their small size of a few micrometers. Another problem was the

* According to the Dalton's law, the total pressure of a gas mixture is the sum of the partial pressure of each gas: $P_{total} = P_1 + P_2 + P_3 + \ldots + P_n$. All experiments were performed under atmospheric pressures. Thus, the sum of all partial pressures is approximately 100 kPa.

instability of the sensor signal, as demonstrated by another similar type of CO_2 experiment of which the result is shown in figure 3.8.

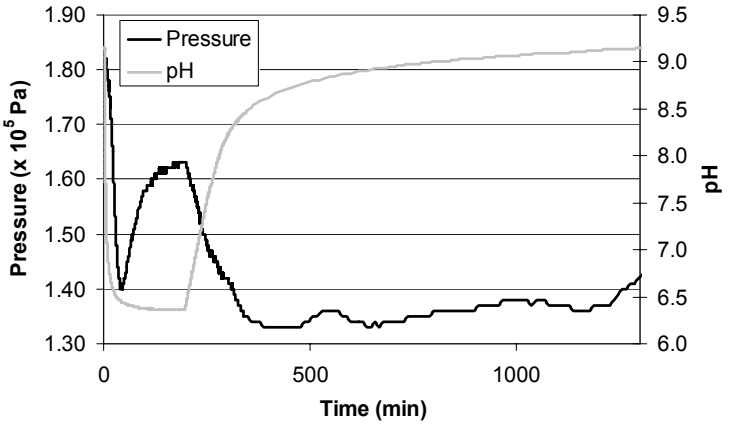

Figure 3.8. Plot of the pH change of a 50 mM sodium bicarbonate solution and the pressure change of the hydrogel based sensor as result of a Pco_2 change from 0.03 kPa (air) to 100 kPa (MAA-co-DETA hydrogel) and vice versa at t = 200 minutes.

At t = 0 minutes, 100 kPa CO_2 was led through the solution. The pH decreased and, as expected, the generated pressure decreased. However, after approximately 50 minutes, the pressure unexpectedly increased while the Pco_2 remained constant at 100 kPa. Then, at t = 200 minutes, the CO_2 flow was switched off and the pH increased again. In contrast to what is expected, the pressure decreased to approximately $1.35x10^5$ Pa where it fluctuates for a long time without returning to its original starting pressure. It is suspected that the instability and reversed behavior in the signal are caused by moving (rearranging) of the microspheres. This behavior is considered to be the largest drawback of using hydrogel microspheres and therefore a thin hydrogel disk was explored as an alternative as will be discussed in the next section.

3.4.2 Thin hydrogel disk

In order to overcome the encountered problems discussed in section 3.4.1, the hydrogel microspheres were replaced by a thin hydrogel disk[11]. The disk was prepared by a simple method and consists of hydroxyethyl methacrylate (HEMA) and dimethylaminoethyl methacrylate (DMAEMA). A prehydrogel mixture of HEMA and DMAEMA was made with a mole ratio of 95:5 and to the total mole amount, 1.5% cross-linker tetraethyleneglycol

dimethacrylate and 3% photo-iniator 2,2-dimethoxy-2-phenylacetophenone was added.

Silicon moulds were prepared with standard cleanroom techniques. By means of reactive ion etching a square cavity was created with 2000 µm sides and a depth of 50 µm. An amount of prehydrogel solution was pipetted in the cavity and covered with transparent Mylar foil which prevents oxygen to interfere with the polymerization reaction but allows UV light to pass. By sliding the foil over the mould, abundant solution is removed until the cavity is exactly filled with the monomer mixture. A mask was placed on top of the foil with a circular aperture (diameter 750 µm) through which UV can pass. The hydrogel was exposed to 366 nm UV light for 90 seconds to achieve a complete polymerization within the aperture region. The polymerization setup is shown in figure 3.9.

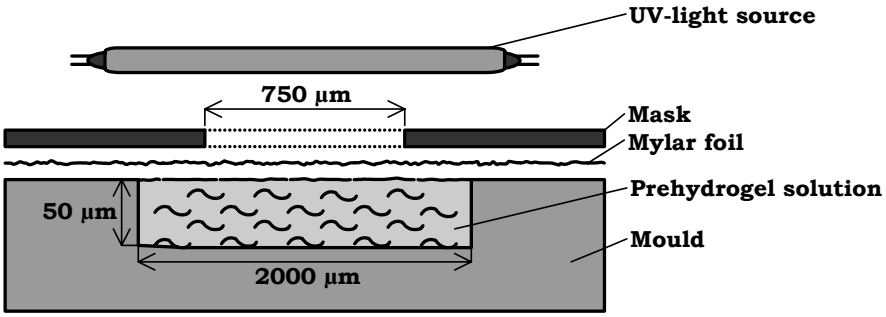

Figure 3.9. Schematic representation of the setup that is used to polymerize HEMA-co-DMAEMA hydrogel disks with a diameter of 750 µm and a thickness of 50 µm.

By using this method, a hydrogel disk with a diameter of 750 µm and a thickness of 50 µm was created. The mould with disk was placed in a pH 6 buffer, which results in swelling of the hydrogel. Consequently, the hydrogel disk releases from the substrate and can easily be removed with a scalpel.

The synthesis of the hydrogel with DMAEMA was a well-considered choice. The pK_a of the monomer DMAEMA is approximately 8. This means that this type of hydrogel will swell and deswell in a pH range around 8, as required for measuring the medical relevant Pco_2 levels. The amine groups in the hydrogel are protonated with decreasing pH around 8, which consequently results in swelling. In the case of confinement, the hydrogel generates more pressure with decreasing pH.

A Honeywell pressure sensor (26PC series), which consists of a silicon pressure sensor chip and a plastic housing, was modified. The housing was removed in order to obtain the bare sensor chip. A hole was drilled in a PCB stick and the pressure sensor chip was glued in it at all sides in such a way that the bondpads and front and back side of the pressure sensor membrane were uncovered. The bondpads on the chip were connected to the electrode tracks on the PCB by wirebonding. The wirebonds and electrode tracks were then insulated with two-component epoxy Hysol (Loctite, EE0079/C8-W795). The cavity of the pressure sensor chip was subsequently filled with silicone rubber (Dow Corning, 734). After hardening of the rubber, a thin layer of Teflon coating (Fluorinert^{tm} electronic liquid (FC40, 3M) was applied to prevent sticking of the hydrogel disk which was placed on top. The disk was then clamped by a porous metal screen that was kept in place by a shrink tube. In figure 3.10 a cross section of the sensor is shown and in figure 3.11 a photo of the manufactured sensor. Note that in this stage no gas permeable membrane was added to the sensor configuration.

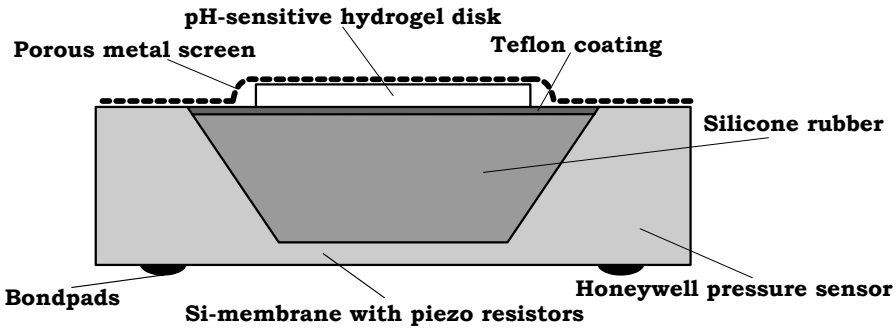

Figure 3.10. Cross section of the CO_2 sensor with hydrogel disk.

Figure 3.11. Photo of the constructed CO_2 sensor with hydrogel disk mounted on a PCB stick.

The measurement setup consists of a voltage supply (Delta Elektronika, E 015-2) to provide voltage to the pressure sensor and a pH meter (PHM 83, Radiometer Copenhagen) to measure the pH. With use of LabVIEW software (National Instruments) the sensor and pH signal were logged versus time.

The hydrogel-based sensor and pH glass membrane electrode were placed in a 100 mM bicarbonate solution* and 100 kPa nitrogen (N_2) was led through the solution. In figure 3.12 the result of a CO_2 experiment is shown.

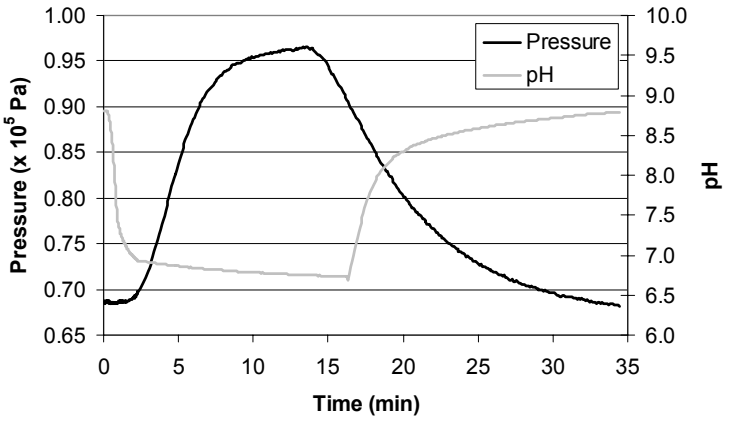

Figure 3.12. Plot of the pH change of a 100 mM sodium bicarbonate solution and the pressure change of the hydrogel-based sensor as result of a gas flow change from 100% N_2 to 100% CO_2 and back to 100% N_2.

The starting pressure was approximately 0.68×10^5 Pa. At t = 0 minutes, the N_2 was replaced by 100 kPa CO_2 and the pH of the solution decreased from 8.9 to 6.7. Consequently, the pressure generated by the hydrogel increased from 0.68×10^5 to 0.96×10^5 Pa. The time that the hydrogel-based sensor needed to reach equilibrium was approximately 13 minutes. At t = 13.3 minutes, the CO_2 flow was replaced by a 100 kPa N_2 flow. The pH increased again to its original value as did the pressure by decreasing.

The response time of the sensor is shorter than that of the sensor with hydrogel microspheres. Although both sensor configurations may not

* At the moment of the experiment, no optimum in bicarbonate concentration had yet been determined and a certain value was chosen.

be compared due to the difference in hydrogel thicknesses (hydrogel microspheres: ~500 µm, hydrogel disk: ~50 µm), the sensor with the hydrogel disk is still reasonably fast despite the fact that a solid piece of gel is used. More important is the fact that the sensor with disk showed little instability in the sensor signal. Furthermore, the behavior of the sensor was as expected. With a decrease in pH the hydrogel nicely generated additional pressure and vice versa.

3.4.3 Conclusions

Two sensors were tested with different hydrogel configurations: hydrogel microspheres and a hydrogel disk. With both configurations CO_2 detection was achieved.

The two sensors are quite different regarding the applied pressure transducer, hydrogel volume and technical assembly procedure. Furthermore, the measurement principles are different: direct detection of hydrogel pressure generation and indirect through silicone rubber. For these reasons, both sensors cannot be compared with respect to the response time. Nevertheless, two important differences are noted. The signal of the sensor with the hydrogel disk was, from the beginning, very stable and the sensor showed the expected behavior. The hydrogel disk was also easier to synthesize and handle, and was reasonably fast despite the fact that a solid piece of gel is used. Therefore, the conclusion is drawn that a thin HEMA-co-DMAEMA pH-sensitive hydrogel disk, or layer, is the best option as sensing material in the hydrogel-based CO_2 sensor. Since a hydrogel with a thickness below 50 µm can easily be made with micromachining techniques, it should be possible to further reduce the response time of the sensor.

3.5 References

1 R.W. Stow, R.F. Bear, B.F. Randell, *Arch. Phys. Med. Rehab.* 1957, **38**, 646.

2 J.W. Severinghaus, A.F. Bradley, *J. Appl. Physiol.* 1958, **13**, 515.

3 G.G. Guilbalt, F.R. Shu, *Anal. Chem.* 1972, **44**, 2161.

4 R.C. Weast, M.J. Astle, W.H. Beyer, CRC Handbook of Chemistry and Physics, 65th ed., 1984, CRC press Inc., Florida, USA.

5 P.W. Atkins, Physical Chemistry, 6th ed., 2001, Oxford University Press, New York, USA.

6 R. Chang, Physical Chemistry for the chemical and biological sciences, 3rd ed., 2000, California, USA.

7 T. Tanaka, D.J. Fillmore, *J. Chem. Phys.* 1979, **70**, 1214.

8 S.Herber, W. Olthuis, P. Bergveld, *Sens. Actuators B* 2003, **91**, 378.

9 S.M. Lee, Dictionary of Composite Materials Technology, 1st ed., 1995, CRC press Inc., Florida, USA.

10 H. Kawaguchi, K. Fujimoto, Y. Nakazawa, M. Sakagawa, Y. Ariyoshi, M. Shidara, H. Okazaki, Y. Ebisawa, *Colloids and Surfaces, A, Physicochemical and Engineering Aspects* 1996, **109**, 147.

11 S. Herber, W. Olthuis, P. Bergveld, A. van den berg, *Sens. Actuators B* 2004, **103**, 284.

Chapter 4

Study of Pressure Generation of Hydrogels under Isochoric Conditions*

In this chapter a method is proposed to study the behavior of stimulus-sensitive hydrogels under isochoric conditions. Freedom of swell movement of such a hydrogel is restricted in all directions by enclosing the hydrogel between a pressure sensor and porous cover. Water and external stimuli can be applied to the hydrogel through the pores of the cover to provoke hydrogel pressure generation. The method is put to the proof by examining the response of a pH-sensitive hydrogel to changes in pH, ionic strength and buffer concentrations. Both equilibrium and dynamic pressure generation are observed. The results show that higher pressures are obtained by incorporating more ionizable groups into the hydrogel or by lowering the ionic strength of the external solution. Furthermore, it is proven that pressures reach equilibrium faster when less titratable groups are incorporated or at higher buffer concentrations. The presented method is a fast en simple manner to characterize the static and dynamic stimulus-dependent behavior of hydrogels.

* This chapter is based on S. Herber, J. Eijkel, W. Olthuis, P. Bergveld, A. van den Berg, *J. Chem. Phys.* 2004, **121**, 2746.

4.1 Introduction

Little is known about the behavior of stimulus-sensitive hydrogels when enclosed[1]. This can be interesting for situations where hydrogels are confined in sensors, like our own hydrogel-based CO_2 sensor, or in actuators. In this chapter a method is presented for studying the response of enclosed stimulus-sensitive hydrogels by constructing a device by means of microfabrication techniques. The use of these techniques was a deliberate choice. Hydrogels are known to have long swelling and shrinking response times due to the fact that the kinetics are controlled by diffusion of ions. Faster response times are obtained by downsizing hydrogels due to shorter diffusion lengths. The characteristic time of swelling is inversely proportional to the square of the size of the hydrogel[2]. To study the dynamic response, a hydrogel was enclosed between a micro pressure sensor and a microfabricated porous cover. The cover contains a sieve with microscaled holes through which water and ions can pass easily to hydrate the hydrogel. The stiffness of this microsieve exceeds the stiffness of the pressure sensor membrane many times. Therefore the pressure sensor membrane will deflect when the hydrogel attempts to swell. Since the deflection of the pressure sensor membrane is much smaller than the thickness of the hydrogel one can speak of isochoric conditions (isochoric: constant volume, a.k.a. isovolumetric). The demonstrated device is not influenced by variations in atmospheric pressure as this pressure is equal on both sides of the pressure sensor membrane.

Other methods to characterize hydrogels are based on free swellable or partly constrained hydrogels. Equilibrium and kinetic studies of unconstrained hydrogels have been performed by Tanaka *et al.*[2-4] They observed the degree of swelling as function of pH and bath ionic strength by measuring the change in diameter of hydrogel spheres using a microscope and camera. Another widely used method to characterize unconfined hydrogels is measuring the change in weight of gels after changing environmental conditions[5-7]. Beebe *et al.* developed a method to study partly confined hydrogels[8]. They studied the swelling of a cylindrical hydrogel in a microchannel. The hydrogel can only deform in radial direction and is modeled by considering a circular section. By means of this method two

models were developed to predict equilibrium swelling and kinetics of pH-sensitive hydrogels.

With our method fully constrained hydrogels can be characterized. In contrast to the above mentioned methods our manner is suitable for measuring pressures generated by hydrogels. Since hydrogel swelling is osmotically driven, this information is also useful for the calculations of Donnan equilibrium as shown in the theoretical section and results. Furthermore the characterization data are useful for sensors and actuators where hydrogels are almost completely confined. Examples of such sensors are hydrogel-actuated capacitive transducers explored by Strong, Wang and McConaghy[9] and Lei *et al.*[10], and the hydrogel-based CO_2 sensor developed in our group[11,12]. An example of a constrained hydrogel as actuator is the peristaltic micropump where hydrogels close an elastic microfiber developed by Van der Linden *et al.* [313]

4.2 Theory

It is assumed that the equilibrium degree of swelling of a polyelectrolyte gel, such as a pH-sensitive hydrogel, is governed by the change in total free energy ΔF ,

$$\Delta F = \Delta F_{mix} + \Delta F_{el} + \Delta F_{ion}, \tag{4.1}$$

where F_{mix} is the ordinary free energy of polymer-solvent mixing, F_{el} the elastic free energy as a consequence of the expansion of the network structure and F_{ion} the free energy due to nonuniform distribution of ions between the inside and outside of the gel[14]. In equilibrium swelling conditions the total change in free energy reaches a minimum. Equation 4.1 can also be rewritten in terms of pressures,

$$\Pi_{tot} = \Pi_{mix} + \Pi_{el} + \Pi_{ion}, \tag{4.2}$$

where Π_{mix}, Π_{el} and Π_{ion} are, respectively, the mixing, elastic and ionic contributions[14-16]. When a hydrogel is under isochoric conditions the elongation of the polymer chains can not take place. Thus, the elastic

contribution Π_{el} remains constant. The same counts for the mixing contribution Π_{mix} because water flow into or out of the hydrogel can not occur. Therefore Π_{tot} only depends on the osmotic pressure Π_{ion}, which is described by the Donnan theory,

$$\Pi_{ion} = RT\left(c_{gel} - c_{sol} \right), \tag{4.3}$$

where c_{gel} and c_{sol} are the concentrations of ions in the gel and the external solution[17]. Due to the presence of the immobile (fixed) charges at the polymer backbone, all mobile ions are distributed over the system according to the so-called Donnan ratio r_D,

$$r_D = \frac{c^+_{sol}}{c^+_{gel}} = \frac{c^-_{gel}}{c^-_{sol}}, \tag{4.4}$$

where c^+_{sol} is the concentration of cations and c^-_{sol} the concentration of anions in the solution, and c^+_{gel} the concentration of cations and c^-_{gel} the concentration of anions in the gel. Thus $c^+_{sol} + c^-_{sol} = c_{sol}$ and $c^+_{gel} + c^-_{gel} = c_{gel}$ as used in equation 4.3. For a 1:1 salt concentration $c^+_{sol} = c^-_{sol} = \frac{1}{2}c_{sol}$ and c_{sol} is equal to the ionic strength. If the fixed charge has a concentration c_x it can be calculated, based on charge neutrality, that

$$r_D = \frac{\sqrt{{c_{sol}}^2 + {c_x}^2} + c_x}{c_{sol}}. \tag{4.5}$$

By using equations 4.3 - 4.5 the osmotic pressure can be rewritten to

$$\Pi_{ion} = \tfrac{1}{2} RTc_{sol}\left(\frac{1}{r_D} + r_D - 2 \right). \tag{4.6}$$

The ion distribution not only causes an osmotic pressure, but also an electrical potential over the gel/solution interface, the Donnan potential Φ_D,

$$\phi_D = \frac{RT}{F} \ln r_D, \tag{4.7}$$

with F the Faraday constant. Because the pH outside as well as inside the gel plays a dominant role in the gel's reaction, the distribution of protons is of importance. With equations 4.4, 4.5 and 4.7 the pH in the hydrogel pH_{gel} can be calculated,

$$pH_{gel} = pH_{sol} + \frac{\phi_D F}{2.3RT}, \tag{4.8}$$

where pH_{sol} is the pH of the external solution.

The swelling kinetics of polyelectrolyte gels can be predicted by the macroscopic continuum model presented by Grimshaw *et al.*[18] Here, a characteristic diffusion-reaction time constant describes the diffusion and reactions of protons in the hydrogel for small changes in pH of an unbuffered external solution. When buffer ions are present in the solution the swelling kinetics can be described by the characteristic buffer-mediated diffusion-reaction time constant derived by Lesho and Sheppard[19],

$$\tau_{bdr} = \frac{\delta^2}{\pi^2 D_{HB}}\left[1 + \frac{\beta_{gel}}{(1+H_0)\beta_{sol}}\right], \tag{4.9}$$

where δ is the gel thickness, D_{HB} the diffusivity of the buffer molecule in the gel and H_0 the hydration (ratio of fluid to solid volume). The β_{gel} and β_{sol} are the modified buffer capacity of the hydrogel and the buffer solution, respectively. The gel thickness and hydration are constant in our situation since the hydrogel is under isochoric conditions. In figure 4.1 the influence of β_{gel} and β_{sol} on the time constant is demonstrated (for H_0 =1). In figure 4.1a is shown that the time constant τ_{bdr} increases linearly with increasing β_{gel}. According to figure 4.1b this time constant approximates $\tau_{bdr}=\delta^2/\pi^2 D_{HB}$ when the buffer capacity of the solution increases. At decreasing solution buffer capacity the time constant increases dramatically.

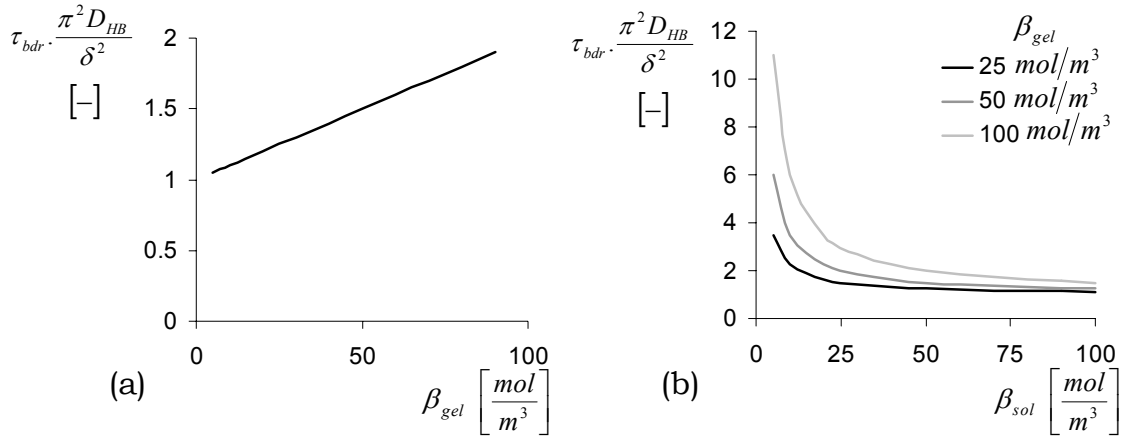

Figure 4.1. (a) The influence of the buffer capacity of the hydrogel on the time constant when the β_{sol} is 50 mol/m³. (b) The influence of the buffer capacity of the external solution on the time constant for various values of β_{gel}.

4.3 Experimental

4.3.1 Materials

The monomer dimethylaminothyl methacrylate (DMAEMA) and comonomer 2–hydroxyethyl methacrylate (HEMA) were bought from Acros. Cross-linker tertraethylene glycol dimethacrylate (TEGDMA) was obtained from Fluka and 2,2-dimethoxy-2-phenylacetophenone (DMPAP) from Aldrich. The DMAEMA was purified by distillation. All other chemicals were used as received. The pressure sensor (type P4.2) was acquired from Sentron Europe BV. The cover was fabricated especially for this purpose in silicon with standard cleanroom techniques. The thickness of the cover is 200 µm. Calculations showed that at this thickness cover deflection is negligible compared to the deflection of the pressure sensor membrane at 1x10^5 Pa gel pressure. The cover contains square pores with 50 µm sides and 50 µm spacing in a matrix of 5x5. The amount of pores is restricted by the overall dimensions of the pressure sensor membrane (450x450 µm^2). The pore size and spacing was chosen because preliminary experiments showed that decreasing the spacing between the pores resulted in little or no pressure generation. It is assumed that in this case more of the hydrogel is expanding out through the pores and a smaller portion of the gel is constrained by the spaces between the pores resulting in little force generation. This could probably be solved by also decreasing the pore size.

Unfortunately decreasing the pore size is not possible due to limitations of the used cleanroom techniques. Increasing the pore spacing would lead to slower response times and was therefore not investigated.

4.3.2 Methods

Prehydrogel solutions were prepared with solvent containing ethylene glycol and water in equimolar amounts. HEMA and DMAEMA with a molar ratio of 95/5 or 97.5/2.5, 1.5 mol% cross-linker TEGDMA and 3 mol% photoiniator DMPAP were added. The mole ratio between the monomers and the solvent was 1 to 1.5. Solutions were stored in dark at 4 oC.

pH buffers were prepared with BIS-TRIS (pH 6-6.5), HEPES (pH 7-8) and TRIS (pH 8.5-9). The ionic strength was adjusted with NaCl.

Devices for characterization were prepared with different prehydrogel solutions. Before adding the prehydrogel solution the pores in the cover were first filled with polydimethyl siloxane (PDMS). After hardening the PDMS forms a silicone rubber plug which prevents the prehydrogel solution to leak out and retards diffusion of oxygen to interfere with the polymerization reaction. Still, UV light is allowed to pass. After the PDMS filling the silicon cover is mounted on the pressure sensor. Since the pressure sensor is covered by a special insulating coating, conventional MEMS bonding techniques could not be used. Therefore the two parts were glued together. Figure 4.2 shows the process scheme used after the gluing.

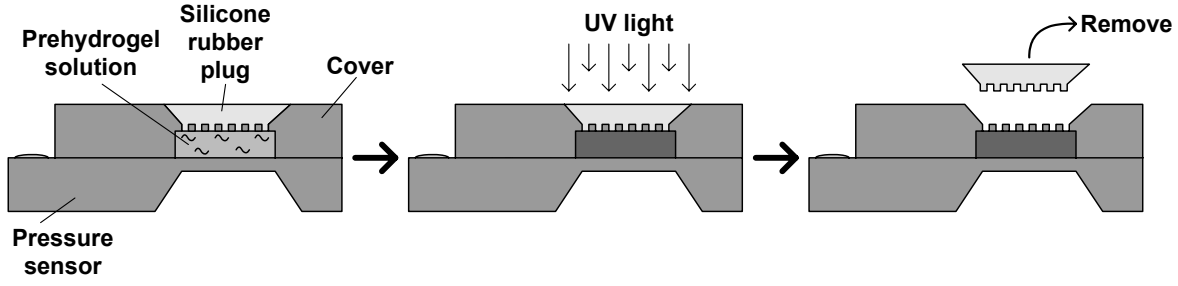

Figure 4.2. Process scheme of the device preparation. First the device is filled with the prehydrogel solution. Then the hydrogel is polymerized in situ by UV light. Thereafter the silicone rubber plug is removed to open the sensor.

The devices were filled with the monomer solution through a small channel in the device by using vacuum. Subsequently, the free-radical

copolymerization reaction was started by UV light for2 minutes with an ELC-403 light curing system of The Electro-Lite Corporation. Due to the non-collimated light source, scattering by the PDMS plug and reflection by the pressure sensor membrane, the UV light is highly diffused and also reaches under the pore matrix of the silicon cover. Therefore the resulting hydrogel forms a homogeneous whole. After the hydrogel formation the PDMS plug is removed to open the sensor. The dimensions of the hydrogel are fixed by the dimensions of the hydrogel cavity (450x450x10 μm^3). The device was mounted on a PCB board and electrical connections were made with the pressure sensor using wirebonding. Epoxy glue was used to isolate the wirebonds. A precision voltage source (Knick "präzisions-spannungsgeber" Berlin 37) was used to supply a constant voltage to the device. The output signal was monitored by a HP 34410A multimeter which was connected to a computer. A LabVIEW program was written to log the signal versus time.

4.4 Results and discussion

First it was investigated whether measurements were made at isochoric conditions (no volume increase). An approximation of the volume increase of the hydrogel through the pores was made by using a microscope (by focusing through a pore on two points of the hydrogel, border and middle, height differences could be determined) and gave a value of ~4% of the total hydrogel volume. Together with the volume increase due to deflection of the pressure sensor membrane 3% (at $1x10^5$ Pa) gives the total maximum volume increase of the hydrogel which is ~7%. Preliminary free swelling experiments showed that the volume of this type of hydrogel at pH9 can increase with ~125% at pH6. When this is compared to the 7% volume increase in the device the hydrogel can be considered as under isochoric conditions.

In order to investigate the influence of the percentage of titratable groups on the pressure generation two devices were prepared, respectively with a hydrogel consisting of 2.5% DMAEMA and 97.5% HEMA, and a hydrogel with 5.0% DMAEMA and 95.0% HEMA. Both hydrogels had a thickness of approximately 15 µm (due to a relative thick glue layer between cover and pressure sensor the hydrogel thickness is larger than 10 µm). To

hydrate the hydrogel, both devices were placed in a pH9 buffer with an ionic strength of 100 mM. At this pH all amine groups (pK_a = 8) are dissociated and no pH-dependent pressure is generated. The only pressure that is generated is caused by hydration of the gel due to the hydrophilic nature of the polymer network. This initial pressure was set to zero. A pressure generation was provoked by placing both devices in a pH6 buffer of the same ionic strength and a buffer capacity of 100 mM. Figure 4.3 shows the result of the experiment.

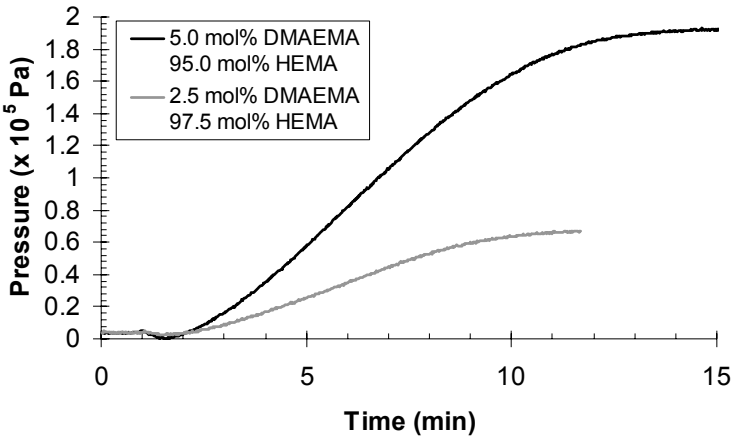

Figure 4.3. The pressures generated by two different hydrogels (thickness 15 µm) vs. time as a result of a pH change from 9 to 6 (ionic strength is 100 mM).

The hydrogel with 2.5% DMAEMA generated a pressure of 0.67×10^5 Pa in 12 minutes. The 5% DMAEMA hydrogel generated a pressure of 1.92×10^5 Pa in 15 minutes. Due to a higher concentration of protonated groups, the ion concentration in the second hydrogel is higher, generating an increased ionic pressure contribution Π_{ion}.

In figure 4.3 it can also be seen that the time constants of both devices are different. The device containing the hydrogel with less amine groups, meaning a lower value for β_{gel}, takes less time to reach equilibrium pressure compared to the other device, as predicted by equation 4.9.

The characteristic buffer-mediated diffusion-reaction time constant (equation 4.9) predicts that the buffer solution capacity has influence on the response time. Therefore experiments were performed to examine this for the enclosed hydrogels. A device was prepared with a 10 µm thick hydrogel that was synthesized of 5% DMAEMA and 95% HEMA. Various buffers were used with buffer capacities of 10, 25 and 50 mM. The ionic

strength of all buffers was fixed at 100 mM. First the device was placed in a pH 9 buffer of 10, 25 or 50 mM to hydrate the gel. This pressure was set to zero and the buffer was exchanged by a pH 6 buffer with the same buffer concentration to provoke pH-dependent pressure generation. The process was repeated for all buffer concentrations and the results are shown in figure 4.4.

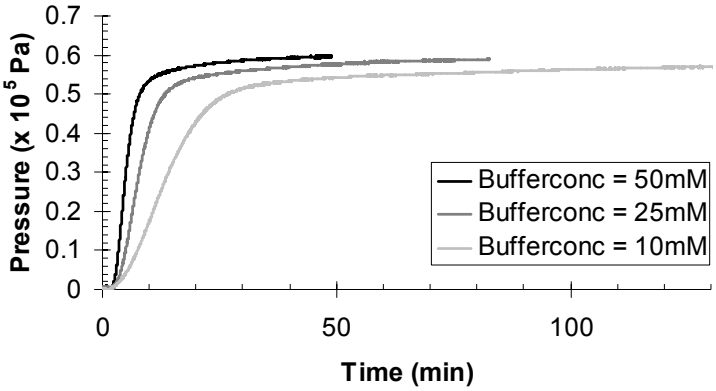

Figure 4.4. The pressure generated by a hydrogel (5% DMAEMA / 95% HEMA, thickness 10 µm) as a result of a pH change from 9 to 6 using buffers with different concentrations but same ionic strength (100 mM).

The figure shows that there is a decrease in response time when higher buffer concentrations are used, as predicted by equation 4.9. The rate of pressure generation is dominated by the diffusion-limited reaction of H^+ ions with titratable groups as in the case of free swelling[18]. With a higher buffer solution capacity, more H^+ ions are available from the nearby buffer molecules and the protonation will occur at higher speed. As a consequence the pressure is generated faster, as observed with this experiment. At lower buffer solution capacity the H^+ ions must be supplied from slow-diffusing buffer molecules from further away.

Furthermore, it is observed that the final pressures are slightly different for the three measurements. More pressure is generated with increased buffer solution capacity despite the fact that the ionic strength and pH were kept constant. Perhaps some affinity exists between the hydrogel network and the used buffer material BIS-TRIS. When the protonated form of BIS-TRIS (present in the solution at pH 6) would be retained in the polymer structure, the ionic pressure contribution would increase, leading to more pressure generation. Another explanation could

be that the protonation of the amine groups is inhibited by the pressure on the polymer network and that higher buffer capacities are better capable to protonate.

The influence of the buffer solution capacity β_{sol} on the pressure decrease was also investigated for three different values of β_{sol}. After the hydrogel was equilibrated at pH6, the device was placed in a pH 9 buffer with the same buffer concentration, and the pressure decreases was measured (see figure 4.5). As predicted by equation 4.9, a decrease in buffer concentration leads to a decrease in rate of pressure decrease.

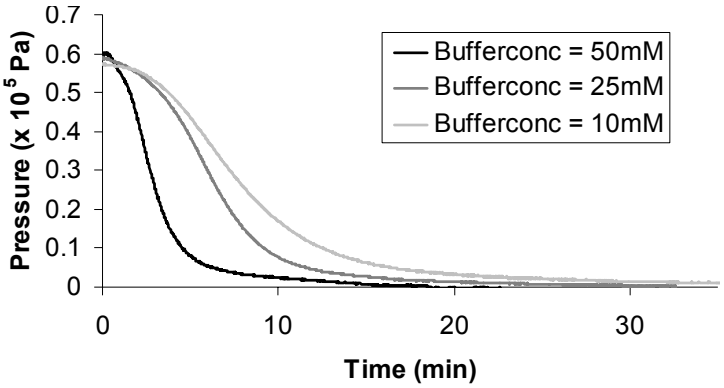

Figure 4.5. Pressure response of a hydrogel (5% DMAEMA / 95% HEMA, thickness 10 µm) as a result of pH change from 6 to 9 of buffers with different concentrations but same ionic strength (50 mM).

In a following experiment the influence of ionic strength is examined. Buffers were prepared with an ionic strength varying between 10 and 100 mM. The pH of all buffers was fixed to 6 and the buffer concentration to 10 mM. The same device (5% DMAEMA and 95% HEMA) was used as in the previous experiment. The device was placed in all buffers, starting at the ionic strength of 100 mM and ending at 10 mM. In figure 4.6 the recorded pressures versus time are shown.

The figure demonstrates an interesting characteristic response to a change in ionic strength of the external solution. Initially, there is a large rapid pressure increase, followed by a small slow pressure decrease. This typical response is the result of two coinciding counteracting processes. The pressure increase is due to the increase of osmotic pressure Π_{ion} caused by the decrease in ionic strength of external solution. For this, no additional

ions have to diffuse into the hydrogel and therefore the pressure increase is, apparently, a fast process.

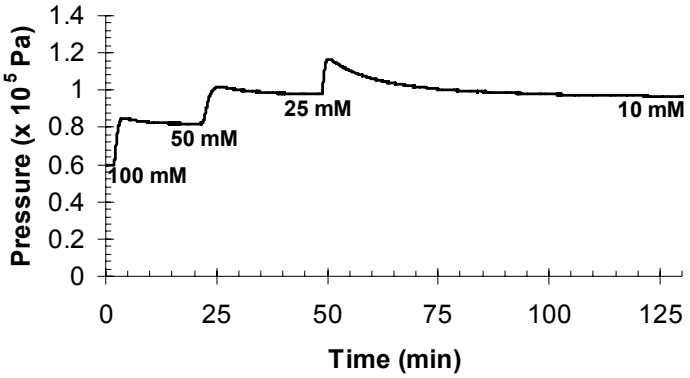

Figure 4.6. The pressure generation of a hydrogel (thickness 10 µm) consisting of 5% DMAEMA and 95% HEMA in pH6 buffers with varying ionic strengths.

At the same time another process takes place. This is due to the Donnan effect. Based on the measurement results shown in figure 4.6 and by using equations 4.5-4.8, the Donnan ratio, fixed charge concentration, Donnan potential and pH_{gel} can be calculated, shown in table 4.1.

Table 4.1. Calculated values for the Donnan ratio, fixed charge concentration, Donnan potential and pH_{gel}.

Ionic Strength c_{sol} (mM)	Measured pressure Π_{ion} (Pa)	Donnan ratio r_D	Fixed charge concentration c_x (mM)	Donnan potential ϕ_D (mV)	pH_{gel}
100	0.60x10^5	1.99	74.4	17.3	6.3
50	0.82x10^5	3.02	75.4	27.9	6.5
25	0.98x10^5	5.02	60.3	40.7	6.7
10	0.97x10^5	9.86	48.8	57.8	7.0

In the table it is demonstrated that the pH inside the hydrogel increases with decreasing ionic strength due to a higher Donnan potential. Subsequently, the fixed charge concentration in the hydrogel decreases and ions diffuse out of the hydrogel. This is a slow process as shown with the preceding experiments, and also observed for free chemically induced

swelling[18]. Due to the small deprotonation of the gel, the osmotic pressure Π_{ion} decreases somewhat which explains the pressure decrease of the characteristic response in figure 4.6. Furthermore, it is shown that the ionic strength decrease from 25 mM to 10 mM results in a slower pressure decrease than for the other cases. According to table 4.1, the pH increase is larger for this ionic strength change compared to the others. This might explain the slower pressure decrease.

The pH-dependent pressure generation was also examined. Another device was used containing a hydrogel composed from 5% DMAEMA and 95% DMAEMA. The device was subsequently placed in a range of buffer solutions of 50 mM (ionic strength 50 mM) and the pressure was measured, always waiting for equilibrium to be reached (see fig. 4.7).

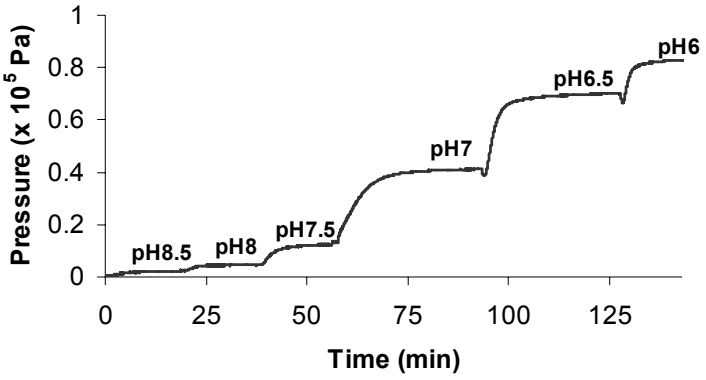

Figure 4.7. Pressure generation vs. time of a 5% DMAEMA 95% HEMA hydrogel (thickness 10 µm) in response to pH steps of 0.5 of the external solution with an ionic strength of 50 mM.

With each pH decrease, the hydrogel generated an additional pressure. Around pH 7 the largest pressure step is generated which moreover took the largest time to reach equilibrium. Thus, the degree of protonation is the largest around this pH. Apparently, the pK_a of the hydrogel is 7. In our case the pK_a can be described as the pH at which half of the maximum pressure is generated. The pK_a can better be extrapolated when the pressure is plotted versus pH, as shown in figure 4.8.

It was expected was that the pK_a of the hydrogel would be around 8 since this is also the pK_a of the monomer DMAEMA. Since the pH inside the hydrogel is not the same as the pH of the external solution, the pressure versus pH_{gel} is also plotted in figure 4.8. Here, the pK_a is approximately 7.3.

As expected, the intrinsic pK_a is higher. Nevertheless, this pK_a is still below 8. It is possible that the pressure exerted on the hydrogel inhibits protonation and consequently decreases the pK_a, which is also observed by others[20].

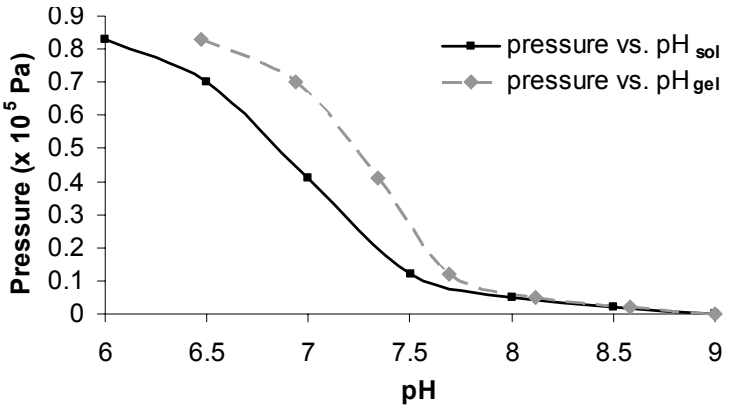

Figure 4.8. Measured equilibrium pressures of a 5% DMAEMA 95% HEMA hydrogel (thickness 10 µm) vs. pH of the external solution pH_{sol} and the calculated pH inside the hydrogel pH_{gel}.

4.5 Conclusions

A method has been demonstrated to study the behavior of hydrogels under isochoric conditions. The device, which has dimensions in the micrometer scale, has the advantage that measurements can be carried out reasonably fast for typical hydrogel characterization and in real-time with the use of a small pressure sensor. It is shown that a pH-sensitive hydrogel can generate pressure under isochoric conditions, dependent on the amount of ionizable groups, the ionic strength of the external solution and the pH. Higher pressures can be obtained by incorporating more titratable groups or by decreasing the ionic strength of the surrounding solution. Furthermore it is concluded that the rate of pressure generation depends on the amount of ionizable groups and the buffer concentration. Equilibrium pressures are reached faster when less ionizable groups are incorporated or when higher buffer concentrations are used. Due to the Donnan effect, the pH inside the hydrogel is not equal to the external solution pH. Experimental data show that the pK_a of the hydrogel is shifted down. It is believed that the presented method is a simple and fast manner to

characterize the static and dynamic stimulus-dependent behavior of hydrogels, and may be used for studying the behavior of other gels such as immuno-sensitive or glucose-sensitive hydrogels. The found characteristics are very useful for designing the hydrogel-based CO_2 sensor. It is now known in which pH range the hydrogel responds and at which ionic strength the response is at its maximum. With these parameters the sensor with highest resolution can be designed. Furthermore it is now known that the response time of the sensor can be influenced by varying the amount of protonable groups.

A restriction of the presented characterization method is the presence of pores in the cover. After all, the pores allow hydrogel to swell through which undermines the definition of isochoric. Nevertheless, the pores are absolutely necessary to exchange ions with the environment.

At the moment two types of covers have been explored: one with 50 µm pores and 20 µm spacing, which did not work (due to the too small spacing), and another with 50 µm pores and 50 µm spacing, with which all experiments were performed. In order to optimize the characterization method more research must be performed on the influence of the cover parameters. Possibilities are changing the pore shape, e.g., rectangular or round pores, or varying the dimensions of the pores and spacing.

4.6 References

1 B. Johnson, D. Beebe, and W. Crone, *Materials Science and Engineering C* 2004, **24**, 575.

2 T. Tanaka and D. Fillmore, *J. Chem. Phys.* 1979, **70**, 1214.

3 English, T. Tanaka, and E. Edelman, *J. Chem. Phys.* 1997, **107**, 1645.

4 J. Rička and T. Tanaka, *Macromolecules* 1984, **17**, 2916.

5 H. Brønsted, J. Kopeček, Polyelectrolyte Gels, Vol. 480, Chap. 17, p.285, 1992, American Chemical Society, Washington DC, USA,.

6 Hüther, B. Schäfer, X. Xu, and G. Maurer, *Phys. Chem. Chem. Phys.* 2002. **2**, 835.

7 O. Okay and S. Sariisik, *European Polymer Journal* 200, **36**, 393.

8 S. De, N. Aluru, B. Johnson, W. Crone, D. Beebe, and J. Moore, *J. of microelectromechanical systems* 2002, **11**, 544.

9 Z. Strong, A. Wang, and C. McConaghy, *Biomedical Microdevices* 2002, **4**, 97.

10 M. Lei, A. Baldi, T. Pan, Y. Gu, R. Siegel, and B. Ziaie, *17th IEEE International Conference on Micro Electro Mechanical Systems* 2004, Maastricht, The Netherlands.

11 S. Herber, W. Olthuis, and P. Bergveld, *Sens. Actuators B* 2003, **91**, 378.

12 S. Herber, W. Olthuis, P. Bergveld, and A. van den Berg, *Sens. Actuators B* 2004, Accepted.

13 H. Linden, S. Herber, W. Olthuis, and P. Bergveld, *The Analyst* 2003, **128**, 325.

14 P. Flory, Principles of polymer chemistry, Chap. XIII, 1953, Cornell University Press, Ithica, USA.

15 F. Horkay, I. Tasaki, and P. Basser, *Biomacromolecules* 2000, **1**, 84.

16 O. Okay and S. Durmaz, *Polymer* 2002, **43**, 1215.

17 F. Donnan, *Chem. Rev.* 1924, **1**, 73.

18 P. Grimshaw, J. Nussbaum, A. Grodzinsky, and M. Yarmush, *J. Chem. Phys.* 1990, **93**, 4462.

19 M. Lesho and N. Sheppard, *Polymer Gels and Networks* 1997, **5**, 502.

20 W. Seitz, private communications.

Chapter 5

Design Parameters and Optimization of the Sensor

The hydrogel-based carbon dioxide sensor consists of a pressure transducer, porous cover, gas permeable membrane, pH-sensitive hydrogel and an electrolyte. The pressure transducer is acquired from Sentron Europe BV. Two designs for the porous cover are presented with a different hydrogel cavity depth (5 and 10 µm). The gas permeable membrane consists of a polydimethylsiloxane layer mounted to a silicon substrate which functions as a carrier. The pH-sensitive hydrogel is synthesized of 2–hydroxyethyl methacrylate and dimethylaminoethyl methacrylate. The optimal electrolyte for maximum sensor resolution consists of 17 mM sodium bicarbonate and 8 mM sodium chloride, and has an ionic strength of 25 mM. The dimensions of the final sensor are 2.92x0.95x0.70 mm^3.

5.1 Introduction

In this chapter, specifications of the pressure sensor and the design parameters of the porous cover (two designs) and gas permeable membrane are presented. A composition drawing of the final sensor is also shown. Furthermore, the exact composition of the pH-sensitive hydrogel and electrolyte is motivated.

5.2 The pressure sensor

The main application of the hydrogel-based sensor is measuring Pco_2 inside the stomach. Therefore, the dimensions of the total sensor, and thus of the pressure sensor, should be small enough to be mounted in a catheter with a maximum diameter of 3 mm. A catheter with this thickness can easily be inserted in the stomach through the nose.

Sentron Europe BV (Roden, the Netherlands) is a company which manufactures pressure sensors (type P4.2, E2303771) especially designed for catheter-tip applications. Because of its small dimensions, this pressure sensor will be used for the hydrogel-based sensor. The pressure sensor exploits the Wheatstone bridge principle. The bridge is made of four piezoresistors located on the four edges of the sensor membrane, close to the edges where the stress is largest when pressure is applied to the center of the membrane. Two of the resistors are positioned parallel to the direction of the stress, and their resistance increases with pressure. The other two resistors are oriented perpendicular to the direction of the stress, and their resistance decreases with pressure. The output of this type of configuration is a differential voltage signal, which is maximal dependent on the applied pressure. In figure 5.1 a schematic diagram of the electrical circuit of the pressure sensor and in figure 5.2 a schematic drawing of the sensor are shown. Detailed information of the chip is given in table 5.1.

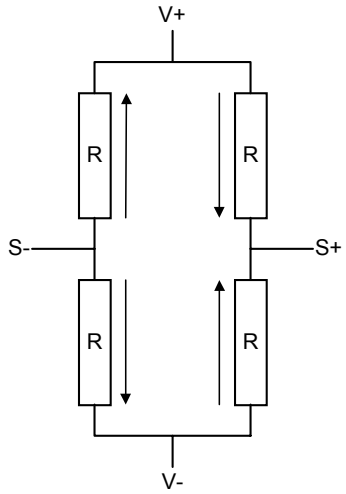

Figure 5.1. Schematic diagram of the electrical circuit of the pressure sensor P4.2 (figure courtesy of Sentron Europe BV, Roden, the Netherlands).

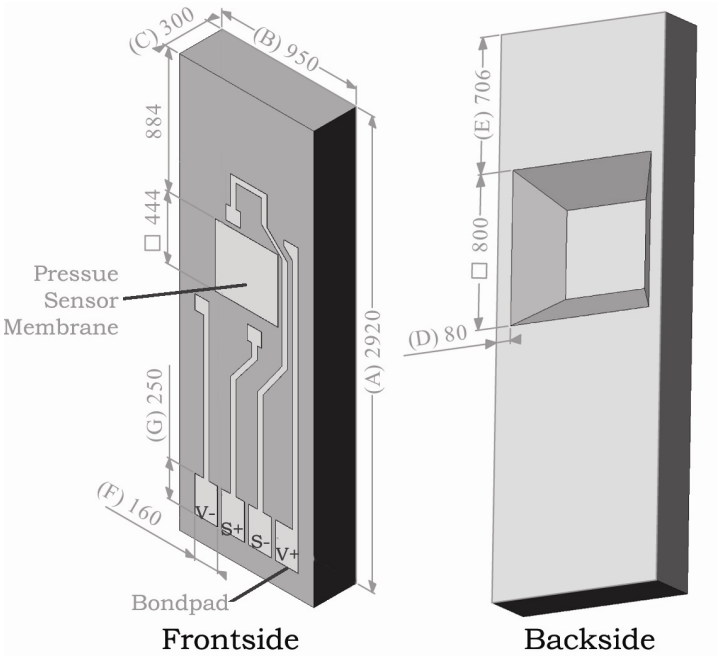

Figure 5.2. Schematic drawing of the front and back side of pressure sensor P4.2.

Table 5.1. Mechanical, electrical and general specifications of pressure sensor P4.2.

Mechanical specifications			
Parameter	Value	Tolerance	Unit
1. Length (A):	2,92	± 0,05	mm
2. Width (B):	0,95	± 0,05	mm
3. Height (C):	0,30	± 0,05	mm
4. Distance between cavity and long side (D):	≥0,030		mm
5. Distance between cavity and short side (E):	0,71	± 0,05	mm
6. Bondpad-Width (F):	0,16	± 0,01	mm
7. Bondpad-Length (G):	0,25	± 0,01	mm
Electrical Specifications			
Parameter	Min.	Max.	Unit
1. Pressure sensitivity (Gain):	8,0	15,0	µV/V/mmHg
2. Linearity of the pressure signals (-300 +300 mmHg, influenced by encapsulation)	-2	+2	% FS
3. Offset (dark):	-12,5	12,5	mV
4. Linearity Offset to Working Voltage:		50	µV
5. Bridge resistance:	3,9	5,0	kΩ
6. Light sensitivity:	-0,1	0,1	mV
7. TCO	-2,3	2,3	mmHg/K
8. Working Voltage (V+ - V-)	-3	+5	V
General specifications			
Parameter	Min.	Max.	Unit
1. Range of pressure	-300	+1000	mmHg
2. Operating temperature	-20	+120	°C
3. Max temperature (≤ 5 minutes)		250	°C

5.3 Design of the porous cover

Two types of covers were designed, realized and tested. The most important difference between both designs is the hydrogel cavity depth. In this section both designs are described in detail.

5.3.1 Design I

A schematic representation of cover design I is given in figure 5.3. The dimensions of the porous cover are based on the dimensions of the pressure sensor. The pressure sensor has a length of 2920 µm and a width of 950 µm (figure 5.2). The porous cover has the same width of 950 µm and a length of 2360 µm. This length is shorter than the length of the pressure sensor in order to keep the bondpads free for wirebonding. The thickness of the porous cover is the same as the thickness of the wafer, i.e., 510 µm.

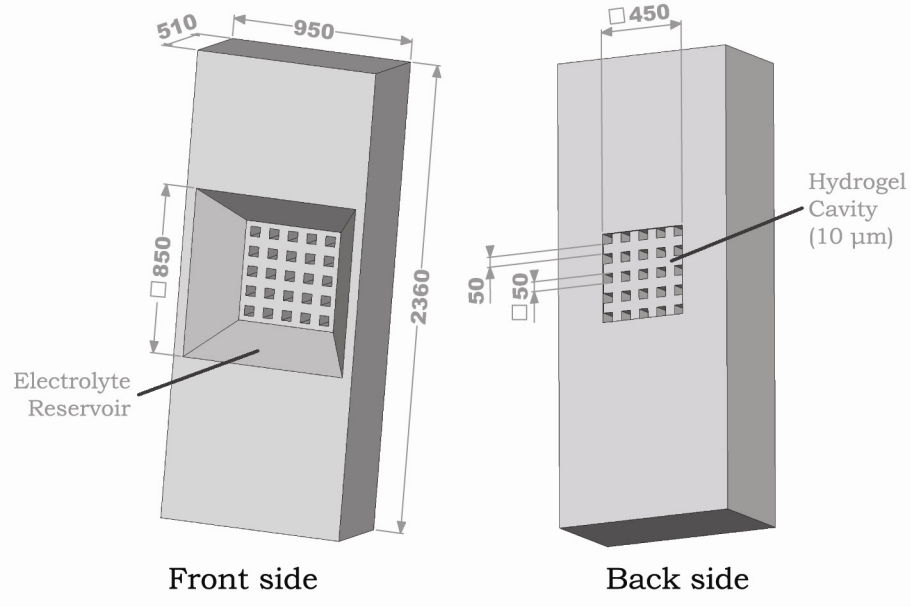

Figure 5.3. Schematic representation of the front and back side of cover design I.

The cover contains a reservoir on the front side for the electrolyte. This reservoir is etched by KOH which is an anisotropic chemical process with a positive tapering (wider in the front and narrower in the back) of 54.74°, as schematically shown in figure 5.3 and 5.4. The etch window on the front side of the reservoir is 850x850 µm^2 and the depth is 300 µm.

The pores of the cover have the dimension of 50x50 μm^2. This dimension was chosen with respect to the experience obtained in previous research[1,2] and the applied etching technique: reactive ion etching (see chapter 6). The limitation of this etching technique is the depth to which can be etched with respect to the etch window dimensions, due to a positive tapering effect with an aspect ratio of approximately 1:10. This is schematically shown in the cross-section of the cover in figure 5.4. Etching a through-hole (from the back side) of 200 μm deep requires an etch window of at least 40x40 μm^2. Therefore, an etch window of 50x50 μm^2 was chosen with a spacing of 50 μm between the pores.

The hydrogel cavity is located on the back side of the cover and has approximately the same length and width as the pressure sensor membrane, namely 450x450 μm^2. The depth of the cavity is 10 μm (reactive ion etching from the back side) as will be the hydrogel thickness.

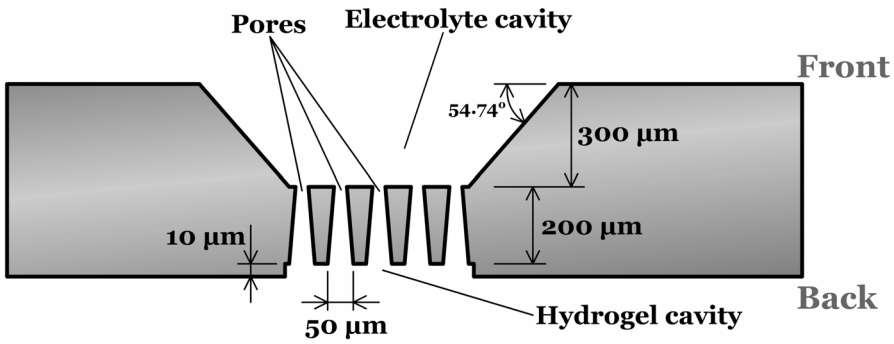

Figure 5.4. Cross-section of cover design I. The pores are etched with reactive ion etching, resulting in a wider opening at the etch side than in the depth.

5.3.2 Design II

Cover design II is based on experimental results obtained with design I (chapter 7) and takes into account the mounting of a gas permeable membrane on the front side. A schematic representation of cover design II is given in figure 5.5. The length, 2920 μm, and width, 950 μm, of cover design II are identical to design I. The thickness, however, is decreased to 200 μm and the hydrogel cavity to 5 μm. The pores are 50x50 μm^2 with a depth of 100 μm and spacing of also 50 μm.

The electrolyte reservoir is made with reactive ion etching instead of KOH etching in order to eliminate the large positive tapering. This way, the

etch window at the front side of the cover is smaller (500x500 µm^3) and, consequently, there is a wider border to mount the gas permeable membrane to. The depth of the reservoir is 95 µm.

Furthermore, cover design II has a filling channel for the electrolyte with a length of 800 µm and a width of 50 µm, as shown in figure 5.5. The channel is etched in the same step as the electrolyte reservoir and has the same depth of 95 µm.

There is also a glue barrier located at the back side of the cover as extra precaution. When the cover is mounted to the pressure sensor, the glue barrier prevents the glue to enter the hydrogel cavity by capillary forces.

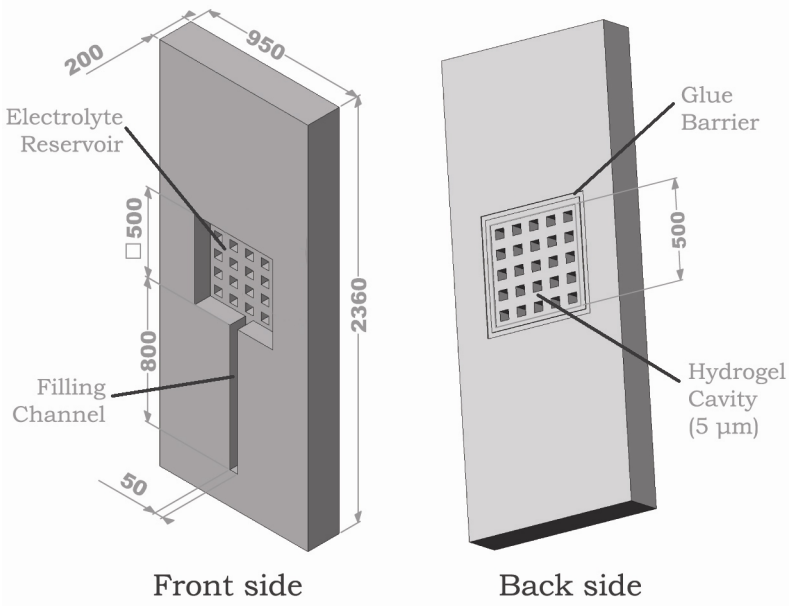

Figure 5.5. Schematic representation of the front and back side of cover design II.

5.3.3 Stiffness of the porous cover

The stiffness of the cover membrane (the part with the pores) should exceed the stiffness of the pressure sensor membrane many times in order to prevent pressure loss due to deflection of the porous cover membrane by the hydrogel. The thickness of the pressure sensor membrane varies between 6.9 and 8.0 µm. The membrane thickness of cover design I and II are 200 and 100 µm, respectively. To compare the pressure sensor membrane with the cover membrane, the deflection of both is calculated when a pressure of 1x10^5 Pa is applied.

For small deflections of a membrane, such as the pressure sensor membrane, the dimensionless linear pressure/deflection membrane formula can be used,

$$Q = K_b \cdot W_0 , \tag{5.1}$$

where Q is the dimensionless load parameter, K_b the bending stiffness and W_0 the center deflection relative to the membrane thickness[3]. For a square membrane with small deflection the bending stiffness, K_b, is described by

$$K_b = \frac{49.6}{12(1-\nu^2)}, \tag{5.2}$$

with υ the Poisson constant. For silicon the Poisson constant is 0.29. With equation 5.2 can be calculated that the bending stiffness, K_b, is 4.51. For the load, Q, the following dimensionless formula can be used,

$$Q = \frac{pa^4}{Eh^4}, \tag{5.3}$$

where p is the pressure (Pa), a the half length of a side (m), E the modulus of elasticity (N/m^2) and h the membrane thickness (m). For silicon, the modulus of elasticity is 122x10^9 N/m^2. For a pressure of 1x10^5 Pa, a membrane thickness of 6.9x10^{-6} m and 222x10^{-6} m as half length, the load, Q, is calculated to be 0.878. By substituting the calculated values for Q and K_b into equation 5.1, the relative center deflection, W_0, can be determined, i.e., 0.195. The absolute center deflection (m), ω_0, is described by

$$w_0 = W_0 \cdot h , \tag{5.4}$$

with h the membrane thickness (m). With a membrane thickness of 6.9x10^{-6} m (Sentron pressure sensor), it can be calculated that the deflection of the membrane center is 1.3 μm.

Using the equations 5.1-5.4 to calculate the center deflection of the cover membrane (without pores) results in 4.7x10^{-10} and 5.8x10^{-11} m for a thickness of 100 and 200 μm, respectively, at a pressure of 1x10^5 Pa.

However, the equations may not be used for the cover since it contains pores.

The deflection of the porous cover membrane can be calculated with ANSYS software. ANSYS is a general purpose finite element modeling package for numerically solving a wide variety of mechanical problems. These problems include static/dynamic structural analysis (both linear and non-linear), heat transfer and fluid problems, as well as acoustic and electro-magnetic problems. An ANSYS simulation was performed of the deflection of a 200 µm thick porous cover membrane as a result of a pressure of $1x10^5$ Pa. According to the simulation, the center deflection is $8.1x10^{-5}$ µm. A similar ANSYS simulation for a membrane thickness of 100 µm shows a membrane deflection of only $7.5x10^{-4}$ µm. Figure 5.6 shows a schematic representation of a (exaggerated) deflection of the 100 µm thick membrane.

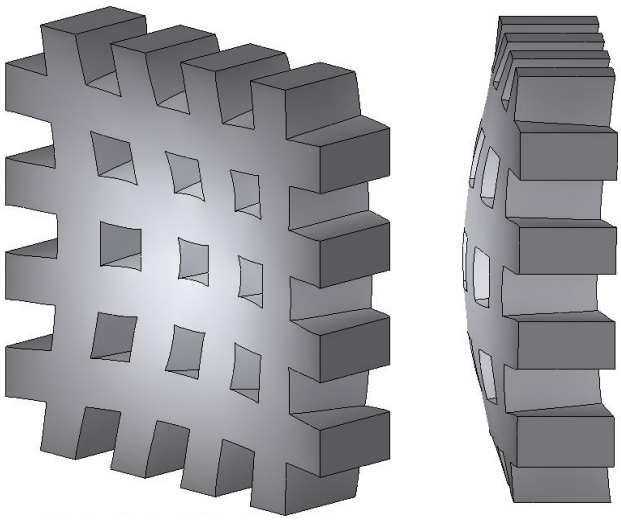

Figure 5.6. Schematic representation of the deflection of a 100 µm thick membrane. Note that the deflection is exaggerated.

By comparing the center deflection values of the ANSYS simulation with the values achieved by using equations 5.1-5.4, the conclusion can be drawn that the pores clearly weaken the cover membrane resulting in more deflection.

It can be calculated that the percentage deflection of the 200 µm thick cover membrane relative to the pressure sensor membrane deflection is merely $6.2x10^{-3}$ %. For the 100 µm thick cover membrane the percentage

is 57.7×10^{-3} %. Since the percentages are very low for both thicknesses, it can be assumed that the deflection of the porous cover membrane by hydrogel pressure generation will not give any noticeable pressure loss.

5.4 Design of the gas permeable membrane and carrier

A schematic representation of the gas permeable membrane can be found in figure 5.7. It consists of a polydimethylsiloxane (PDMS) gas permeable layer mounted on a silicon substrate which functions as membrane carrier. PDMS is the world's most common silicone and its applications range from contact lenses and medical devices to elastomers, caulking, lubricating oils and heat resistant tiles. A property of PDMS is that it is highly permeable for carbon dioxide gas[4]. Furthermore, PDMS is very flexible, which has the advantage that no pressure change will occur in the electrolyte reservoir when the pressure sensor membrane deflects due to the hydrogel.

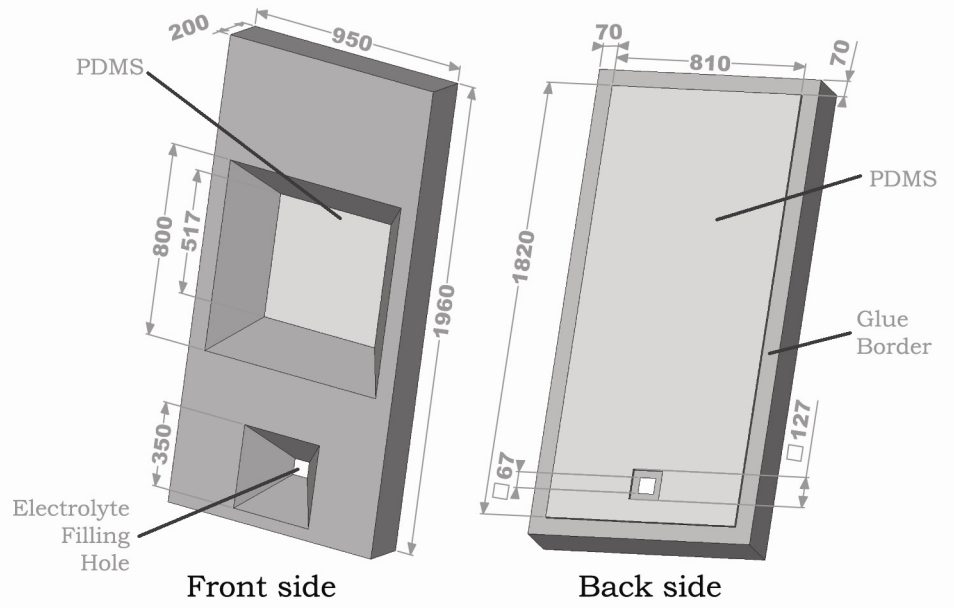

Figure 5.7. Schematic representation of the front and back side of the gas permeable membrane and carrier.

The width of the membrane carrier is the same as the width of the pressure sensor and porous cover, namely 950 µm. The length is 1960 µm and the thickness 200 µm. The PDMS membrane has a thickness of 14 µm.

In figure 5.7 is also shown that there is a glue border at the back side of the gas permeable membrane carrier. The gas permeable membrane carrier can easily be mounted on the porous cover by capillary gluing at this border. Furthermore, the gas permeable membrane carrier contains an electrolyte filling hole. After mounting the gas permeable membrane carrier to the porous cover, the filling hole is located above the filling channel in the cover. Through the filling hole and the filling channel in the cover the electrolyte reservoir and pores can be filled. Detailed information on the filling technique can be found in chapter 6 of this thesis.

5.5 Final sensor composition drawing

In figure 5.8 a composition drawing is shown of the complete sensor with cover design II. The drawing consists of an exploded view of all single parts and an assembly of the complete sensor. The dimensions of the complete sensor will be 2.92x0.95x0.70 mm^3.

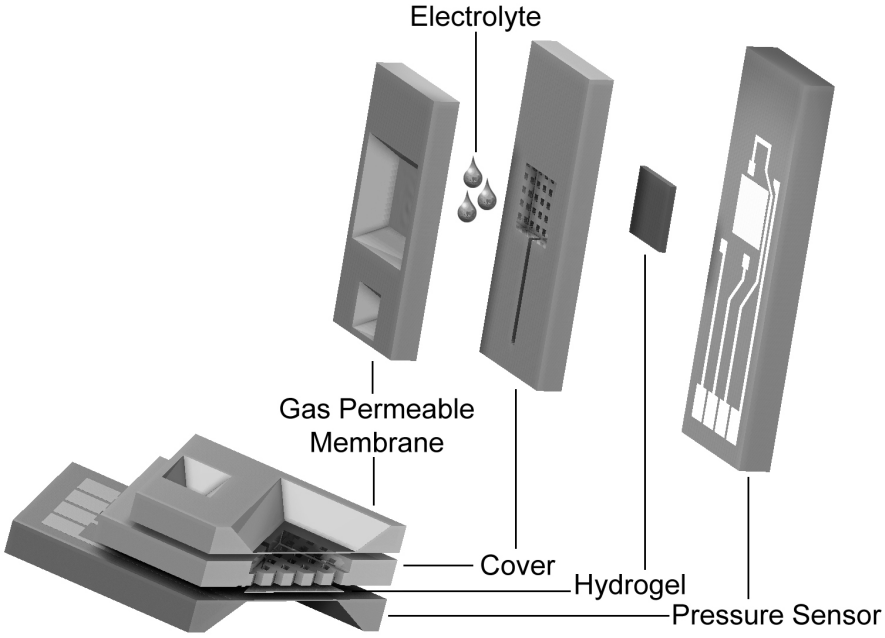

Figure 5.8. Exploded view of all parts and assembly drawing of the final hydrogel-based CO_2 sensor.

5.6 The pH-sensitive hydrogel

In chapter 4 the study of pressure generation of hydrogels under isochoric conditions has been presented. In this study the pH-dependent pressure generation is investigated of 2–hydroxyethyl methacrylate-co-dimethylaminoethyl methacrylate (HEMA-co-DMAEMA) hydrogel. It was found that this hydrogel has an apparent pK_a of 7, which makes this type of hydrogel suitable for Pco_2 measurements in the medically interesting range (see chapter 3) and is the reason that it is applied in the final sensor.

It is possible to decrease the density of the HEMA-co-DMAEMA network which has the advantage that there is an increased diffusion rate of ions and, consequently, faster swelling/pressure generation equilibrium. By adding solvent to the prehydrogel solution, the HEMA and DMAEMA monomers are more diluted. After polymerization the solvent can be flushed away, leaving a network with decreased density. Beside water, ethyleneglycol is used in the solvent which prevents crack formation after polymerization[5]. In chapter 6, detailed information can be found on the composition, synthesis and polymerization of this hydrogel.

5.7 Electrolyte composition

In this section, motivation is given for the used bicarbonate concentration and the chosen ionic strength of the electrolyte.

5.7.1 Bicarbonate concentration

By adding sodium bicarbonate to the electrolyte the pH response to Pco_2 changes is doubled, as described in chapter 3. In that chapter a plot is shown which represents the relation between Pco_2 and pH for various bicarbonate concentrations. With use of this plot, again shown in figure 5.9 with some modifications, the optimal sodium bicarbonate solution is determined.

The apparent pK_a of HEMA-co-DMAEMA hydrogel is 7. This means that the pressure, generated by the hydrogel, varies with pH changes in the pH range around 7. To measure the Pco_2 within the medical range (3-20 kPa), the corresponding pH range should overlap pH 7. The optimal bicarbonate concentration is found when the middle of the medical pH

range is exactly 7. In figure 5.9 is shown that a bicarbonate concentration of 17 mM is the determined optimum for the electrolyte. The medical pH range at this concentration is from 6.6 to 7.4 with 7.0 as middle.

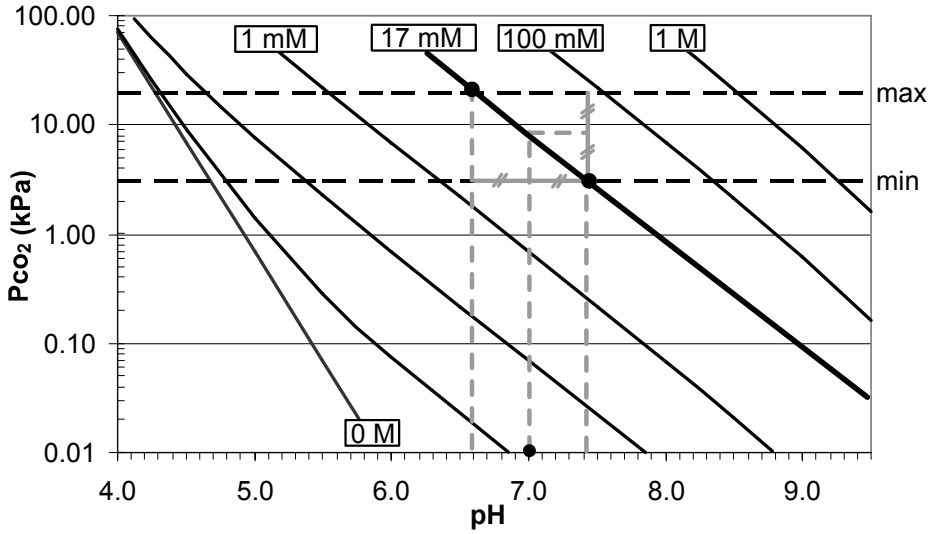

Figure 5.9. The relation between Pco_2 and pH for various bicarbonate concentrations.

5.7.2 Ionic strength

During the study of pressure generation of a pH-sensitive hydrogel under isochoric condition the influence of ionic strength was also examined, as described in chapter 4. The pressure generation was measured for various ionic strengths at pH 6. At this pH the hydrogel is completely ionized and will consequently generate the maximum pressure. In figure 5.10 the result of this experiment is shown again.

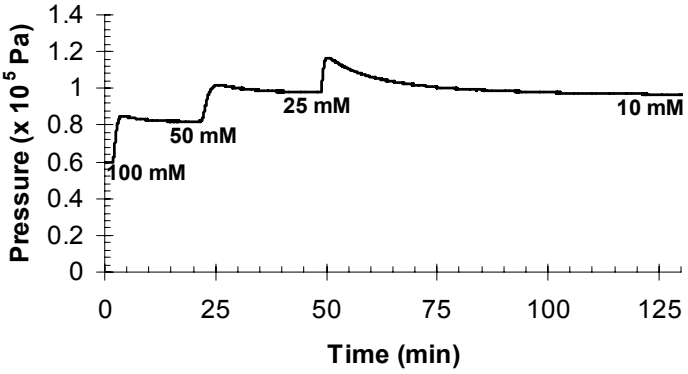

Figure 5.10. The pressure generation of a hydrogel (thickness 10 µm) consisting of 5% DMAEMA and 95% HEMA in pH6 buffers with varying ionic strengths.

As can be seen in the figure, the maximum pressure is generated at an ionic strength of 25 mM. Therefore, to obtain the highest sensor resolution, the ionic strength of the electrolyte should also be set to 25 mM. The ionic strength of a solution is defined by

$$I = 1/2 \sum \left(z_i^2 \cdot c_i \right), \tag{5.5}$$

where c_i is the concentration and z_i the valence factor of the i^{th} ion. The electrolyte already contains 17 mM sodium bicarbonate (fully dissociated). With equation 5.5 can be calculated that this gives the solution an ionic strength of 17 mM. To increase the ionic strength to 25 mM, sodium chloride is used. By means of equation 5.5 it is determined that 8 mM sodium chloride should be added.

5.8 References

1 S. Herber, W. Olthuis, P. Bergveld, *Sens. Actuators B* 2003, **91**, 378.

2 S. Herber, W. Olthuis, P. Bergveld, A. Van den berg, *Sens. Actuators B* 2004, **103**, 284.

3 R. E. Oosterbroek, Modeling, Design and Realization of microfluidic components (thesis) 1999, University of Twente, Enschede, The Netherlands.

4 B. van der Schoot, P. Bergveld, *Analytica Chimica Acta* 1984, **166**, 93.

5 J. Bomer, private communications.

Chapter 6

Technological Aspects of the Sensor

In this chapter, the realization of two types of porous covers and a gas permeable membrane carrier is shown. These sensor parts are made of silicon with standard cleanroom techniques. The gas permeable membrane is made of polydimethylsiloxane attached to the carrier. The sensor is manually assembled by means of a special tool and consists of aligning and gluing the sensor parts, and filling the sensor with the hydrogel and electrolyte. The recipes for the prehydrogel solution and electrolyte are also given in this chapter. Furthermore, the measurement setup is described, which basically consists of two mass flow controllers to accurately mix carbon dioxide and nitrogen, and a temperature controller.

6.1 Introduction

In this chapter, a detailed description of how and with which techniques the hydrogel-based CO_2 sensor is manufactured. This includes recipes of the hydrogel and the electrolyte, and the brand names of used materials. Furthermore, the measurement conditions are described.

6.2 The electrolyte

The electrolyte consists of water, sodium bicarbonate and sodium chloride. The deionized (DI) water was supplied by a Millipore Elix 3 water purification system. The sodium bicarbonate was obtained from Merck (Darmstadt, Germany) and an amount of 17 mM was added to the DI water. Furthermore, 8 mM sodium chloride was added, also acquired from Merck. This composition is an optimum as discussed in chapter 5.

6.3 The prehydrogel solution

The prehydrogel solution consists of a solvent and monomers, which are polymerized by ultraviolet light after the sensor is filled with the solution. The prehydrogel solution was prepared with 2–hydroxyethyl methacrylate (HEMA) and dimethylaminoethyl methacrylate (DMAEMA) with a molar ratio of 95/5, and solvent containing ethylene glycol (Merck) and water in equimolar amounts. The HEMA and DMAEMA were obtained from Acros Organics (Geel, Belgium). To the total mole amount of monomers (HEMA&DMAEMA) 1.5 mol% cross-linker tertraethylene glycol dimethacrylate (TEGDMA) and 3 mol% photoinitiator 2,2-dimethoxy-2-phenylacetophenone (DMPAP) were added. The TEGDMA was acquired from Fluka (Buchs, Switzerland) and the DMPAP from Aldrich (Steinheim, Germany). The mole ratio between the monomers and the solvent was 1 to 1.2. The obtained solution was transparent and colorless, and was stored at a temperature of 4 ^{o}C in dark in order to prevent early polymerization due to UV in daylight.

6.4 The porous cover

Two designs for the porous cover were made. The first design, design I, originates from an early stage of the research project. The second design, design II, is based on experience obtained with design I and takes the mounting of the gas permeable membrane carrier into account. In this section, the realization of both designs is presented.

6.4.1 Design I

The porous cover consists of an electrolyte reservoir, hydrogel cavity and pores. In figure 6.1 the process scheme is shown.

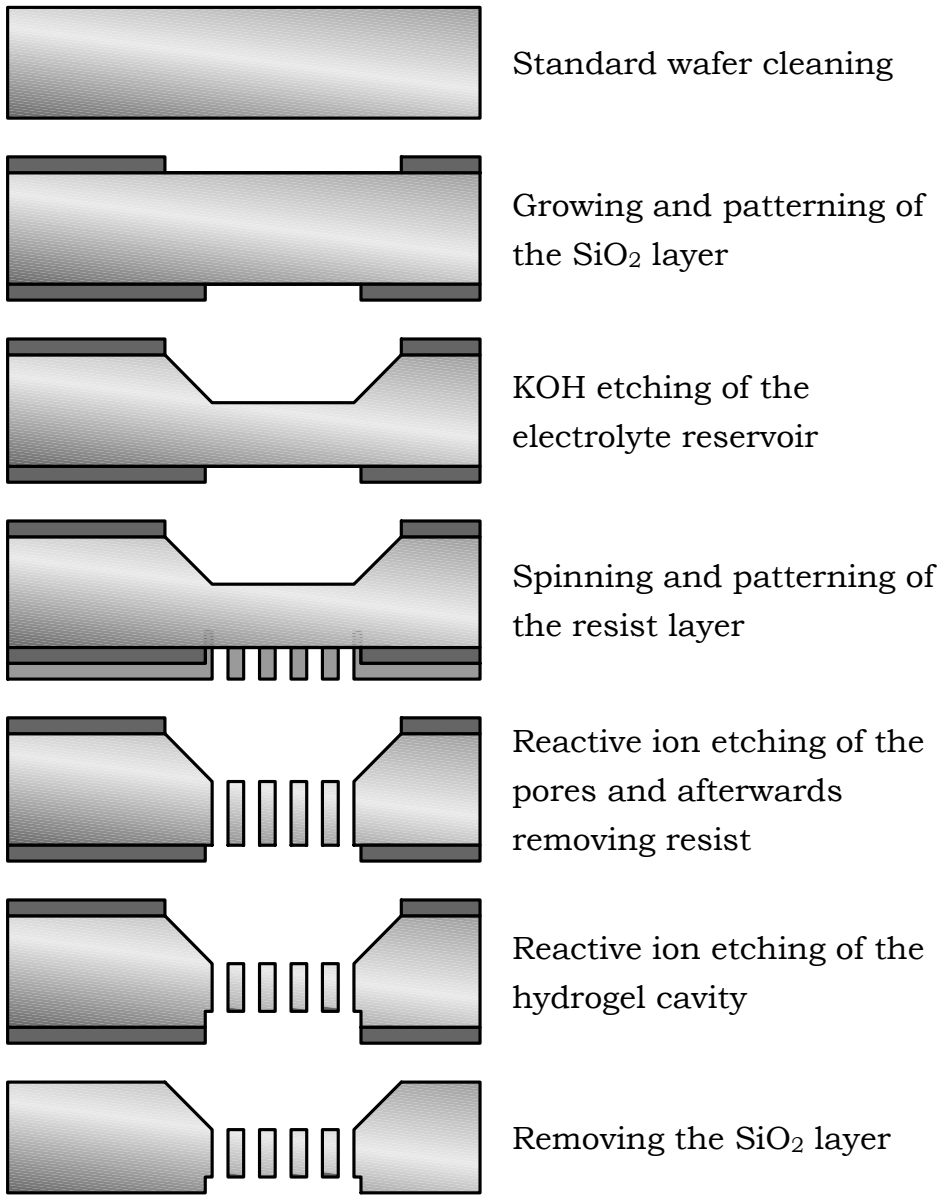

Figure 6.1. Process scheme of porous cover design I.
Note that the figures are not drawn on scale and in proportions.

The covers were fabricated using a 100 mm p-type <100> 510 µm thick single polished silicon wafer (Okmetic, Finland). First, the wafer was oxidized in a wet oxidation furnace for 5 hours to grow a 1.5 µm thick SiO_2

layer. The oxide was patterned on both sides of the wafer using buffered hydrofluoric acid (BHF) to create etch-masks for the bicarbonate reservoir (unpolished side) and hydrogel cavity (polished side). Subsequently, the bicarbonate reservoir was chemically etched with KOH to a depth of 300 µm, while the wafer was in a special holder to protect the other side from etching. Next, resist was spun on the opposite of the wafer (polished side) covering the hydrogel cavity etch-mask. The resist was patterned to form the holes etch-mask and reactive ion etching (RIE) was used to etch the 210 µm deep holes. Finally, the resist was removed to reveal the underlying SiO_2 etch-mask for the hydrogel cavity which was then etched by RIE to a depth of 10 µm. The last step was dicing of the wafer (Disco DAD-321) resulting in the covers with outer dimensions of 2.36x0.95x0.51 mm^3. In figure 6.2 a photo is shown of the manufactured cover.

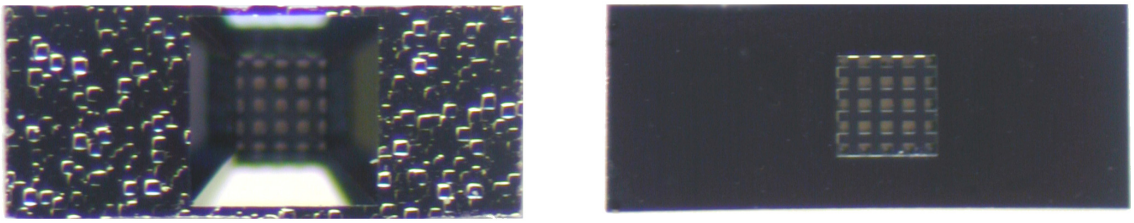

Top view (unpolished side) *Bottom view (polished side)*

Figure 6.2. Photo of the manufactured porous cover design I. Note that the unpolished side can clearly be distinguished from the polished side.

6.4.2 Design II

The design II covers were fabricated on a 100 mm p-type <100> 510 µm thick single polished silicon wafer (Okmetic, Finland). The inner circular area (diameter of 8 cm) of the wafer was etched from the (unpolished) backside to a thickness of 200 µm by KOH while using a nitride etch-mask. The outer ring maintained its original thickness of 510 µm to preserve wafer integrity. Note that only the outer ring contains the nitride layer and that the rest of the processing takes place on the inner circular area. The further process scheme is quite similar to that of design I and is schematically shown in figure 6.3.

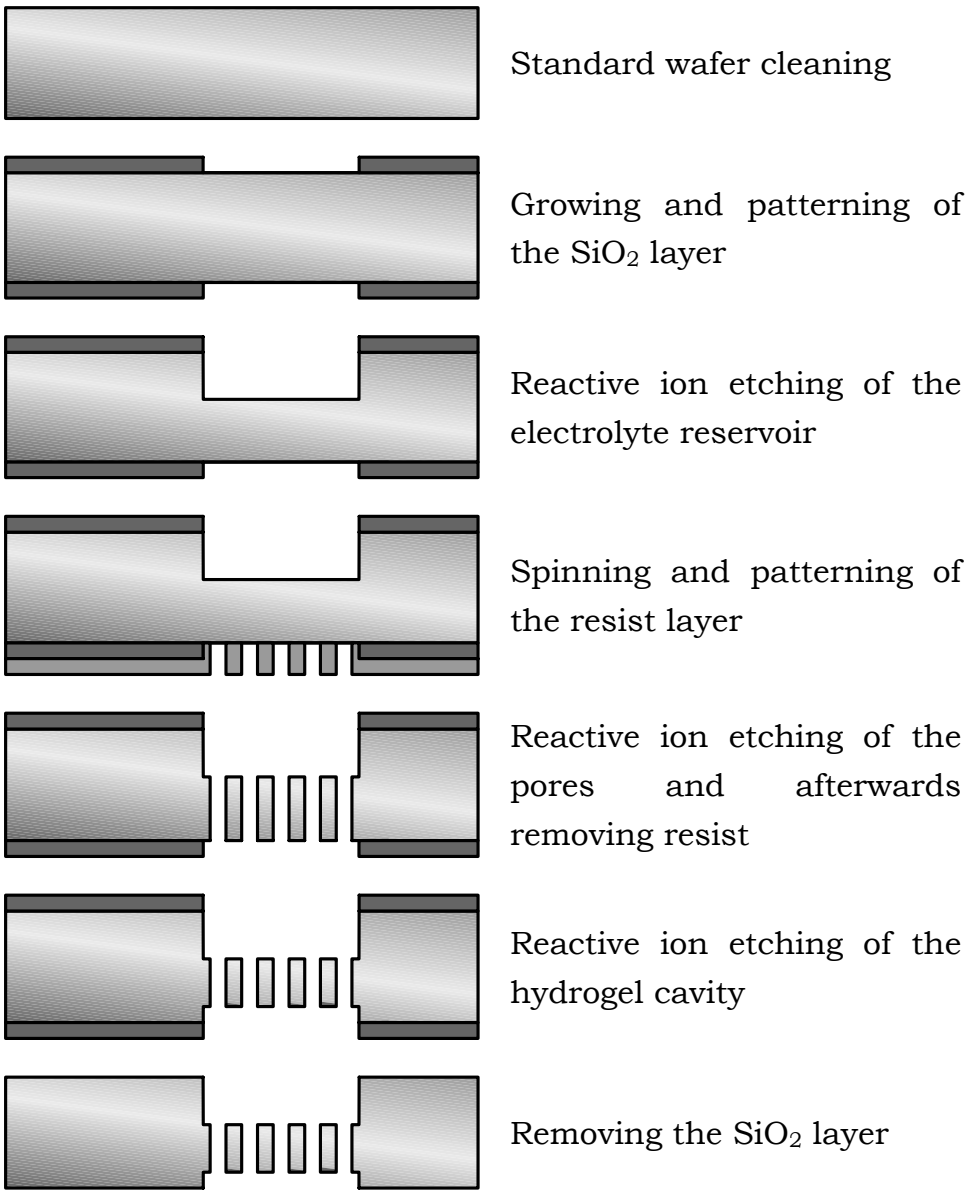

Figure 6.3. Process scheme of porous cover design II after the KOH etching to decrease the wafer thickness. Note that the figures are not drawn on scale and in proportions.

The wafer was oxidized in a wet oxidation furnace for 5 hours to grow a 1.5 μm thick SiO_2 layer. The oxide was patterned on both sides of the wafer using BHF to create etch-masks for the bicarbonate reservoir (unpolished side) and hydrogel cavity (polished side). Subsequently, the bicarbonate reservoir and electrolyte filling channel (not shown) were etched with reactive ion etching to a depth of 95 μm. Next, resist was spun on the opposite of the wafer (polished side) covering the hydrogel cavity etch-mask.

The resist was patterned to form the holes etch-mask and reactive ion etching (RIE) was used to etch the 105 µm deep holes. Finally, the resist was removed to reveal the underlying etch-mask for the hydrogel cavity which was subsequently etched by RIE to a depth of 5 µm.

The last step was dicing of the wafer resulting in the covers with outer dimensions of 2.36x0.95x0.20 mm^3. In figure 6.4 a photo is shown of the porous cover design II.

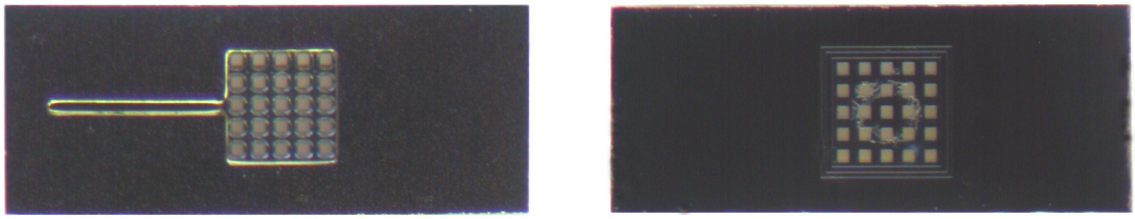

Top view (unpolished side) *Bottom view (polished side)*

Figure 6.4. Photo of the manufactured porous cover design II. Note that the unpolished side can not be distinguished from the polished side due to the KOH etching of the inner circular area of the wafer, resulting in a smooth surface.

6.5 The gas permeable membrane and carrier

For the manufacturing of the gas permeable membranes, research was performed to find the relation between the thickness of spun polydimethylsiloxane (PDMS) and the spin speed. The PDMS was acquired from Dow Corning (Sylgard 184) and consists of an elastomer and a curing agent, which were mixed with a weight ratio of 10 to 1. The mixing was performed with a Sarstedt CM-9 at 2000 rpm for 15 minutes. Afterwards, enclosed air bubbles were removed by placing the mixture in a vacuum clock for another 15 minutes. The PDMS was spun on wafers at various spin speeds for 20 seconds. The PDMS was cured in a furnace at 80 ^oC for 1.5 hours. With a Dektak surface profiler (Veeco 8) the thickness of the PDMS for each spin speed was measured. The result is shown in figure 6.5.

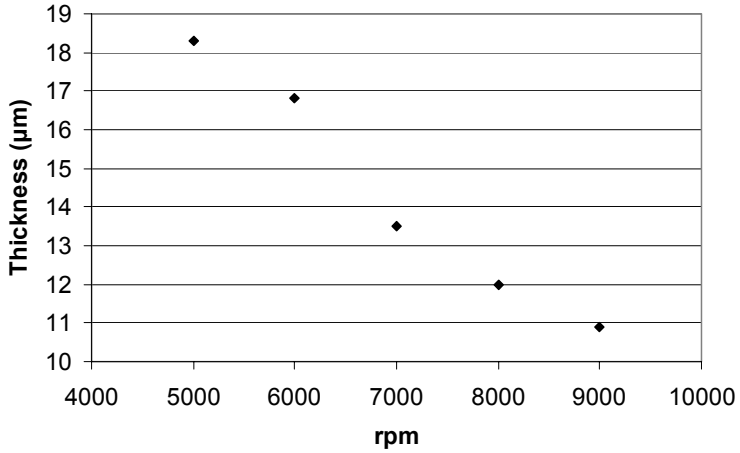

Figure 6.5. Plot of thickness of spun PDMS versus the spin speed in rounds per minute (rpm). Spin time was 20 seconds.

The PDMS thickness varies between 11 and 18 µm for spin speeds from 9000 to 5000 rpm. A thickness of 14 µm was chosen for the gas permeable membrane which corresponds with a spin speed of 7000 RPM.

In figure 6.6 the process scheme for manufacturing the carrier and gas permeable membrane is shown. The membranes were fabricated on a 100 mm p-type <100> 510 µm thick single polished silicon wafer (Okmetic, Finland). The wafer thickness was decreased to 200 µm (from the unpolished side) with the same technique as described for cover design II. The wafer was subsequently oxidized in a wet oxidation furnace for 5 hours to grow a 1.5 µm thick SiO_2 layer. Then the oxide layer was patterned using lithography and BHF to form the etch-mask for the holes at the (unpolished) side which was also used to reduce the wafer thickness. The holes were etched with KOH, however, not completely, but until a layer of approximately 10 µm silicon remained. This was done in order to preserve a surface to spin the PDMS on. On this surface is the SiO_2 layer with which PDMS has a good adhesion. Note that when the PDMS is spun first and afterwards the holes are KOH etched, the PDMS releases due to underetching.

PDMS was made by mixing elastomer and curing agent with a weight ratio of 10 to 1. The PDMS was immediately spun on the wafer at 7000 rpm for 20 seconds. Subsequently, the PDMS was cured by placing the wafer for 90 minutes on a hotplate with a temperature of 100 ^{o}C. Then, aluminum was sputtered and patterned to form an etch-mask for the PDMS. RIE was used to etch the PDMS selectively after which the aluminum was removed

using aluminum etch (H_3PO_4, HNO_3, $C_2H_4O_2$, H_2O with a volume ratio of 16:1:1:2, respectively). Next, RIE was used to remove the remaining 10 µm silicon layer at the bottom of the holes and BHF to remove the SiO_2 layer in order to open the holes and free the PDMS membranes.

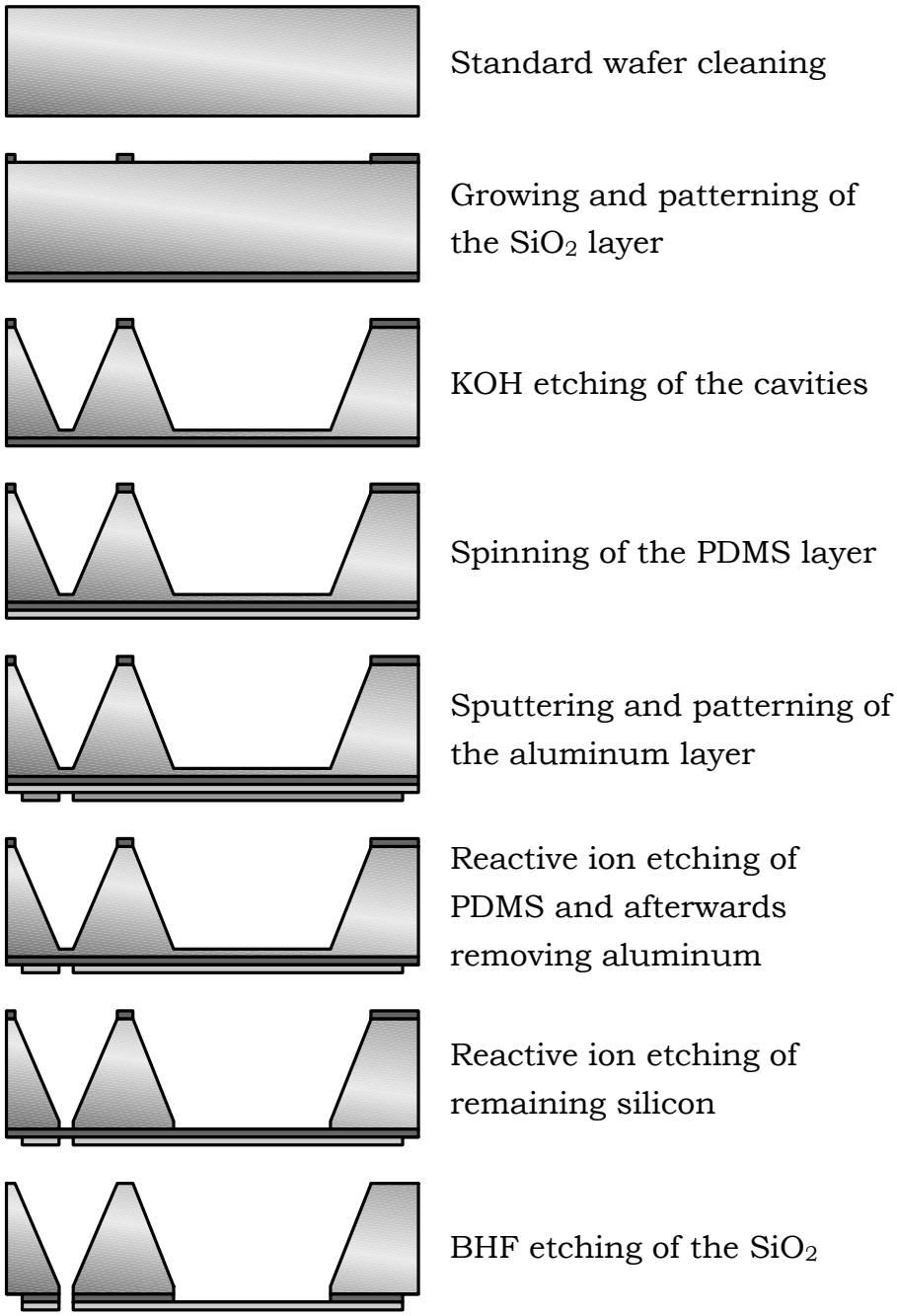

Figure 6.6. Process scheme of the manufacturing of the gas permeable membrane and carrier. Note that the figures are not drawn on scale and in proportions.

The thickness of the PDMS was measured with a Dektak surface profiler. The result is shown in figure 6.7. The thickness of the PDMS layer varies between 12 and 14 µm. Compared to previous Dektak measurements (not shown), the surface of the PDMS layer is much rougher. This is probably caused by the sputtering and afterwards removing of the aluminum etch-mask. This is, however, not a problem for the final application.

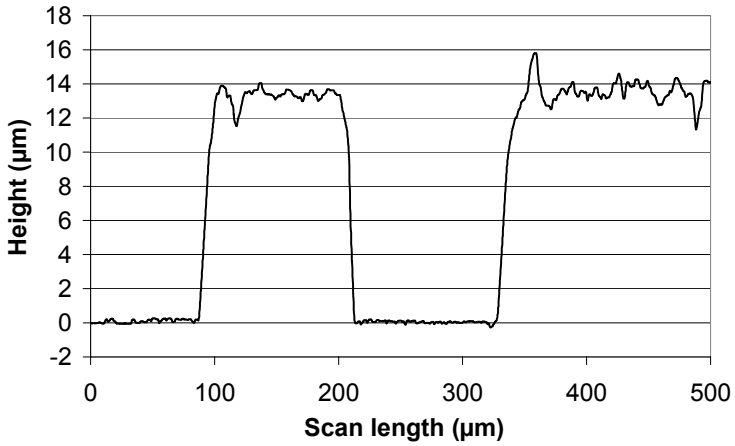

Figure 6.7. Dektak surface profile of the PDMS layer.

The last step in the processing was dicing the wafer, which resulted in the membrane chips with outer dimensions of 1.96x0.95x0.20 mm^3. A photo of the manufactured membranes is shown in figure 6.8.

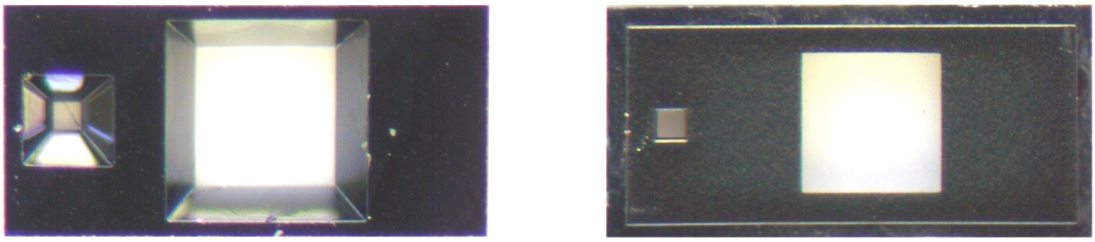

Top view Bottom view

Figure 6.8. Photo of the gas permeable membrane on carrier.

6.6 The sensor assembly

In this section a description of the pretreatment of the pressure sensor and the porous cover is given. Subsequently, detailed information is provided on

the assembly of the porous cover on the pressure sensor and the attachment of the gas permeable membrane carrier on top.

6.6.1 Pretreatment

Before the sensor parts can be assembled, some pretreatment has to be performed. First, the pressure sensor is glued to a PCB stick with cyanoacrylate. The back side of the pressure sensor membrane is precisely aligned above a 0.5 mm hole, which is drilled through the PCB. This way the atmospheric pressure is the reference pressure of the sensor. The bondpads of the pressure sensor are connected to the PCB leads by means of wirebonding.

The pretreatment procedure of the porous cover is schematically shown in figure 6.9. Note that the process scheme is focused on cover design II since this design includes the mounting of the gas permeable membrane carrier on top, shown later in this chapter. The process schemes for cover design I are, however, exactly the same as for design II.

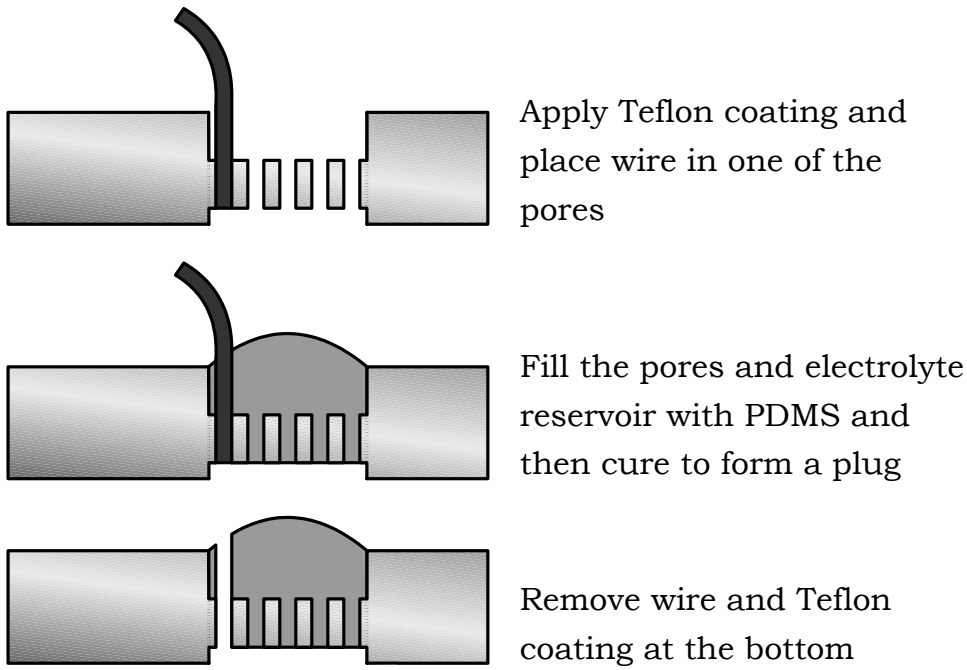

Figure 6.9. Process scheme of the pretreatment of the porous cover. Note that the figures are not drawn on scale and in proportions.

The first step is to apply a Teflon coating on the porous cover which allows easy removal of the PDMS plug to be applied in a later stadium. The Teflon coating was applied by immersing the cover in Fluorinert™ electronic liquid (FC40, 3M) and afterwards drying for 15 minutes in a furnace at 60 °C. Then a thin metal wire (diameter ~45 µm) is placed in one of the pores of the cover. Subsequently, the electrolyte reservoir and the pores are filled with PDMS by means of vacuum while holding a special mould in the hydrogel cavity. Separate trial and error tests showed that this method gives the best result. By curing of the PDMS in a furnace at 80 °C for 90 minutes, a plug is formed. Next, the wire is removed, leaving a small channel for filling the hydrogel cavity with the prehydrogel solution after combining the cover with the pressure sensor. Furthermore, the Teflon layer at the bottom of the cover is removed by means of a tissue and subsequently immersing in isopropanol for five minutes in an ultrasonic bath. Otherwise, the adhesion of the cover to the pressure sensor is of low quality.

For the further assembly process a special tool was manufactured. With this tool it is possible to align and clamp the parts of the sensor in order to apply glue. The special tool is shown in figure 6.10. The tool consists of two parallel metal wires, stretched by a tension spring between two screws. Furthermore, there is a clamp to hold the PCB stick.

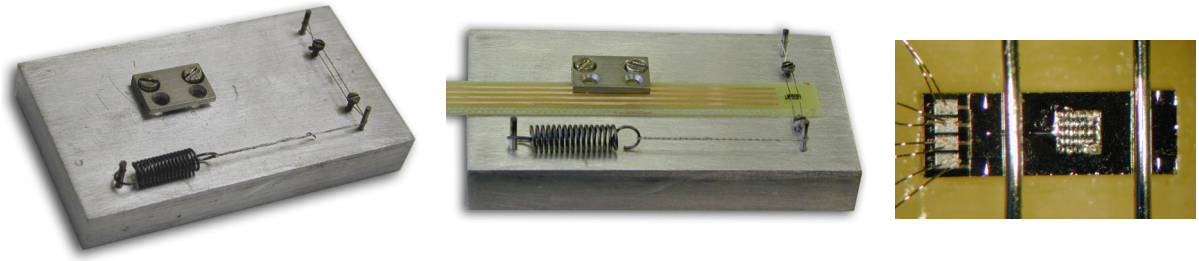

The holder | The holder with PCB stick | Close-up

Figure 6.10. Pictures of the special tool used for the sensor assembly.

The distance between the wires is determined by the thickness of the screws (M1.6). By turning the screws, the two wires can be moved up or down. This way, they can press sensor parts on each other with an adjustable force, while maintaining good accessibility to the sides of the parts. For an alignment of two parts, the wires are first moved downward

until the wires exert a small force on the stacked parts. The alignment can then take place by means of a microscope and a pair of tweezers. Subsequently, the wires are moved downward further until they exert a sufficiently large force to fix the aligned parts tightly. Then, the glue is applied at the sides of the stack which will also flow between the two parts by capillary forces.

6.6.2 Assembly of the porous cover to the pressure sensor on PCB stick

The next part in the sensor assembly is attaching the porous cover to the pressure sensor. This process scheme is shown in figure 6.11. Note that the PCB stick is not shown in the further process scheme.

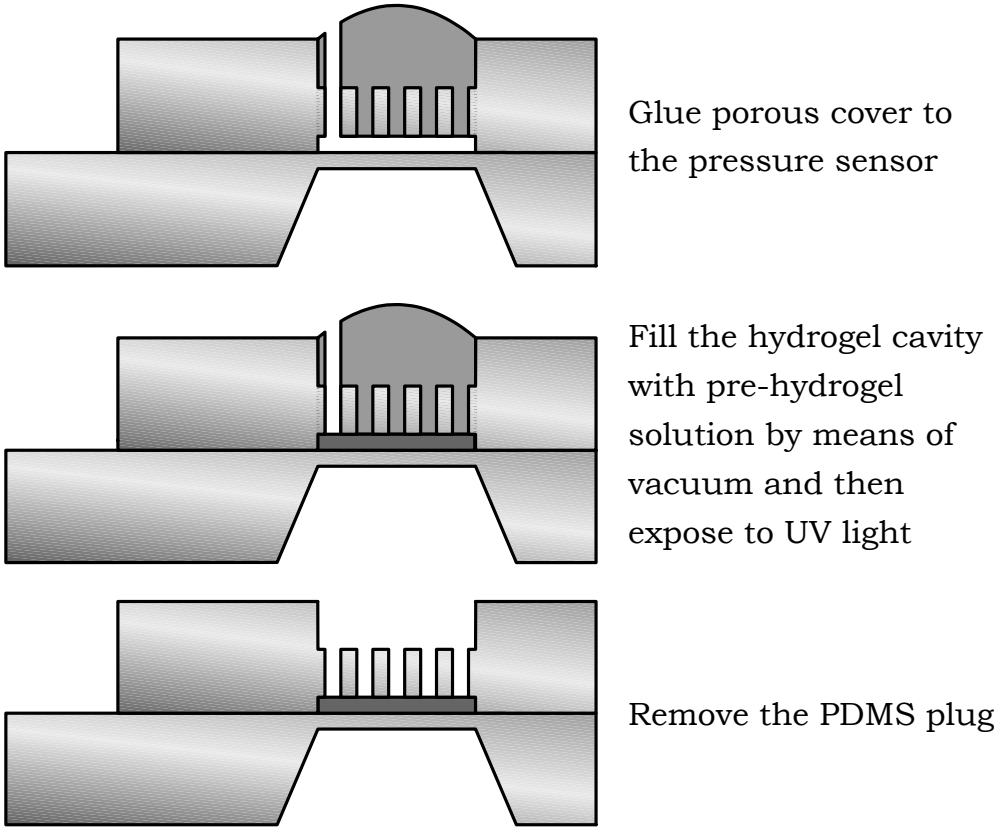

Figure 6.11. Process scheme of the assembly of the porous cover to the pressure sensor. Note that the figures are not drawn on scale and in proportions.

With use of the special tool, the porous cover is aligned on the pressure sensor and subsequently fixed tightly. Then both parts are

definitely bonded together with two-component epoxy glue Hysol (EE0079/HD0070, Loctite). The glue is applied to all sides and will flow between both parts by capillary forces. The Hysol is cured by placing the clamped parts including the special tool in a furnace at 60 ^{o}C for one hour. Then, a droplet of prehydrogel solution is placed on the PDMS plug, covering the filling channel. The device is placed in a vacuum clock and vacuum is applied. This way, the air in the hydrogel cavity is removed. By increasing the pressure in the vacuum clock back to the atmospheric pressure, the prehydrogel solution is forced to flow into the hydrogel cavity. The remaining prehydrogel solution on top of the device is removed and the device is exposed to UV light (ELC-403 light curing system, The Electro-Lite Corporation) for 2 minutes. The UV absorption of PDMS is very low and free-radical copolymerization reaction of the prehydrogel solution is started. Due to the non-collimated light source, scattering by the PDMS plug and reflection by the pressure sensor membrane, the UV light is highly diffuse and also reaches under the pore matrix of the silicon cover. Therefore, the resulting hydrogel reaches a homogeneous composition. After the hydrogel formation the PDMS plug is removed to open the sensor.

A scanning electrode microscope (SEM) photo of the PDMS plug (obtained from a design I cover) is shown in figure 6.12. As can be seen, the plug has exactly the inverse shape of the electrolyte reservoir and pores.

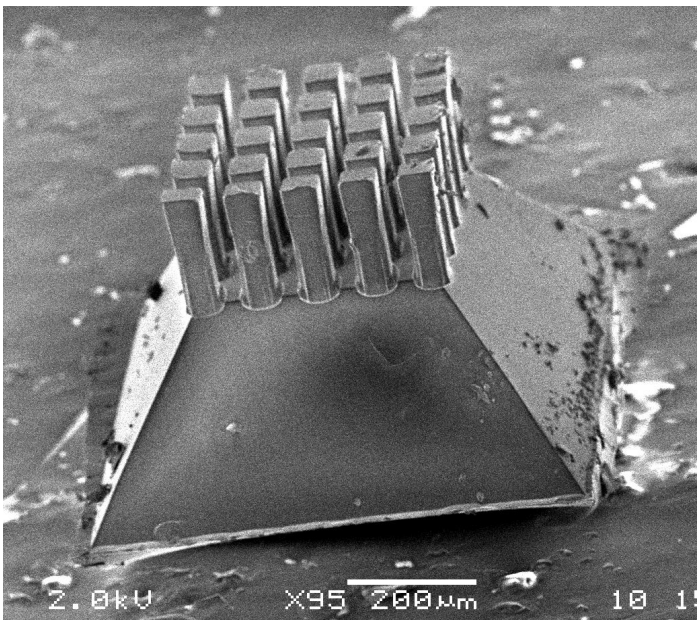

Figure 6.12. SEM photo of the PDMS plug, removed from a design I cover.

Before the gas permeable membrane carrier is mounted, the semi-finished sensor can be tested in order to verify that the polymerization of the hydrogel was successful. The tests include hydration of the hydrogel and a CO_2 measurement cycle.

The advantage of the presented *in situ* polymerization is that the hydrogel has the exact dimensions of the hydrogel cavity. When a beforehand prepared hydrogel disk is placed between the porous cover and pressure sensor, the chance of a functioning device is low. In this case there are two critical dimensions, i.e. the depth of the hydrogel cavity and the thickness of the hydrogel disk. These can differ in such a way that the chance of a successful sensor is dramatically decreased (all attempts to create a sensor with this method failed). With the *in situ* polymerization the critical dimensions are eliminated.

6.6.3 Assembly of the gas permeable membrane carrier to the stack of porous cover and pressure sensor

When the semi-finished sensor is tested successfully (the hydrogel is hydrated properly and there is CO_2 response), the gas permeable membrane carrier can be mounted on top. The process scheme is shown in figure 6.13.

With the special tool, the gas permeable membrane carrier is aligned and fixed on the stack of cover and pressure sensor. Two-component epoxy Hysol is used to glue them together. After curing the Hysol, the device is placed in a beaker with the electrolyte. By means of vacuum, the electrolyte reservoir and the pores are filled with the electrolyte through the filling hole of the gas permeable membrane carrier and through the filling channel of the porous cover. The last step is closing the filling hole with a droplet of one-component silicone glue (Dow Corning, 734). The glue cures under humid conditions and also when floating on water. The device is placed two hours in a closed box with a relative humidity of 100% to cure the silicone glue and simultaneously prevent the electrolyte to evaporate through the gas permeable membrane. After the curing, the sensor is ready for use.

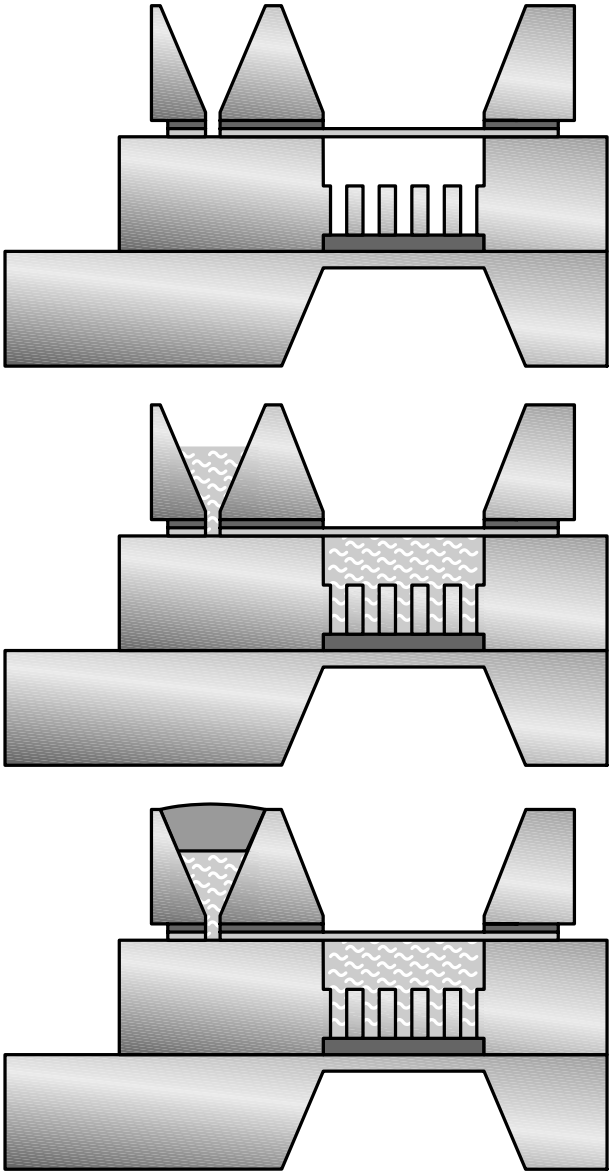

Figure 6.13. Process scheme of the assembly of the gas permeable membrane carrier to the stack of porous cover and pressure sensor. Note that the figures are not drawn on scale and in proportions.

A photo of the assembled sensor is shown in figure 6.14. The outer dimensions are 2.92x0.95x0.70 mm^3. The storage of the sensor should always occur under a relative humidity of 100% or in water in order to prevent evaporation of the electrolyte through the gas permeable membrane.

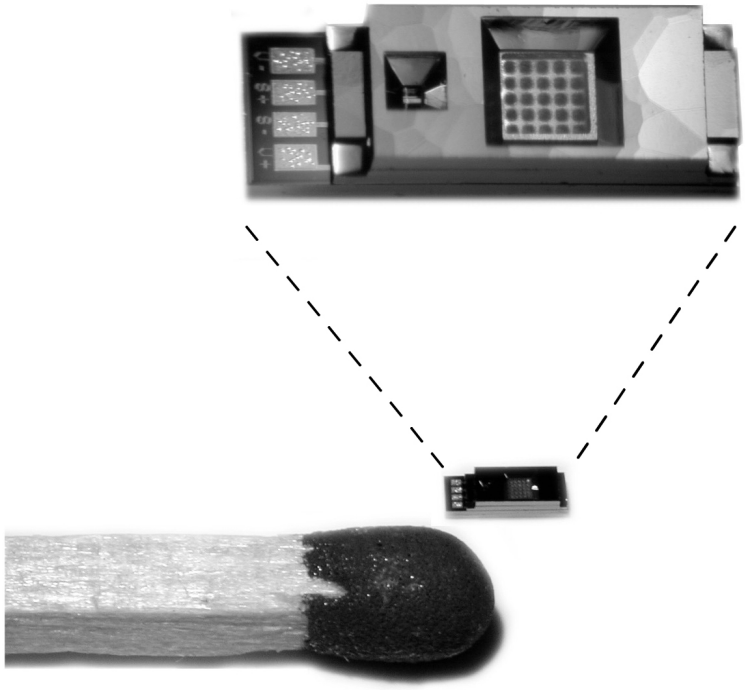

Figure 6.14. Photo of the assembled sensor.

6.7 The measurement setup

A schematic representation of the measurement setup is shown in figure 6.15. One of the most important parts of the measurement setup is the gas mixing system, which consists of two Bronkhorst mass flow controllers (model: F-201C-RAA-11-Z), two gas bottles, two reduction valves and a humidifier. One of the mass flow controllers is connected to a gas bottle with 100% nitrogen through a reduction valve, and the other controller to a bottle with 50% nitrogen and 50% carbon dioxide also through a reduction valve. The output of the mass flow controller with 100% nitrogen is connected to a humidifier, in which the gas is led through DI water to increases the relative humidity to 100%. This was done to prevent the sensor from drying out. After the humidifier, both gasses are mixed and transported to the sensor with a flow of 50 ml/min. With the gas mixing system it is possible to vary the partial CO_2 pressure from 1 to 50 kPa with steps of 0.5 kPa. Note that the flow of the 50/50% N_2/CO_2 gas is very low relative to the 100% N_2 gas flow, and that its influence on the humidity is therefore neglectable. Therefore an additional humidifier is not necessary.

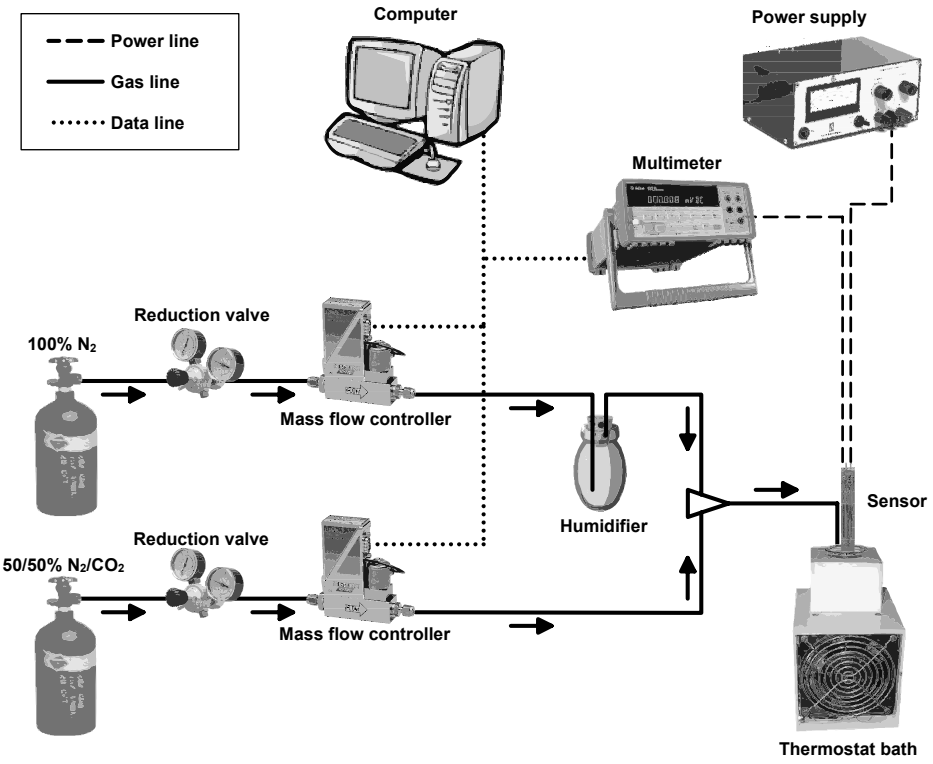

Figure 6.15. Photo of measurement setup.

The gas mixture flows through a glass tube which is placed in a thermostat bath. The bath's temperature is accurately controlled by an external controller and no additional stirring takes place. Inside the glass tube the hydrogel-based sensor is present which is connected to a home-made precision power supply (0.500 volt). A multimeter (34401A, Hewlet Packard) measures the output voltage of the sensor.

The multimeter and the two mass flow controllers are connected to a computer. By means of a LabVIEW (National Instruments) program specially written for this purpose, both mass flow controllers are regulated. Furthermore, the LabVIEW program translates the output voltage of the sensor to a pressure, and logs this data versus time.

6.8 Conclusions

The electrolyte and prehydrogel solution are prepared with simple methods and widely-available chemicals. The sensor parts are made with standard

cleanroom techniques. However, the assembly of the single parts to a complete sensor is laborious with a lot of manual actions and therefore the yield is not high. Nevertheless, this method is suitable in this stage of the research since it is relatively simple and requires no additional complicated (cleanroom) equipment. Yet, it enables the exploration of the sensor capabilities. It is not advised to use the current assembly method for future commercial manufacturing of the sensor, but to adapt it to mass fabrication techniques. Suggestions for such techniques are given in chapter 8.

Chapter 7

Characterization and Discussion*

The sensor is characterized and the best results are obtained with a sensor with cover design II and a gas permeable membrane. This sensor responds well to changes in Pco_2 at 37 ^oC with a maximum pressure generation of $0.29x10^5$ Pa at 20 kPa CO_2. The response time varies between 2 and 4 minutes, and the sensor shows linear temperature sensitivity due to the construction manner. The sensor enables detection of Pco_2 changes as small as 0.5 kPa, which is limited by the used measurement setup. Hydrochloric acid has no influence on the response of the sensor. The sensor was still functioning four months after manufacturing. However, the maximum pressure generation was decreased. From the obtained data it is determined that the reaction kinetics is the response time limiting factor of the sensor.

7.1 Introduction

In this chapter the characterization results of the hydrogel-based carbon dioxide sensor are shown and matched with the medical requirements. This includes a series of experiments with sensors with both types of covers, and also with the gas permeable membrane. Furthermore, the response time limiting factor of the sensor is determined and finally, some conclusions are drawn.

* This chapter is partly based on S. Herber, J. Bomer, W. Olthuis, P. Bergveld, A. van den Berg, *Biomedical Microdevices* 2005, **7**(3).

7.2 CO_2 measurements with cover design I

A series of experiments have been performed with a sensor with cover design I and without a gas permeable membrane. The thickness of the used hydrogel is 10 µm and all experiments were performed at room temperature without any temperature controlling.

7.2.1 Hydration

Before the CO_2 response of the sensor is studied, the hydrogel in the sensor is hydrated. The sensor was connected to the measurement setup and LabVIEW software was started to log the sensor signal versus time. Then, the sensor was placed in a beaker with DI-water. The hydration process of the hydrogel in the sensor is shown in figure 7.1. Note that no CO_2 was bubbled through the water.

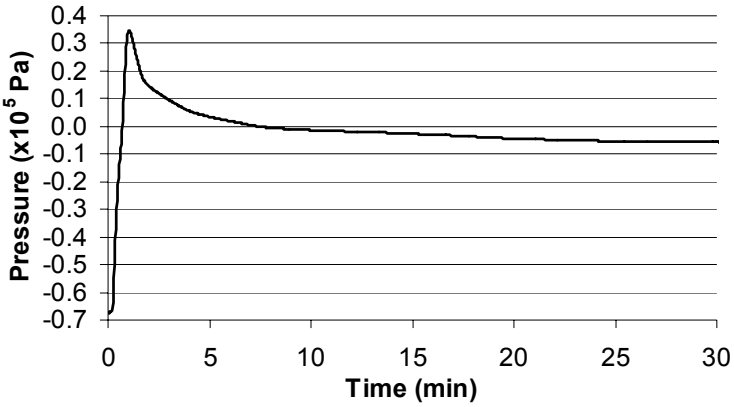

Figure 7.1. First time hydration of the hydrogel in the sensor with cover design I.

The hydrogel shows a good adhesion to the pressure sensor membrane and porous cover after polymerization. This results in the negative offset pressure at start when the hydrogel is shrunken due to evaporation of the solvent. The gel consequently pulls the pressure sensor membrane towards the porous cover. Note that additional offset pressure can be caused by the construction of the sensor, as will be discussed in section 7.3.4.

At t = 0 minutes, the sensor was placed in the solution which resulted in an increase in pressure to approximately 0.35×10^5 Pa due to the uptake of water by the hydrophilic hydrogel. Then, the pressure slowly decreased to about -0.05×10^5 Pa and equilibrium was reached after

approximately 25 minutes. The peak is caused by unpolymerized monomers that are still present in the hydrogel after polymerization. These unpolymerized monomers are hydrophilic and consequently attract water. The monomers will, however, diffuse out of the hydrogel, which results in the shown decrease in pressure.

The shown hydration response of the hydrogel in the sensor is representative for all sensors that were made and tested. Throughout this chapter all starting pressures at 2 kPa CO_2 are set to zero. Thus, all pressures shown in the plots are relative to the starting pressure at 2 kPa CO_2.

7.2.2 CO_2 measurement cycle

After the hydration the sensor was placed in the electrolyte consisting of 17 mM sodium bicarbonate and 8 mM sodium chloride resulting in an ionic strength of 25 mM. Then, 2 kPa CO_2 was bubbled through the solution and in approximately one hour the sensor equilibrated with the pH and ionic strength of the electrolyte. By means of LabVIEW software a measurement cycle was performed to increase the CO_2 with steps of 3 kPa from 2 to 20 kPa and back to the initial 2 kPa. Each CO_2 step is automatically performed when the pressure reaches equilibrium (when the standard deviation of the pressure measurement points of the last 180 seconds is below 5 Pa). The result of the experiment is shown in figure 7.2.

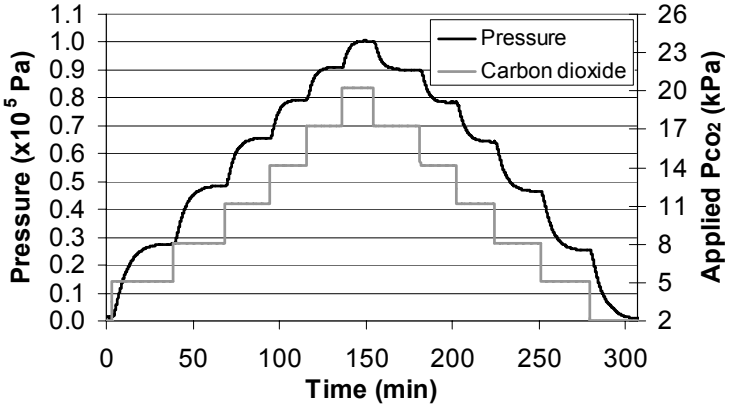

Figure 7.2. Plot of a CO_2 measurement cycle performed with a sensor with cover design I.

With every increase in Pco_2, the hydrogel generated an additional pressure up to $1.0x10^5$ Pa at 20 kPa CO_2. With the stepwise decrease in

Pco_2, the hydrogel generated less pressure until, at 2 kPa CO_2, the original pressure was reached. So, the process is fully reversible and the sensor shows no noticeable hysteresis and works in the medically interesting range.

According to figure 7.2, the Pco_2 steps around low Pco_2 levels provokes more change in pressure than steps around high Pco_2 levels. The reason for this is that a step at low Pco_2 results in a larger pH change of the electrolyte than at higher concentrations. In section 3.2.2, this relation between Pco_2 and pH for a specific bicarbonate concentration is already described. When a 17 mM bicarbonate solution is considered (see figure 5.9), the pH changes from 7.77 to 7.37 in response to a Pco_2 step from 2 to 5 kPa. The Pco_2 step from 17 to 20 kPa results in a pH change from 6.84 to 6.77. So, in the first CO_2 step the ΔpH is 0.40 and in the last step 0.07. Since the first step results in a larger pH change, the hydrogel consequently generates more additional pressure than during the last step. This might also explain the longer equilibration time in the first step compared to the last step.

With use of figure 7.2, the equilibration pressures are determined and plotted versus the Pco_2. The result is shown in figure 7.3.

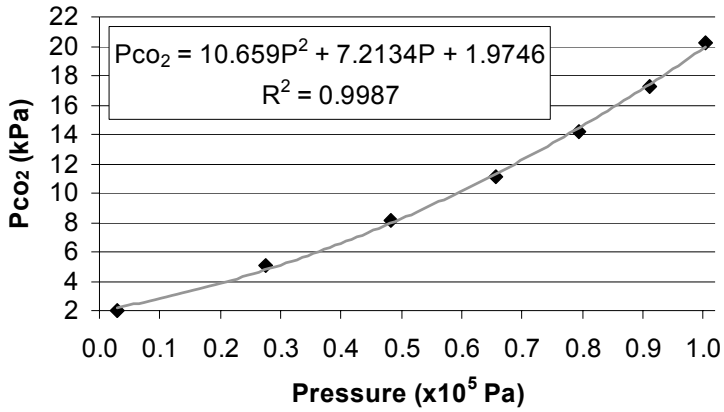

Figure 7.3. Plot of the Pco_2 versus the pressure for the measured equilibrium pressures and a fitted trendline representing the calibration curve of the sensor.

A trendline is fitted, which represents the calibration curve of this sensor. This second-order polynomial fit equation is also shown in figure 7.3 and is described by

$$Pco_2 = 10.659P^2 + 7.2134P + 1.9746, \qquad (7.1)$$

where P is the pressure in 10^5 Pa and Pco_2 the partial pressure of carbon dioxide in kPa.

The 90% response time of the sensor is also determined with use of figure 7.2. This is done for the steps up as well as the steps down and the result is shown in figure 7.4. The response time for the steps up varies between 7 and 20 minutes and for the steps down between 10 and 16 minutes. This does not meet the requirements for the medical application and was the reason for designing the new covers.

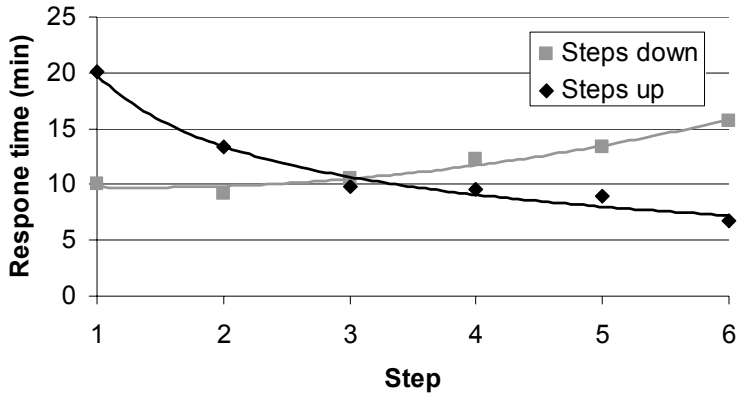

Figure 7.4. Plot of the 90% response time of the sensor as result of 3 kPa CO_2 steps up and down.

7.2.3 Small CO_2 steps

As already mentioned in chapter 6, the smallest Pco_2 step that can be applied with the used measurement setup is 0.5 kPa CO_2. This is limited by the combination of mass flow controllers and the gas mixture of 50% CO_2/50% N_2. An experiment was performed where the Pco_2 was increased with the small steps from 2.0 to 3.5 kPa CO_2. Note that a step of 0.5 kPa CO_2 from 2.0 to 2.5 kPa CO_2 results in a pH change of the electrolyte of only ~0.093. The result is shown in figure 7.5.

With every increase in Pco_2 the pressure increased obviously with steps of approximately $0.05x10^5$ Pa. Since the pressure increase due to a Pco_2 step is quite large and well measurable, it is expected to be possible to measure steps as small as 0.1 kPa CO_2, as required for the medical application.

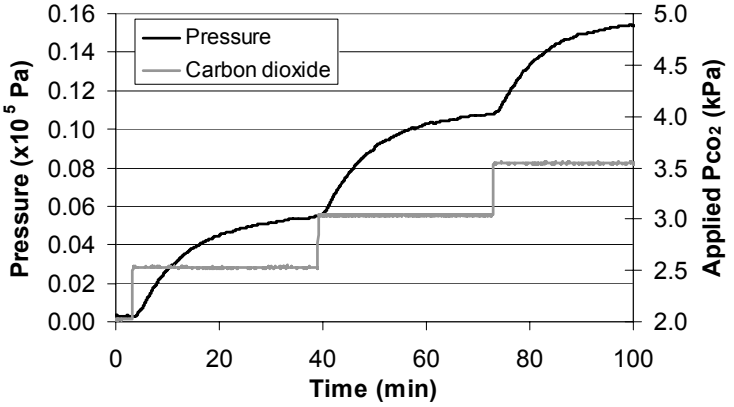

Figure 7.5. Plot of the sensor response to small CO_2 steps of 0.5 kPa (limited by the used measurement setup).

7.3 CO_2 measurements with cover design II

The cover was redesigned in order to decrease the response time. The depth of the hydrogel cavity was decreased from 10 to 5 µm and the hydrogel thickness after the *in situ* polymerization will then also be 5 µm, which should consequently result in a faster response time. Furthermore, the redesigned cover takes the mounting of the gas permeable membrane carrier into account.

In this section, characterization results are shown of experiments with sensors with the redesigned cover (II) and the gas permeable membrane. Based on experience obtained with the previous experiments, it is expected that the sensor is temperature sensitive and therefore all experiments are performed with additional temperature controlling.

7.3.1 First time hydration

As for the sensor with cover design I, the first time hydration of the hydrogel in the sensor is also investigated for design II. This was done with a semi-finished sensor, i.e. without the gas permeable membrane. The response of the sensor after immersing in DI-water is shown in figure 7.6. During the experiment no CO_2 was bubbled through the solution.

Again, there is a negative starting pressure due to the shrunken state of the hydrogel (and possibly also due to the construction manner of the sensor, see section 7.3.4). At t = 0 minutes, the sensor was immersed in the DI-water and the hydrophilic hydrogel immediately generated pressure due

to the uptake of the water. The pressure increased to a peak of approximately $0.15x10^5$ Pa after which it decreased and reached equilibrium. As already explained in the previous section, the peak is caused by the presence of unpolymerized monomers in the hydrogel that diffuse out and consequently result in pressure decrease. Note that the response in figure 7.6 is reasonable different than in figure 7.1 with respect to the part after the peak until reaching equilibrium. This is probably due to initial settling (twining) of the hydrogel in the cavity.

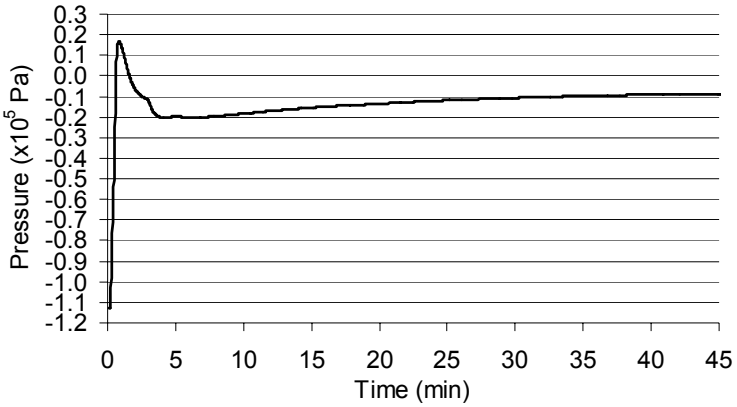

Figure 7.6. First time hydration of the hydrogel in the sensor with cover design II.

To verify that the unpolymerized monomers cause the peak, the sensor was dehydrated and subsequently hydrated again. The result is shown in figure 7.7.

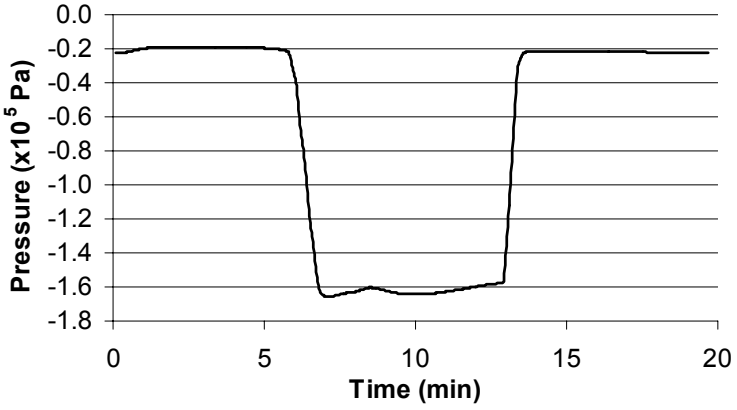

Figure 7.7. Result of dehydration and hydration of the hydrogel in the sensor with cover design II.

The sensor was placed outside the water and after approximately 6 minutes the hydrogel was dehydrated by evaporation. This resulted in a

pressure decrease to approximately -1.7x10^5 Pa. Then, after 5 minutes, the sensor was immersed again in the DI-water. Consequently, the pressure increased again to its initial value. However, there is no peak, which confirms the hypothesis that there are, initially, unreacted monomers present in the hydrogel after polymerization. This means that the built-in efficiency of the monomers, reflecting the degree of polymerization, is not 100%. In addition, the reactivity ratios of the two monomers DMAEMA and HEMA are important. The reactivity ratio of a monomer (e.g. HEMA) describes its preference for adding its own monomer (HEMA) versus the other monomer (DMAEMA) during polymerization[1,2]. The built-in efficiency and the reactivity ratio have great influence on the polymerization and determine the ultimate hydrogel composition. Thus, a prehydrogel solution of 5% DMAEMA and 95% HEMA does not necessarily result in a hydrogel with the exact same ratio between the polymers (pHEMA: pDMAEMA).

7.3.2 The gas permeable membrane

With the semi-finished sensor, it was verified whether the *in situ* polymerization was successful. This was done by placing the complete sensor in the electrolyte, consisting of 17 mM sodium bicarbonate and 8 mM sodium chloride, and observing the response to Pco_2 changes. The result of a CO_2 measurement cycle is shown in figure 7.8. As can be seen, the sensor responds obviously to the Pco_2 changes with a maximum pressure of 0.33x10^5 Pa at a partial CO_2 pressure of 20 kPa.

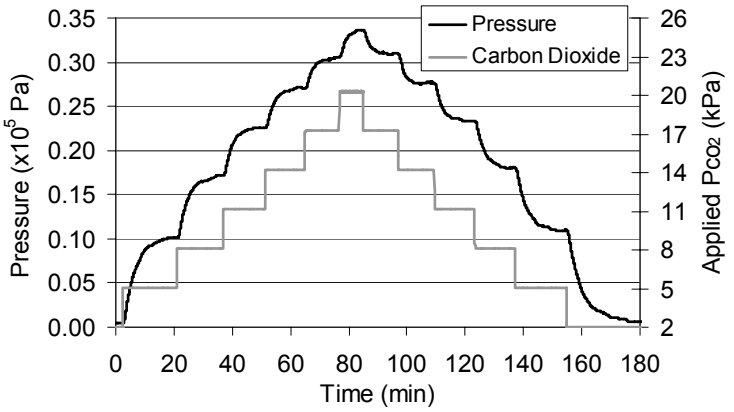

Figure 7.8. Plot of a CO_2 measurement cycle performed at 25 °C with a sensor with cover design II and without the gas permeable membrane.

To investigate the influence of the addition of the gas permeable membrane, the semi-finished sensor was completed and another CO_2 measurement cycle was performed with the sensor submerged in the electrolyte. The result is shown in figure 7.9. Apparently, the membrane allows CO_2 to diffuse through properly since there was obvious CO_2 response. The maximum pressure generation occurred at 20 kPa CO_2 and was 0.30×10^5 Pa, which is slightly lower than during the previous measurement cycle. This difference might be due to the bonding method of the gas permeable membrane where the sensor is placed in a furnace at 60 ^oC to cure the epoxy glue. This might have led to a change in hydrogel configuration (e.g. reordering of the chains) and consequently a change in maximum pressure generation. More information on the influence of the gas permeable membrane on the response time is provided in section 7.4.

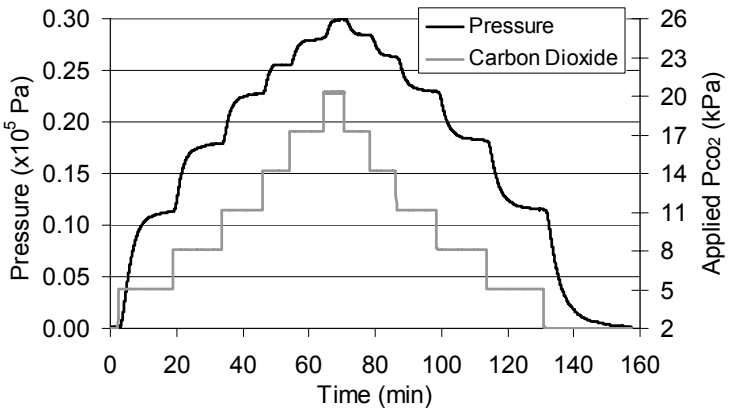

Figure 7.9. Plot of a CO_2 measurement cycle performed at 25 ^oC with a sensor with cover design II and with the gas permeable membrane.

7.3.3 CO_2 measurement cycle

A second sensor was constructed and a CO_2 measurement cycle was performed at 25 ^oC, while measuring in the gas mixture environment. The result is shown in figure 7.10. The sensor responds well to the Pco_2 steps with little hysteresis. The maximum pressure generation occurred at 20 kPa CO_2 with a pressure of 0.28×10^5 Pa.

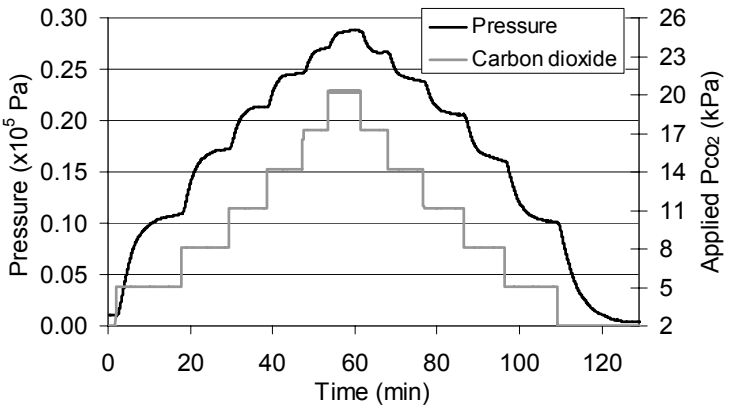

Figure 7.10. Plot of a CO_2 measurement cycle performed at 25 °C with a sensor with cover design II and with the gas permeable membrane.

Since the operating temperature of the sensor will be the same as the human body temperature, another CO_2 measurement cycle was performed at 37 °C. The result of the measurement is shown in figure 7.11.

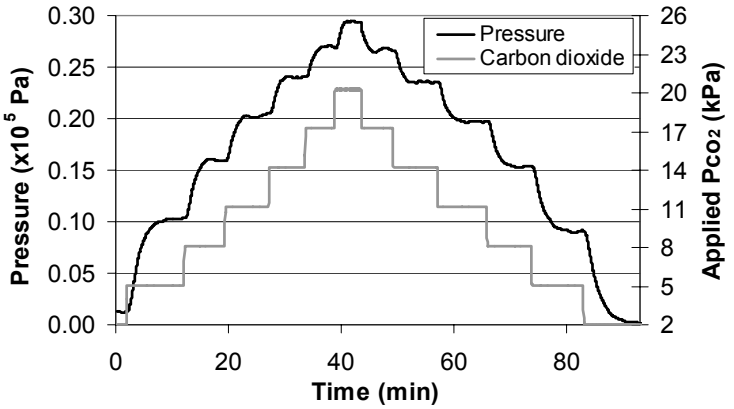

Figure 7.11. Plot of a CO_2 measurement cycle performed at 37 °C with a sensor with cover design II and with the gas permeable membrane.

The sensor functions also properly at this temperature. The maximum pressure generation of 0.29×10^5 Pa at 20 kPa CO_2 is comparable with the 0.28×10^5 Pa at 25 °C. So, the temperature has little influence on the maximum pressure generation. However it has great influence on the offset (set to zero in figure 7.11). More information on the temperature sensitivity is provided in section 7.3.4. Note that the time scales on the x-axis of all plots may be compared with each other with respect to the sensor response rate, because all CO_2 measurement cycles are performed automatically. Therefore e.g. at 37 °C (figure 7.11: total time is ~100

minutes) the sensor is faster than at 25 °C (fig. 7.10: total time is ~130 minutes).

With the result of figure 7.11, the calibration curve of the sensor is determined. The Pco_2 is plotted versus the pressure and a calibration curve is fitted, as shown in figure 7.12.

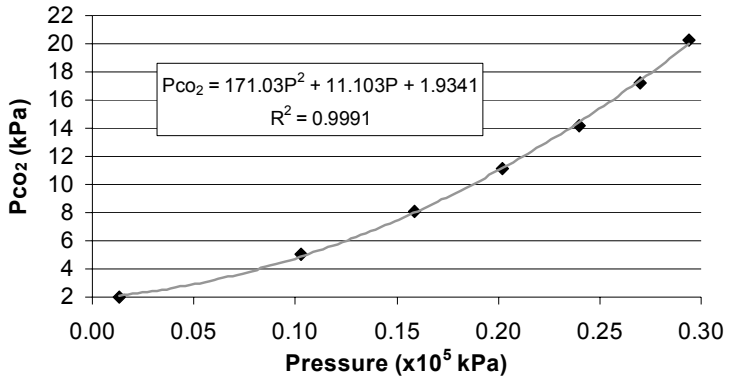

Figure 7.12. Plot of the Pco_2 vs. the pressure for the measured equilibrium pressures and a fitted trendline representing the calibration curve of the sensor.

As for the sensor with cover design I and 10 µm thick hydrogel, the curve is described by a second-order polynomial,

$$Pco_2 = 171.03P^2 + 11.103P + 1.9341\,, \qquad (7.3)$$

where P is the pressure in 10^5 Pa and Pco_2 the partial pressure of carbon dioxide in kPa.

In order to investigate the influence of temperature on the response time of the sensor, the 90% response times for the steps up at both temperatures were determined and plotted versus the steps, as shown in figure 7.13. At 25 °C the response time varies between approximately 4 and 8 minutes, and at 37 °C between 2 and 4 minutes, which meets the requirements of the medical application Thus, the sensor responds faster when the temperature increases, which is discussed further in section 7.3.4.

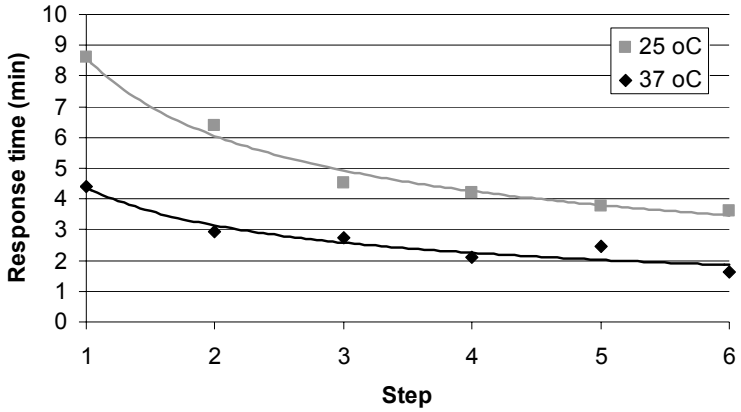

Figure 7.13. Plot of the 90% response time of the sensor at a temperature of 25 °C and 37 °C for the Pco_2 steps up.

7.3.4 Temperature sensitivity

It is suspected that the sensor is temperature sensitive since it contains water, which is known to expand with rising temperature. The expansion of the water in the pores and reservoir of the cover will not deliver a pressure increase because of the flexibility of the PDMS gas permeable membrane. However, the water in the hydrogel will possible generate additional pressure with increasing temperature. Furthermore, it is most likely that there is temperature sensitivity due to the stress caused by the mechanical fixation of the cover to the pressure sensor, and due to the different thermal expansion coefficients of silicon and epoxy. During the early development of the piezoresistive pressure sensor by Ko *et al.*[3], comparable temperature sensitivity was observed due to the different thermal expansion coefficients of the used materials and the offset by stress. Note that due to the Wheatstone bridge configuration of the inherent temperature sensitive piezoresistors, the pressure sensor's temperature sensitivity is relatively small (see table 5.1).

Because of these possible different causes of temperature sensitivity, the sensor's overall temperature sensitivity can not be predicted. Therefore, an experiment was performed to investigate the temperature sensitivity of the sensor. The temperature of the thermostat bath was decreases from 37 °C to 25 °C with steps of 3 °C while maintaining the Pco_2 constant at 2 kPa. The response of the sensor is shown in figure 7.14.

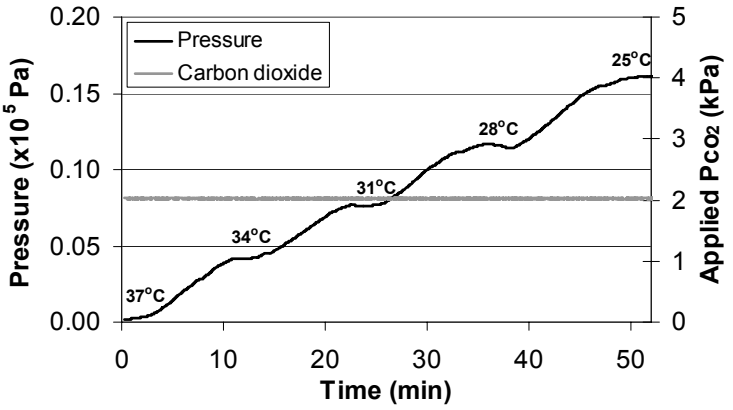

Figure 7.14.Response of the sensor to a temperature decrease from 37 °C to 25 °C with steps of 3 °C.

The plot demonstrates clearly that the sensor is temperature sensitive since the pressure increased with every decrease in temperature. Figure 7.14 is converted into figure 7.15 to demonstrate the relation between pressure and temperature for this sensor. As can be seen, the sensor is linearly sensitive to temperature with a slope of approximately -0.013×10^5 Pa/°C at 2 kPa CO_2.

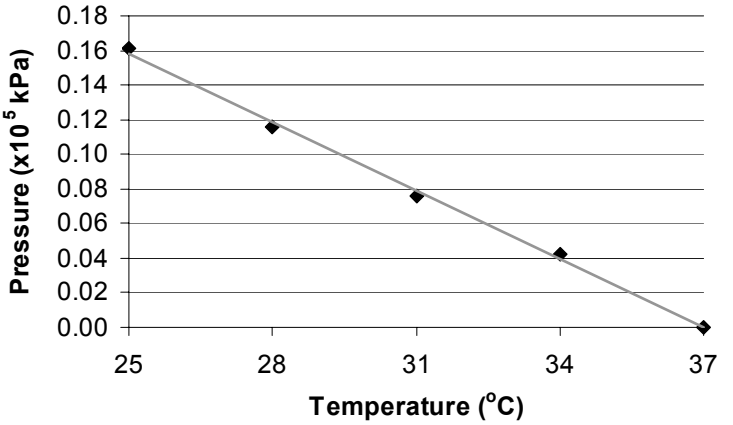

Figure 7.15. Relation between pressure, generated by the hydrogel, and temperature at a constant 2 kPa CO_2.

To determine whether the hydrogel, the mechanical fixation or a combination is responsible for the temperature sensitivity, dummy sensors were made without a hydrogel and without a gas permeable membrane. The temperature experiments were repeated with the two dummy sensors and the result is shown in figure 7.16 (the pressure offset is not set to zero). Both sensors have an offset in pressure and show temperature sensitivity.

In the first case there is a negative offset and a positive temperature sensitivity of approximately 0.013x10^5 Pa/^{o}C. In the second case there is a positive offset and a negative temperature sensitivity of circa -0.017x10^5 Pa/^{o}C. Apparently, the direction of the temperature sensitivity is a function of the sign of the offset. Since the temperature sensitivity of a dummy sensor is in the same order as for a complete sensor, the conclusion is drawn that the sensitivity is all due to the mechanical fixation. Any possible temperature sensitivity due to the hydrogel can not be determined in this case.

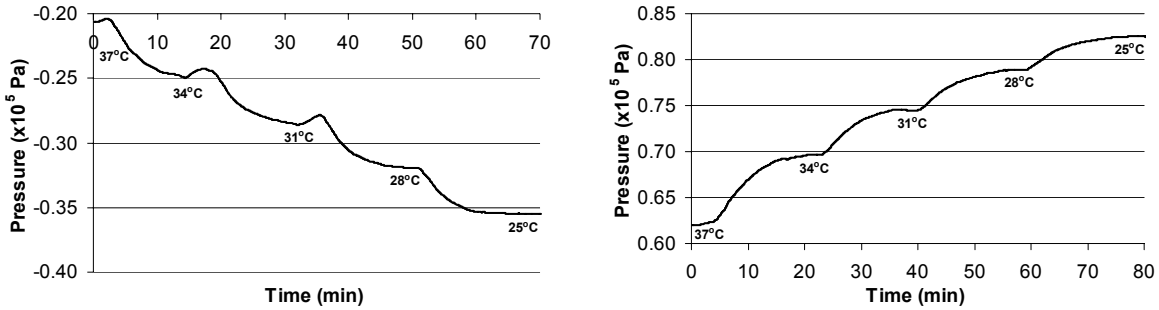

Figure 7.16.Response of two dummy sensors (without hydrogel and gas permeable membrane) to a temperature decrease from 37 ^{o}C to 25 ^{o}C with steps of 3 ^{o}C.

7.3.5 Small CO_2 steps

Another experiment was performed to verify if the sensor is able to detect small Pco_2 steps at 37 ^{o}C. The Pco_2 was increased from 2 to 3.5 kPa CO_2 with steps of 0.5 kPa CO_2. Note that the steps are the smallest possible with the used measurement setup. The result of the experiment is shown in figure 7.17.

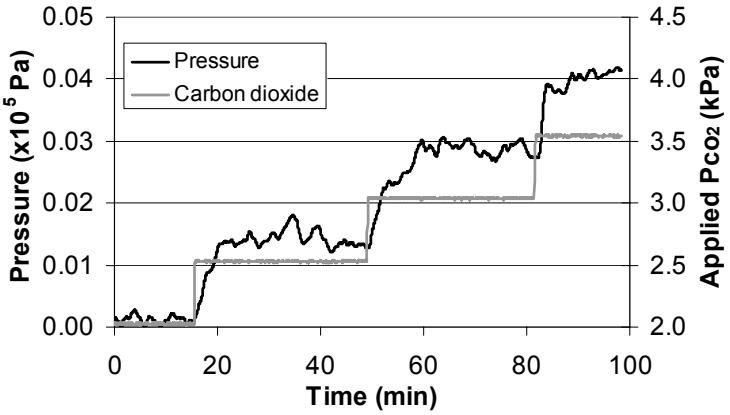

Figure 7.17. Plot of the sensor response to small CO_2 steps of 0.5 kPa (limited by the used measurement setup).

The sensor responds obviously to the small Pco_2 steps with an increase of approximately $0.015x10^5$ Pa per 0.5 kPa CO_2 step. There is some fluctuation in the measurement signal, which is probably caused by small imperfections in temperature controller. Since the sensor is temperature sensitive (section 7.3.4), it responds to these small temperature variations with fluctuations in the pressure signal. The temperature was controlled at +/- 0.1 °C. According to figure 7.15, a temperature fluctuation of 0.2 °C results in a pressure signal fluctuation of approximately $3x10^2$ Pa, which is of the order as observed in figure 7.17.

To demonstrate that the fluctuations are caused by imperfect temperature control at 37 °C, the result of an earlier experiment is shown in figure 7.18. During this experiment the same measurement protocol was used. However, it was performed at the much more stable room temperature and without a gas permeable membrane. In this case the measurement signal is much more stable.

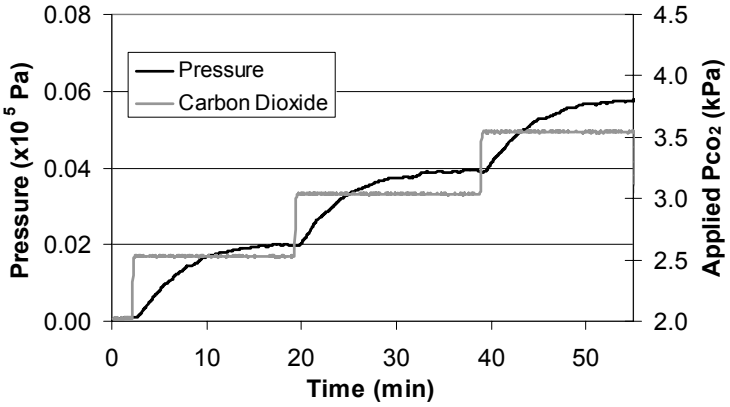

Figure 7.18. Plot of the response of a sensor without gas permeable membrane to small CO_2 steps of 0.5 kPa at room temperature.

7.3.6 Influence of HCl vapor and fluid

Since the ultimate goal of the sensor is measuring Pco_2 inside the stomach it should be resistant to gastric juices. One of these juices is hydrochloric acid (HCl), which can reach concentrations up to 1 M. The HCl fluid can not enter the sensor due to the presence of the hydrophobic gas permeable membrane. However, the membrane allows water vapor to pass. So, possibly it also allows HCl vapor to diffuse through. In table 7.1 the partial pressure of HCl over aqueous HCl is given for different concentrations at different temperatures.

Table 7.1. Partial pressure (Pa) of HCl over aqueous HCl solutions. Source: Chemical Safety Data Sheet SD-39, Properties and essential information for safe handling and use of hydrochloric acid, aqueous and hydrogen chloride, anhydrous (Manufacturing Chemists Association).

	Temperature (°C)						
%HCl	0 °C	10 °C	20 °C	30 °C	40 °C	50 °C	60 °C
2		0.00156	0.00587	0.0201	0.0627	0.187	0.507
4	0.0024	0.0092	0.032	0.103	0.307	0.853	2.20
6	0.0088	0.0312	0.101	0.300	0.827	2.17	5.33
8	0.0157	0.0777	0.237	0.687	1.81	4.59	10.8
10	0.0560	0.179	0.527	1.48	3.76	9.20	20.9
12	0.132	0.407	1.17	3.12	7.73	18.1	40.7
14	0.320	0.947	2.61	6.67	16.1	36.7	80.0
16	0.747	2.13	5.71	14.1	32.9	73.3	156
18	1.80	4.93	12.7	30.4	68.7	148	307
20	4.21	11.2	27.3	64.0	141	295	587

The approximate concentration of water is 55.4 mol/L and the concentration HCl in the stomach is maximally 1 mol/L. Thus, the mol percentage HCl is 1/55.4 x 100% ≈ 2%. According to table 7.1 the partial pressure of 2% HCl at 40 °C is 0.0627 Pa. At 37 °C, as in the stomach, this partial pressure is slightly lower. The partial pressure of HCl can functionally be compared with the partial pressure of CO_2, since every molecule of both species delivers one proton in the electrolyte after diffusing through the gas permeable membrane. The partial pressure of CO_2 in the stomach (≥3 kPa) is much higher than that of HCl (~0.0627 Pa). Therefore, it is expected that the HCl has no or little influence on the sensor response.

Two experiments were performed to verify this. In the first experiment, the sensor was placed in the vapor of HCl. In the worst case scenario, the HCl enters the sensor and titrates the hydrogel, resulting in a rapid and large increase in pressure. A schematic representation of the used setup is shown in figure 7.19a. The sensor was hanging inside the gas chamber and the hydrochloric acid was pipetted at the bottom.

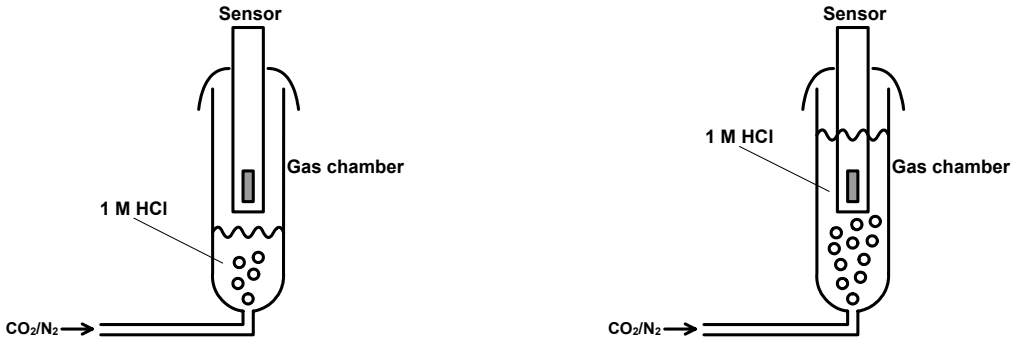

(a) vapor *(b) immersing*

Figure 7.19. Schematic representation of the measurement setup used to investigate the influence of HCl vapor (a) and after immersing in 1 M HCl (b).

In figure 7.20 the response of the sensor is shown. The 1 M HCl was pipetted at t = 1 minute and in response there was a slight decrease in pressure, which might be caused due to a small change in temperature by the pipetting (the Δpressure corresponds to a ΔT of ~0.2 °C, according to figure 7.15). However, there is no rapid and large increase in pressure and therefore the conclusion is drawn that HCl vapor has negligible influence on the sensor response.

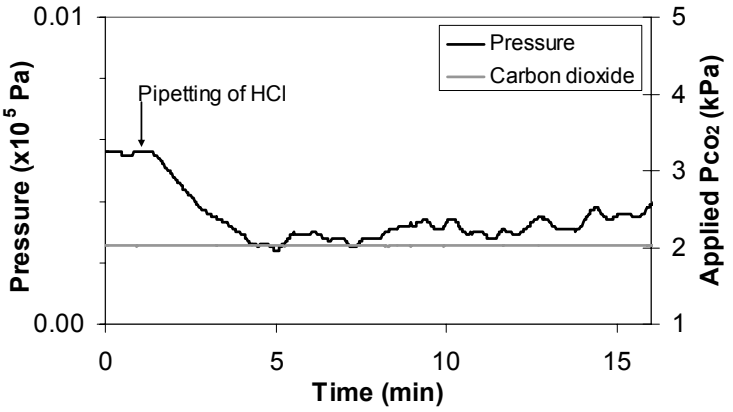

Figure 7.20. Response of the sensor to HCl vapor. Note that the scale of the y-ax is a very narrow pressure range compared to the previous experiments.

During the second experiment the sensor was fully immersed in the hydrochloric acid, as shown in figure 7.19b. The immersing was done at t = 1 minute and the response is shown in figure 7.21.

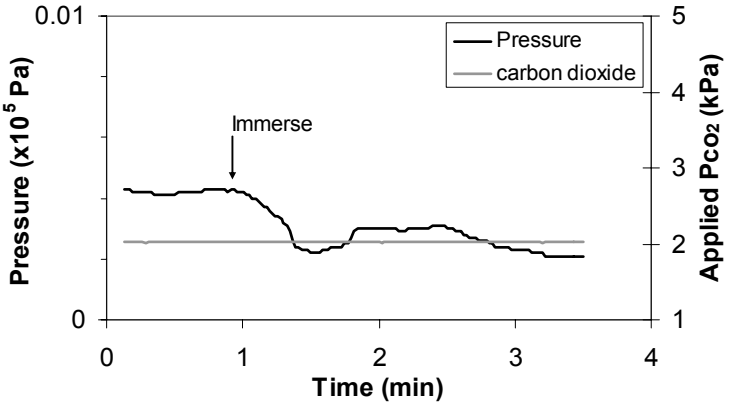

Figure 7.21. Response of the sensor to HCl immersing. Note that the scale of the y-ax is a very narrow pressure range compared to the previous experiments.

Again, there is only a small decrease in pressure, but no rapid and large increase. So, the HCl solution cannot enter the sensor through the hydrophobic gas permeable membrane or through possible cracks caused by imperfect sealing of the sensor with the epoxy glue. Furthermore, this also means that there is good adhesion of the gas permeable membrane to the carrier.

7.3.7 Long-term stability of the sensor

To investigate the long-term stability of the sensor, an experiment was performed with the sensor, as used for the experiments of section 7.3.3, four months after manufacturing. During this period the sensor was preserved by immersing in the electrolyte, which was in equilibrium with the partial CO_2 pressure of air. The Pco_2 was increased from 2 to 20 kPa with steps of 3 kPa to investigate the response and the maximum pressure generation, as shown in figure 7.22. The sensor still responds obviously to the Pco_2 steps. However, the maximum pressure generation at 20 kPa CO_2 is lower than before (approximately two times) as can be concluded from the comparison with figure 7.11.

A probable cause for this might be of mechanical nature. The fixation between the pressure sensor and porous cover might have deteriorated due to aging, hydration or cracking of the epoxy glue. Consequently, the distance between both parts is slightly increased, which would result in less pressure generation and a decrease in offset. This offset decrease was also observed: after manufacturing the offset was approximately -0.1×10^5 Pa and after four months it was -0.6×10^5 Pa. Despite the degradation in

performance this experiment demonstrates that the sensor still functions properly after four months.

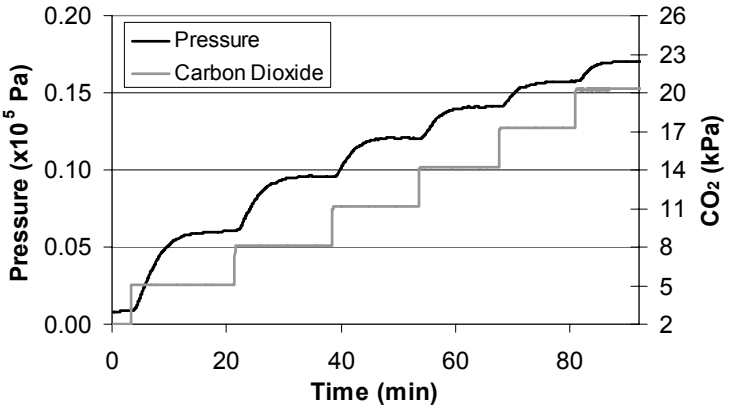

Figure 7.22. Response to Pco_2 steps of the sensor four months after manufacturing at 37 °C.

7.4 The response time

The dynamic response of the hydrogel-based Pco_2 sensor is governed by several diffusion processes and reaction kinetics. This is schematically represented in figure 7.23.

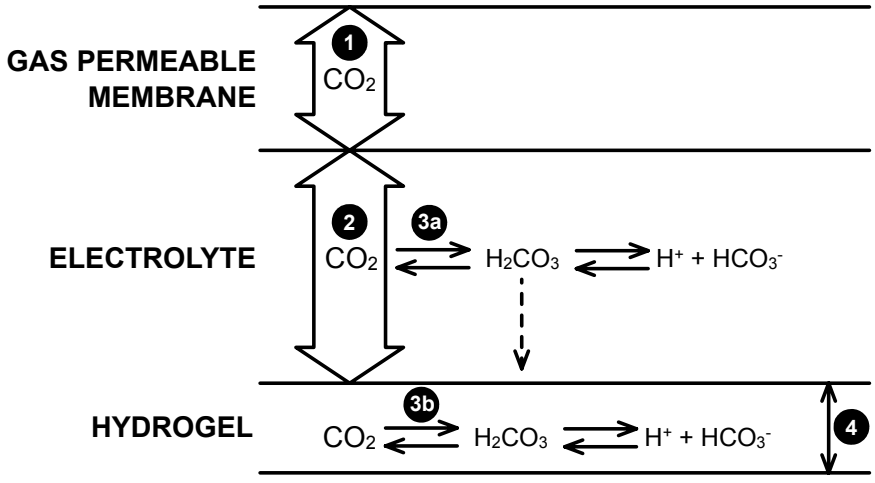

Figure 7.23. Diffusion processes and reaction kinetics that take place in the hydrogel-based CO_2 sensor with different processes indicated by 1, 2, 3 and 4.

The first process is the CO_2 diffusion through the gas permeable membrane, which consists of polydimethylsiloxane (PDMS) and is known to

be very permeable to CO_2 [4]. In an approximation, the time of diffusion, τ_m (s), of the CO_2 through the gas permeable membrane is described by

$$\tau_m = \frac{d_m^2}{D_m}, \tag{7.2}$$

where d_m is the membrane thickness (m) and D_m the diffusion coefficient of CO_2 in the membrane (m^2/s) [5].

Next, the carbon dioxide diffuses into the bulk electrolyte and the conversion reaction of CO_2 to protons takes place (3a). The time of CO_2 diffusion is relatively faster than the conversion time (will be discussed further). So, it is assumed that the conversion reaction occurs everywhere in the bulk at approximately the same time. Therefore, it is more likely that a proton converted near the hydrogel (3b) is consumed by the gel than a proton further away from the bulk electrolyte. Since the solution is already saturated with CO_2 in that time, the converted/consumed CO_2 near the hydrogel is immediately replenished. In addition, the pH of the bulk is around 7 (low concentration of protons) and therefore the concentration difference of protons over a certain diffusional length in the electrolyte is low, which consequently results in a slow proton diffusion process.

For these reasons, the second process in the sensor is the diffusional transport of CO_2 through the electrolyte towards the pH-sensitive hydrogel, which can be expressed with flux. It is assumed that the hydrogel actually works as a sink for CO_2 until a specific amount of amine groups are protonated, which depends on the ΔpH induced by the ΔPco_2. Flux is defined as the rate of flow through a given surface and is described by Fick's first law of diffusion,

$$J = -D_e \frac{\partial c}{\partial x}, \tag{7.3}$$

where J is the flux ($mol/m^2.s$), D_e the diffusion coefficient of CO_2 through the electrolyte (m^2/s) and $\partial c/\partial x$ the CO_2 concentration gradient over the thickness of the electrolyte layer ($mol.m^{-3}/m$) [6]. The negative sign indicates

that diffusion proceeds from higher to lower concentration. Multiplying the flux with the surface area gives the diffusion rate,

$$R_{dif} = -D_e \cdot A \frac{\partial c}{\partial x}, \tag{7.4}$$

where A is the surface area in m^2 and R_{diff} the diffusion rate in mol/s. By assuming that the hydrogel works as a continuous sink (∂c remains constant) until protonation is completed, the above equation is applicable for the hydrogel-based sensor. By dividing the amount of protonable groups by the diffusion rate, the time for the CO_2 diffusion process can be calculated.

The third process is the conversion of CO_2 into protons and bicarbonate ions (3b). This process consists of two steps. The first step is the hydration of CO_2 and dehydration of carbonic acid,

$$CO_2 + H_2O \underset{k_2}{\overset{k_1}{\rightleftharpoons}} H_2CO_3 . \tag{7.5}$$

The forward reaction is slow[4] with k_1=0.03 s^{-1} and might have influence on the response time of the sensor. The reverse reaction is faster with k_2=20 s^{-1}. The second step is the dissociation of the carbonic acid into a proton and bicarbonate ion,

$$H_2CO_3 \leftrightarrow H^+ + HCO_3^- . \tag{7.6}$$

This reaction is believed to occur instantaneously[4] and is therefore not further considered.

The fourth process is the rate of pressure generation by the hydrogel. This process is not taken into account, since this process depends on the proton supply rate and therefore depends on the third process. Note that when a sensor without a gas permeable membrane is transferred from a pH9 buffer to a HCl solution, the pressure generation occurs in the order of seconds due to the presence of many protons.

Summarized from the text above, process one, two or three can be the response time limiting factor of the sensor. With the obtained experimental results and the differences between cover design I and II, the response time limiting factor is determined below.

As already mentioned in chapter 5, the thickness of the membrane is 14 µm. The diffusion coefficient of carbon dioxide through PDMS, D_m, *is* 1.1×10^{-9} m^2/s [5]. Substituting these values in equation 7.2 gives a diffusion time of 0.178 seconds, which is much faster than the time constant found during the CO_2 measurement cycle without gas permeable membrane (figure 7.8). Therefore the gas permeable membrane is probably not the response time limiting factor. However, the hydrogel consumes many protons which are produced as a product of the reaction between H_2O and CO_2 (chapter 1). Thus, a lot of CO_2 has to be converted and consequently a lot of CO_2 has to diffuse through the gas permeable membrane. Therefore it is still possible that the membrane is the response time limiting factor. To investigate this, the measurement cycles with and without the gas permeable membrane are compared (taken from figure 7.8 and 7.9). The 90% response time for the steps up are determined and plotted, as shown in figure 7.24. There is only a slight difference in response time and therefore the conclusion is drawn that the gas permeable membrane is not the response time limiting factor of the sensor.

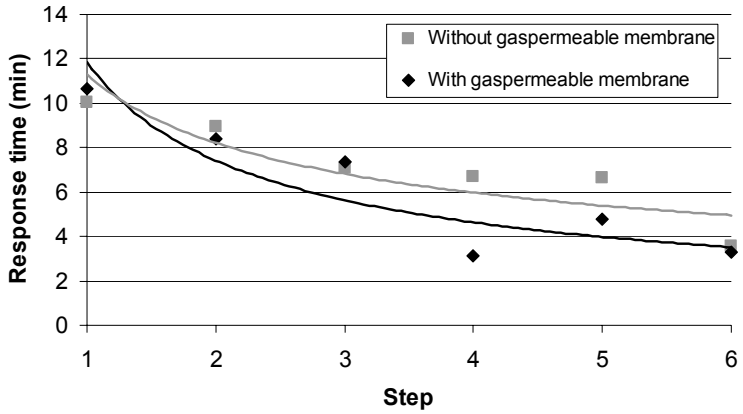

Figure 7.24. Plot of the 90% response time of the sensor with and without gas permeable membrane as result of 3 kPa CO_2 steps up.

The two most relevant differences between both cover designs are the decrease in diffusion length in the electrolyte layer (from 500 µm to 200 µm) and the decrease in hydrogel thickness (from 10 µm to 5 µm). In table

7.2, the expected gain in response time is shown for process two, three and a combination of both.

Table 7.2. Expected gain in response time for the different processes due to the cover change from design I to II.

Process	Gain due to decrease in		Total gain
	diffusion length	hydrogel thickness	
Diffusion of CO_2 (second process)	2½x	2x	5x
Reaction kinetics (third process)		2x	2x
Combination of both process			10x

When the process of CO_2 diffusion is the determining factor, the response time would be five times faster. In this case, the diffusion rate is 2½ times higher due to the decrease in diffusion length from 500 µm to 200 µm (see equation 7.4). Furthermore, the hydrogel thickness is decreased with a factor two and therefore the amount of protonable groups is also decreased two times. Thus, two times less CO_2 has to diffuse to the hydrogel. Multiplying both factors gives the total response time gain of five.

When the reaction kinetics is the decisive factor, the response time would only be two times faster. In this case there are two times less protonable groups due to the decrease in hydrogel thickness. Therefore, two times less CO_2 has to be converted, which results in a gain of response time with a factor two.

When both processes have an equal share on the response time, the total gain would be ten as a result of the product of five and two.

To determine which process is the response time limiting factor, the response times are compared for a sensor with cover design I and design II (taken from figure 7.4 and 7.13). As can be seen in figure 7.25, the response time of design II is approximately two times faster than that of design I. From this, the conclusion is drawn that the reaction kinetics of the hydration is the response time limiting factor of the sensor.

Note that it is expected that the CO_2 steps from high to low levels would result in faster pressure decrease steps since the dehydration of carbonic acid is faster than the hydration. However, as can be seen in e.g.

figure 7.10, this is not the case. Probable another process, such as CO_2 diffusion, has an additional influence on the response time. This is not further investigated.

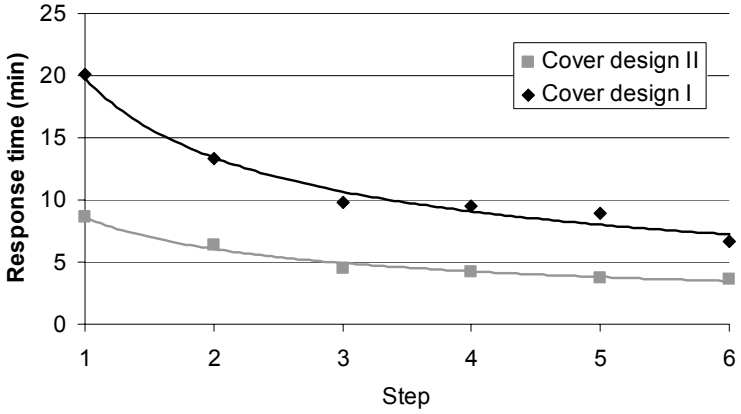

Figure 7.25. Response times to Pco_2 steps up of a sensor with cover design I and with design II.

The temperature has also a large influence on the response time. As already demonstrated in section 7.3.3, the sensor is faster after an increase in temperature. Since the reaction kinetics occurs faster at higher temperature and is the response time limiting factor, the sensor responds faster at higher temperature. Note that at higher temperature the pK_a of the hydrogel and bicarbonate buffer also shift slightly. This can result in a slightly different response of the sensor, but was not observed in section 7.3.3.

The response time of the sensor might be improved by adding the enzyme carbonic anhydrase to the electrolyte. Carbonic anhydrase is known to catalyze the hydration of carbon dioxide and the dehydration of carbonic acid[7,8]. Other research has already demonstrated that the response time of sensors based on bicarbonate electrolyte is improved after adding carbonic anhydrase[9-11]. However, the lifespan of a sensor with carbonic anhydrase might be decreased due to the limited lifetime of the enzyme and it might also require extra conditioning. Furthermore, carbonic anhydrase might influence the ionic strength of the electrolyte and might function as counterion when its isoelectric point is below the pK_a of the hydrogel. This means that all concentrations of all chemical as used up to now should be adapted.

It was experimentally verified that carbonic anhydrase in a solution can not withstand bubbling through of gas, which is observed by the origination of foam. Since the sensor is filled with electrolyte by means of vacuum, which can easily result in boiling and thus bubbling, the sensor filling method should also be adapted for the use of carbonic anhydrase. For the mentioned reasons, it was decided not to perform additional experiments with carbonic anhydrase.

7.5 Conclusions

The sensor without a gas permeable membrane and with a 10 µm thick hydrogel (cover design I) responds well to carbon dioxide within the medically interesting range of 3 to 20 kPa CO_2. At 20 kPa CO_2 a maximum pressure of $1.0x10^5$ Pa is generated. The response time varies between 7 and 20 minutes, which does not fulfill the medical requirement of a response time below 10 minutes. The sensor is able to detect Pco_2 steps as small as 0.5 kPa, which was limited by the measurement setup.

The sensor with a 5 µm thick hydrogel (cover design II) and a gas permeable membrane also responds well to carbon dioxide within the desired range of 3 to 20 kPa CO_2 at a temperature of 25 ^oC and 37 ^oC. The maximum pressure generation at 37 ^oC is $0.29x10^5$ Pa at 20 kPa CO_2. The response time varies between 2 and 4 minutes at 37 ^oC, which agrees quite well with the medical requirement of below 10 minutes.

The sensor is linearly sensitive with the temperature due to the fixation manner of the porous cover to the pressure sensor. However, this might not be a significant problem since the temperature in the stomach is reasonably stable at 37 ^oC. Nevertheless, it is advised to apply other bonding techniques in the future and apply an additional temperature sensor for automatic compensation of the temperature sensitivity.

The sensor is obviously able to detect Pco_2 steps as small as 0.5 kPa, which is not in agreement with the medical resolution requirement of 0.1 kPa. Nevertheless, it is expected that the sensor is able to detect such low steps, but this could not be verified due to the limitations of the used measurement setup.

It is experimentally verified that 1 M HCl, which can be present inside the stomach, has no influence on the response of the sensor.

Four months after manufacturing, the sensor is still able to detect Pco_2 changes. However, the maximum pressure generation is decreased, which might be caused by aging, hydration or cracking of the epoxy glue. Nevertheless, it is promising that the sensor still functions despite the fact that it is manufactured by hand.

The response time limiting factor of the sensor is the reaction kinetics, i.e. the hydration of carbon dioxide. This was determined with the experimentally found results and differences between the two cover designs. Adding carbonic anhydrase to the electrolyte of the sensor might improve the response time of the sensor, but might also cause unexpected behavior of the gel.

The performed experiments have resulted in a considerable characterization of the sensor. However, only after an improved (mass) fabrication method, it is useful to fully characterize the sensor (CO_2 response, accuracy, reproducibility, hysteresis, long-term stability, etc). Nevertheless, the characterization results show that the sensor is considered to fulfill most of the medical requirements.

7.6 References

1 P.C. Hiemenz, Polymer Chemistry: the basic concepts, 1984, Marcel Dekker inc., New York, USA.

2 G. Odian, Principles of Polymerization, 3rd ed., 1991, John Wiley & Sons inc., New York, USA

3 W.H. Ko, J. Hynecek, S.F. Boettcher, *IEEE Trans. Electron Devices* 1979, **26**, 1896.

4 B. van der Schoot, P. Bergveld, *Analytica Chimica Acta* 1984, **166**, 93.

5 A. Varlan, W. Sansen, Micromachined conductometric $p(CO_2)$ sensor, Sens. Actuators B, 1997, 44, 309.

6 R. Chang, Physical Chemistry for the Biological Sciences, 1st ed., 2000, University Science Books, California, USA.

7 G.J. Schwartz, *J. Nephrol.* 2002, **15**, 61.

8 S.J. Dodgson, R.E. Tashian, G. Gross, N.D. Carter, The Carbonic Anhydrases, 1991, Plenum, New York, USA.

9 C. Cammaroto, L. Diliberto, M. Ferralis, R. Mance, A. Sanna, M. Giordano, *Sens. Actuators B* 1998, **48**, 439.

10 S. Hanstein, D. de Beer, H.H. Fella, *Sens. Actuators B* 2001, **81**, 107.

11 M. D. Marazuela, M. C. Moreno Bondi, G. Orellana, *Sens. Actuators B* 1995, **29**, 126.

Chapter 8

Conclusions and Recommendations

In this final chapter some overall conclusions are drawn, followed by a reiteration of the conclusions of the preceding chapters. Subsequently, recommendations are given for techniques to manufacture the sensor on wafer scale in the cleanroom for mass production. Furthermore, suggestions are provided on how to manufacture the sensor in a catheter and how to modify the sensor for other applications.

8.1 Conclusions

Overall, the research project of the hydrogel-based carbon dioxide sensor has reached an advanced and promising stage. The sensor is considered to fulfill most of the medical requirements of measuring gastric carbon dioxide levels for diagnosing gastrointestinal ischemia[1-6]. The behavior of the sensor is extensively studied and appears to be well-predictable. The best qualities of the sensor are the lack of a reference electrode and the use of an existing pressure sensor that is easily accepted in the medical field. Furthermore, the sensor is quite robust, which facilitates its use in medical circumstances. Below the conclusions per chapter are reiterated.

Chapter 1

Regarding the medical requirements of gastric carbon dioxide detection, most available measurement principles are not suitable. Optical sensors are large and expensive, have a high lower detection limit and require advanced readout equipment. Most electrochemical carbon dioxide sensors work at high operating temperatures, are cross-sensitive (other gases or humidity) and are only suitable for measuring low concentrations of carbon dioxide. The Severinghaus concept[7] has proven to be beneficial: it operates at room temperature, is well predictable and is fully reversible. The principle is based on converting the partial pressure of carbon dioxide into a certain pH. Severinghaus used a pH glass electrode to measure this pH, but this electrode is difficult to miniaturize. Although the micro-sized ISFET may be a good alternative, a reference electrode is needed, as for most other presented alternatives like iridium oxide or polymeric membrane electrodes. The reference electrode is known to suffer from drift and is difficult to miniaturize and maintain.

As already mentioned, the Severinghaus concept has some nice advantages, which makes it suitable for gastric Pco_2 measurements. However, no suitable pH measurement method can be found in literature that meets the medical requirements and/or does not require a reference electrode. One possible method, never explored for this purpose, is determining the pH by means of a pH-sensitive hydrogel. In the medical field a lot of experience exists with catheter-tip pressure sensors. When such an existing pressure sensor would be modified with a hydrogel, a new type of CO_2 sensor can be created which would be accepted easily in the medical field

Chapter 2

Stimulus-sensitive hydrogels are very interesting materials for the fabrication of sensors and actuators. Because the kinetics of the swelling process is dictated by diffusion, miniaturization is indispensable to make sensors and actuators with good characteristics.

It has been shown that with the chemical modification of hydrogels a large number of different sensors can be made. These include sensors for dissolved ions, gases, enzyme substrates and antigens. To convert the

swelling signal to an electrical signal a number of possibilities exist like conductometry and light transmission.

Stimulus-sensitive hydrogel actuators have a number of advantages over existing μTAS[8,9] actuators. Their high resilience gives them superior dust tolerance over actuators made from hard materials and it makes them suitable for cell-handling applications. The fact that hydrogel actuators can be controlled with small voltages and currents gives them an extra benefit over conventional μTAS actuators. In contrast with these conventional actuators no elaborate interfacing electronics is needed to control hydrogel actuators and direct interfacing with microcontrollers is possible. By integrating the microelectronic circuits needed for the operation of the μTAS system on the same chip surface, a further degree of miniaturization is achieved. This could lead to the development of extremely small total analysis systems that can operate for very long time periods and need only a small energy source.

The fabrication of gel sensors and actuators with UV photolithography makes them compatible with the conventional fabrication techniques used in μTAS system fabrication and opens up the opportunity of mass production.

Chapter 3

Two sensors were tested with different hydrogel configurations: hydrogel microspheres and a hydrogel disk. With both configurations CO_2 detection was achieved[10,11].

The two sensors are quite different regarding the applied pressure transducer, hydrogel volume and technical assembly procedure. Furthermore, the measurement principles are different: direct detection of hydrogel pressure generation and indirect through silicone rubber. For these reasons, both sensors cannot be compared with respect to the response time. Nevertheless, two important differences are noted. The signal of the sensor with the hydrogel disk was, from the beginning, very stable and the sensor showed the expected behavior. The hydrogel disk was also easier to synthesize and handle, and was reasonably fast despite the fact that a solid piece of gel is used. Therefore, the conclusion is drawn that a thin HEMA-co-DMAEMA pH-sensitive hydrogel disk, or layer, is the best option as sensing material in the hydrogel-based CO_2 sensor. Since a

hydrogel with a thickness below 50 µm can easily be made with micromachining techniques, it should be possible to further reduce the response time of the sensor.

Chapter 4

A method has been demonstrated to study the behavior of hydrogels under isochoric conditions[12]. The device, which has dimensions in the micrometer scale, has the advantage that measurements can be carried out reasonably fast for typical hydrogel characterization and in real-time with the use of a small pressure sensor. It is shown that a pH-sensitive hydrogel can generate pressure under isochoric conditions, dependent on the amount of ionizable groups, the ionic strength of the external solution and the pH. Higher pressures can be obtained by incorporating more titratable groups or by decreasing the ionic strength of the surrounding solution. Furthermore it is concluded that the rate of pressure generation depends on the amount of ionizable groups and the buffer concentration. Equilibrium pressures are reached faster when less ionizable groups are incorporated or when higher buffer concentrations are used. Due to the Donnan effect, the pH inside the hydrogel is not equal to the external solution pH. Experimental data show that the pK_a of the hydrogel is shifted down. It is believed that the presented method is a simple and fast manner to characterize the static and dynamic stimulus-dependent behavior of hydrogels, and may be used for studying the behavior of other gels such as immuno-sensitive or glucose-sensitive hydrogels. The found characteristics are very useful for designing the hydrogel-based CO_2 sensor. It is now known in which pH range the hydrogel responds and at which ionic strength the response is at its maximum. With these parameters the sensor with highest resolution can be designed. Furthermore it is now known that the response time of the sensor can be influenced by varying the amount of protonable groups.

A restriction of the presented characterization method is the presence of pores in the cover. After all, the pores allow hydrogel to swell through which undermines the definition of isochoric. Nevertheless, the pores are absolutely necessary to exchange ions with the environment.

At the moment two types of covers have been explored: one with 50 µm pores and 20 µm spacing, which did not work (due to the too small

spacing), and another with 50 µm pores and 50 µm spacing, with which all experiments were performed. In order to optimize the characterization method more research must be performed on the influence of the cover parameters. Possibilities are changing the pore shape, e.g., rectangular or round pores, or varying the dimensions of the pores and spacing.

Chapter 6

The electrolyte and prehydrogel solution are prepared with simple methods and widely-available chemicals. The sensor parts are made with standard cleanroom techniques. However, the assembly of the single parts to a complete sensor is laborious with a lot of manual actions and therefore the yield is not high. Nevertheless, this method is suitable in this stage of the research since it is relatively simple and requires no additional complicated (cleanroom) equipment. Yet, it enables the exploration of the sensor capabilities. It is not advised to use the current assembly method for future commercial manufacturing of the sensor, but to adapt it to mass fabrication techniques.

Chapter 7

The sensor without a gas permeable membrane and with a 10 µm thick hydrogel (cover design I) responds well to carbon dioxide within the medically interesting range of 3 to 20 kPa CO_2. At 20 kPa CO_2 a maximum pressure of 1.0×10^5 Pa is generated[13]. The response time varies between 7 and 20 minutes, which does not fulfill the medical requirement of a response time below 10 minutes. The sensor is able to detect Pco_2 steps as small as 0.5 kPa, which was limited by the measurement setup.

The sensor with a 5 µm thick hydrogel (cover design II) and a gas permeable membrane also responds well to carbon dioxide within the desired range of 3 to 20 kPa CO_2 at a temperature of 25 ^oC and 37 ^oC. The maximum pressure generation at 37 ^oC is 0.29×10^5 Pa at 20 kPa CO_2. The response time varies between 2 and 4 minutes at 37 ^oC, which agrees quite well with the medical requirement of below 10 minutes.

The sensor is linearly sensitive with the temperature due to the fixation manner of the porous cover to the pressure sensor. However, this might not be a significant problem since the temperature in the stomach is

reasonably stable at 37 ^{o}C. Nevertheless, it is advised to apply other bonding techniques in the future and apply an additional temperature sensor for automatic compensation of the temperature sensitivity.

The sensor is obviously able to detect Pco_2 steps as small as 0.5 kPa, which is not in agreement with the medical resolution requirement of 0.1 kPa. Nevertheless, it is expected that the sensor is able to detect such low steps, but this could not be verified due to the limitations of the used measurement setup.

It is experimentally verified that 1 M HCl, which can be present inside the stomach, has no influence on the response of the sensor.

Four months after manufacturing, the sensor is still able to detect Pco_2 changes. However, the maximum pressure generation is decreased, which might be caused by aging, hydration or cracking of the epoxy glue. Nevertheless, it is promising that the sensor still functions despite the fact that it is manufactured by hand.

The response time limiting factor of the sensor is the reaction kinetics, i.e. the hydration of carbon dioxide. This was determined with the experimentally found results and differences between the two cover designs. Adding carbonic anhydrase to the electrolyte of the sensor might improve the response time of the sensor, but might also cause unexpected behavior of the gel.

The performed experiments have resulted in a considerable characterization of the sensor. However, only after an improved (mass) fabrication method, it is useful to fully characterize the sensor (CO_2 response, accuracy, reproducibility, hysteresis, long-term stability, etc). Nevertheless, the characterization results show that the sensor is considered to fulfill most of the medical requirements.

8.2 Recommendations

One of the major improvements would be manufacturing the complete sensor with standard cleanroom techniques instead of the manual assembly technique. This will dramatically increase the yield and it is expected that the sensors will be more stable and accurate. Below,

recommendations are given for manufacturing the sensor with standard cleanroom techniques, followed by suggestions on how to mount the sensor in a catheter. At the end ideas are provided on how to adapt the sensor to make it suitable for other applications.

8.2.1 Manufacturing the sensor on wafer scale

Spinning prehydrogel solution

In this thesis a technique is described to polymerize a pH-sensitive hydrogel *in situ* on top of a pressure sensor membrane. This can also be achieved with cleanroom techniques by spinning of the prehydrogel solution on a wafer with pressure sensors. By using photolithography, the prehydrogel solution can be polymerized and patterned on the pressure sensor membrane. This should be done in a nitrogen atmosphere to prevent oxygen to interfere with the polymerization. The most important parameters for the spinning process are the spin speed, the spin time and the viscosity of the prehydrogel solution. Early research already demonstrated the feasibility of the technique, as shown in figure 8.1. Prehydrogel solution was spun on wafers at various spin speeds for 20 seconds and subsequently polymerized by photolithography. Then, the thickness of the dehydrated hydrogel was measured with a Dektak surface profiler (Veeco 8). Although there was a slightly nonuniform thickness of hydrogel patterns over the wafer, the method is certainly applicable after optimization. Note that polyvinylpyrrolidone was added to the prehydrogel solution to increase the viscosity; however, this is not recommended for the CO_2 sensor application.

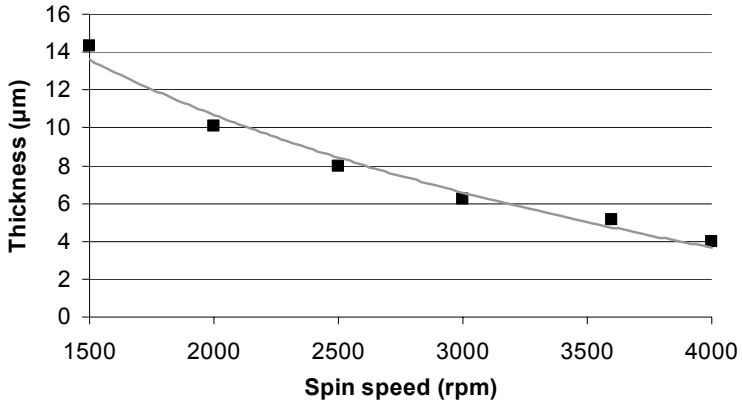

Figure 8.1. Average thickness of dehydrated hydrogel patterns after polymerization at various spin speeds for 20 seconds.

After the spinning and photolithography, it is recommended to place the wafer with patterned hydrogels in DI water for 24 hours to allow unreacted monomers to diffuse out.

To improve the attachment of the hydrogel to the wafer surface an adhesion promoter or primer can be used. Hexamethyldisilane (HMDS) is such a promoter, which is well suitable and can even improve the initial hydration of the gel[14].

To improve the response time of the sensor, it is possible to further decrease the thickness by the hydrogel. By spinning, a thickness of e.g. 2.5 µm can easily be achieved. Of course this would also decrease the maximum pressure generation. However, this might not be a problem since it is expected that the stability and accuracy of the sensor will be improved by the fabrication with standard cleanroom techniques.

The spinning and polymerization of the hydrogel is the most crucial process during the manufacturing of the sensor with standard cleanroom techniques. After all, its dimensions in dehydrated state should exactly agree with the dimensions of the hydrogel cavity in the porous cover. It is recommended that the thickness of the dehydrated hydrogel is slightly less (ca. 5-10%) than the cavity depth. In this case, the hydrogel will fit exactly in the cavity when hydrated, resulting in a small offset pressure. Additional pressure will be generated when the pH is decreased by carbon dioxide.

Low-temperature bonding

After spinning and patterning of the hydrogel, the wafer with porous covers can be mounted on top. Conventional anodic bonding occurs at 450 ^{o}C and higher. However, a bonding technique at lower temperature is preferred in order to preserve the hydrogel, which can resist temperatures up to approximately 150 ^{o}C. A suitable technique might be polymer or adhesive bonding where the bonding temperature can be lower than 100 ^{o}C and high bonding strengths can be achieved. A potential intermediate bonding material might be benzocyclobutene (BCB) that gives very strong void-free bonds[15-18]. Possibly, additional problems might occur such as imperfect sealing and poor long term stability, and may need further investigation. Perhaps, supplementary sensor packaging is required. Note that the bondpads of the pressure sensor should remain uncovered after bonding in order to apply the wirebonds.

Gas permeable membrane

At the moment the gas permeable membrane is attached to a silicon carrier. However, it is recommended to directly mount the membrane to the porous cover so an additional carrier wafer is not required. This will also reduce the thickness of the sensor.

A method to attach a polydimethylsiloxane membrane directly to a silicon surface can be achieved by exposing the PDMS surface to oxygen plasma and immediately afterwards bringing both surfaces together at room temperature[19-21]. PDMS comprises repeating units of $–O-Si(CH_3)_2-$. It is believed that oxygen plasma introduces silanol groups (Si-OH) at the expense of the methyl groups ($Si-CH_3$) [20]. These silanol groups react with the silanol groups of the silicon resulting in Si-O-Si bonds after loss of water molecules. These covalent bonds form a tight irreversible seal.

To use the method described above, a dummy wafer has to be pretreated. First, a coating should be applied which prevents adhesion of PDMS. Then PDMS can be spun on top and patterned with the same technique as described in chapter 6 or by using photopatternable PDMS[19]. Then, the oxygen plasma treatment can take place and immediately afterwards the PDMS membranes can be aligned and stamped on the wafer stack of covers and pressure sensors. This process together with the prehydrogel spinning and low temperature bonding processes are shown in figure 8.2. The dummy wafer can be re-used.

Note that it is also possible to use other types of gas permeable membranes in stead of PDMS, such as e.g. Teflon. Teflon also allows CO_2 to diffuse through and it better inhibits water vapor to diffuse through. However, the “welding” method of PDMS presented above is not applicable on Teflon. Furthermore, Teflon is more difficult to process.

After the processing as shown in figure 8.2, the sensors should be filled with the electrolyte using the method presented in chapter 6. This can be performed per diced sensor after mounting it in a catheter. Also, an automated process can be used where all sensors are simultaneously filled by means of vacuum and afterwards the filling holes are closed by computer-controlled dispensing of droplets silicone glue. After curing of the glue, the wafer can be diced in order to obtain the single sensors.

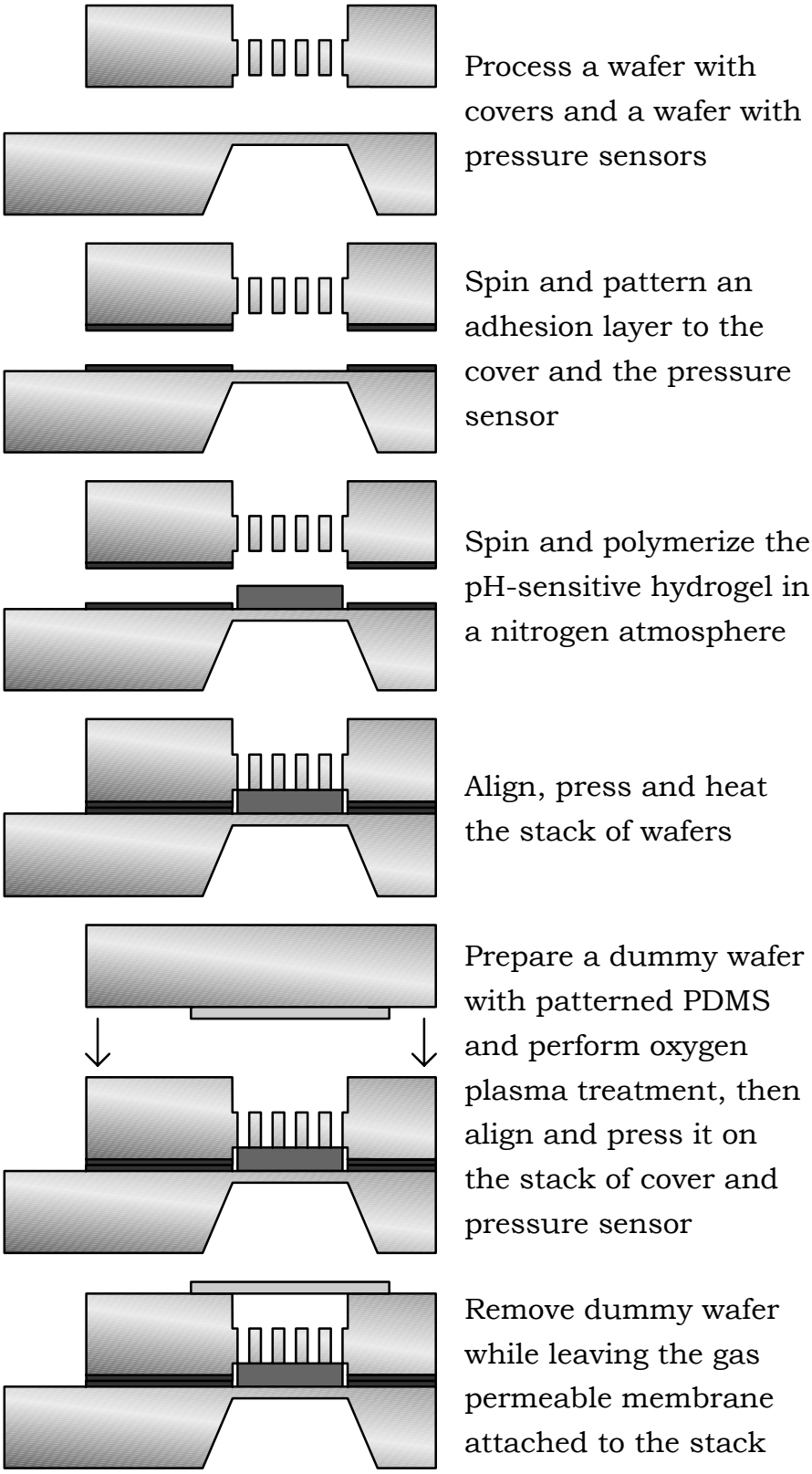

Figure 8.2. Process scheme of the sensor assembly by using standard cleanroom techniques. Note that the figures are not drawn on scale and in proportions.

8.2.2 The electrolyte

The electrolyte is optimized with respect to the ionic strength and pH range. However, more optimization is suggested:

- hygroscopic materials can be added to prevent/inhibit water vapor diffusion through the gas permeable membrane, for instance glycerol;
- preservatives can be added which are also suitable for oral intake, such as sorbic acid or sodium benzene formic acid, to prevent bacterial and fungi growth;
- the enzyme carbonic anhydrase[22,23] can be added to the electrolyte in order to improve the response time of the sensor.

Before adding one of the above suggested materials, it is recommended to investigate what its influence is on the ionic strength and pH of the electrolyte.

8.2.3 Mounting the sensor in a catheter

The ultimate goal of the hydrogel-based sensor is measuring the partial pressure of carbon dioxide in the stomach. Therefore the sensor should be mounted in a catheter. A proposed method is demonstrated in figure 8.3.

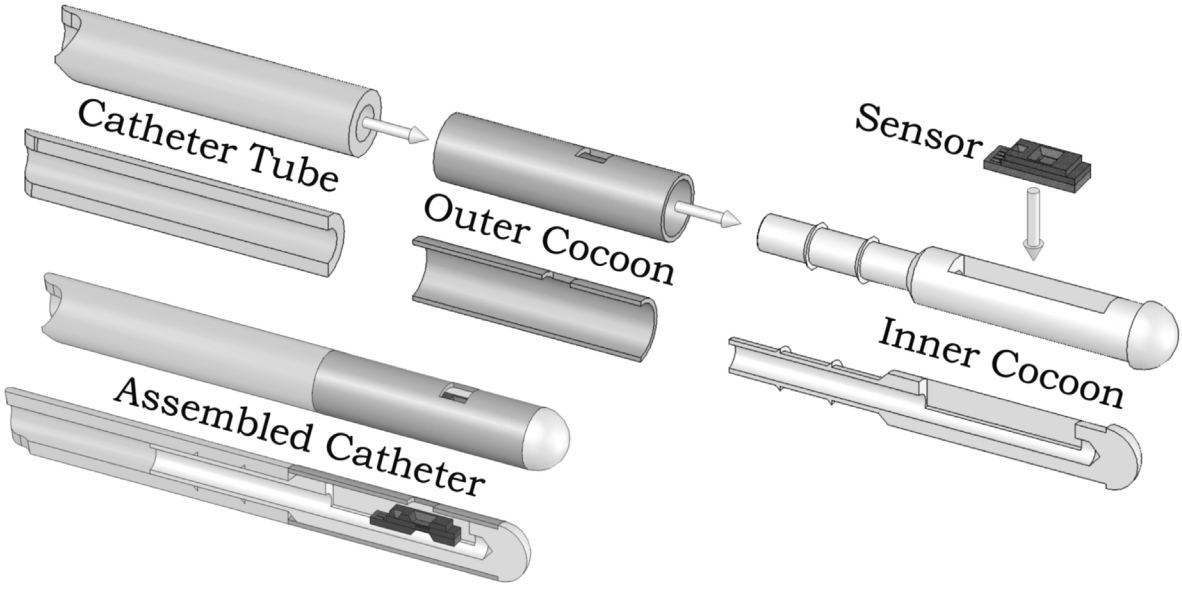

Figure 8.3. Schematic representation and cross-sectional view of the catheter parts and the assembled catheter (outer diameter is 2 mm).

The catheter consists of a catheter tube, the sensor, an outer cocoon and an inner cocoon. The assembly method is as follows: the sensor is wirebonded en subsequently placed in a cavity of the inner cocoon. Then the outer cocoon is moved over the inner cocoon. Next, the top side of the sensor is glued to the outer cocoon with silicone glue. This way the chance of stress is reduced to a minimum. Subsequently, the catheter tube is attached to the inner cocoon. The tube and the outer cocoon are both glued to the inner cocoon with silicone glue. Note that the wiring runs through the tube and that the back side of the pressure sensor membrane (reference pressure) is in contact with the (atmospheric) pressure in the catheter tube. The outer diameter of the assembled catheter is 2 mm, which is small enough to be led through the nose into the stomach.

To compensate for the temperature sensitivity of the sensor it is recommended to simultaneously measure the temperature. The temperature sensitivity of the pressure sensor itself is eliminated by exploiting the Wheatstone bridge principle (see chapter five, figure 5.1). The bridge consists of four piezoresistors and the output is a differential voltage signal independent of temperature fluctuations. However, a single piezoresistors has inherent temperature sensitivity and can therefore also be used as a temperature sensor when its resistance is compensated for the present pressure generated by the hydrogel. In figure 8.4 the measured temperature sensitivity of a single piezoresistors is shown.

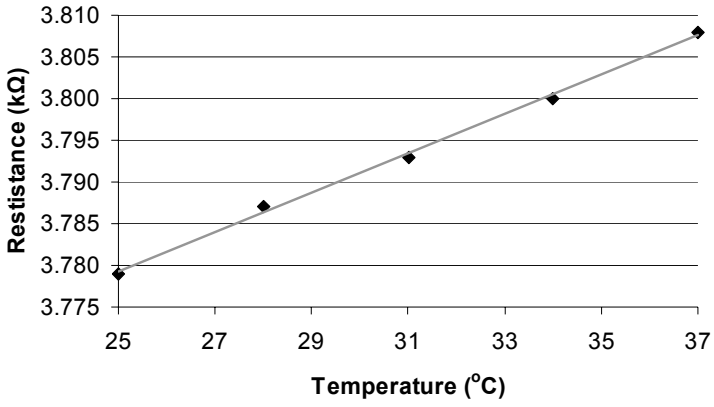

Figure 8.4. Measured temperature sensitivity of a single piezoresistor of the Sentron pressure sensor (type P4.2, E2303771).

The temperature was increased from 25 to 37 °C with steps of 3 °C and the resistance was measured with a multimeter (34401A, Hewlet Packard). As

can be seen, the piezoresistor has a linear temperature coefficient within the investigated range. In practice a multiplex system should be used to alternative measure the pressure and temperature.

8.2.4 Sensor modifications to measure other analytes and in other environments

For the gastric CO_2 measurements the hydrogel-based sensor is proposed which exploits a pH-sensitive hydrogel. However, it is possible to simple adapt the sensor in such a way that it can measure other analytes by using other types of hydrogels, such as:

- a glucose-sensitive hydrogel[24,25] to measure glucose levels;
- an antigen-sensitive hydrogel[26] to measure antigens;
- a hydrogel with incorporated crown ethers[27-29] to measure specific ions.

It might well be possible that such an adapted sensor for other analytes requires a different membrane type or no membrane at all. Furthermore, it is probable that an electrolyte with different composition should be used.

It is also possible to modify the sensor in such a way that it can measure CO_2 in other environments within a different range, such as the Pco_2 in greenhouses or in air. In this case the bicarbonate concentration and/or hydrogel pK_a should be adapted to match the new Pco_2 range.

An extra feature of the sensor would be a calibration option, which can be realized by integrating a simple coulometric pH actuator system[30]. By applying a voltage over two electrodes in the electrolyte, protons can be generated at the anode (electrolysis), which titrate the hydrogel, and hydroxyl ions at the cathode,

anode: $2H_2O + 4e^- \rightarrow 4H^+ + O_2(g)$, (8.1)

cathode: $2H_2O + 2e^- \rightarrow 2OH^- + H_2(g)$. (8.2)

As can be seen, also hydrogen and oxygen gas is generated during the electrolysis. This can be avoided by integrating a platinum catalyst[30], which catalyzes the regeneration of water from the two gasses,

$$2H_2(g) + O_2(g) \rightarrow 2H_2O\,. \qquad (8.3)$$

In the sensor the anode should be placed near the hydrogel and the cathode as far away as possible. A short voltage pulse would be enough to provoke some pressure generation, which can be used for the calibration.

8.3 References

1 A.B. Groeneveld, J.J. Kolkman, *J. Crit. Care* 1994, **9**, 198.

2 J.J. Kolkman, J.A. Otte, A.B. Groeneveld, *Br. J. Anaesthesia* 2000, **84**,101.

3 J.J. Kolkman, Gastric Pco_2 tonometry: Methodology and clinical potential for detection of ischemia (thesis), 1997, Thesis Free University Amsterdam, Amsterdam, The Netherlands.

4 J.J. Kolkman, M.D. L.J. Zwaarekant, K. Boshuizen, A.B. Groeneveld, S.G. Meuwissen, *J. Clinical Monitoring* 1997, **13**, 115.

5 J.A. Otte, E. Oostveen, R.H. Geelkerken, A.B. Groeneveld, J.J. Kolkman, *J. Appl. Physiol.* 2001, **91**, 866.

6 J.J. Kolkman, *Scand J Gastroenterology* 2004, in press.

7 J.W. Severinghaus, A.F. Bradley, *J. Appl. Physiol.* 1958, **13**, 515.

8 A. van den Berg and T.S.J. Lammerink, *Topics in Current Chemistry* 1998, **194**, 22.

9 R.P. Feynman, *J. Microelectromech. Syst.*, 1992, **1**, 60.

10 S.Herber, W. Olthuis, P. Bergveld, *Sens. Actuators B* 2003, **91**, 378.

11 S. Herber, W. Olthuis, P. Bergveld, A. van den berg, *Sens. Actuators B* 2004, **103**, 284.

12 S. Herber, J. Eijkel, W. Olthuis, P. Bergveld, A. van den Berg, *J. Chem. Phys.* 2004, **121**, 2746.

13 S. Herber, J. Bomer, W. Olthuis, P. Bergveld, A. van den Berg, *Biomedical Microdevices*, accepted for publication.

14 D. Kuckling, J. Hoffmann, M. Plötner, D. Ferse, K. Kretschmer, H.J. Adler, K.F. Arndt, R. Reichelt, *Polymer* 2003, **44**, 4455.

15 F. Niklaus, P. Enoksson, E. Kälvesten, G. Stemme, *J. Micromech. Microeng.* 2001, **11**, 100.

16 F. Niklaus, H. Andersson, P. Enoksson, G. Stemme, *Sens. Actuators B* 2001, **92**, 235.

17 J. Oberhammer, F. Niklaus, G. Stemme, *Sens. Actuators B* 2004, **110**, 407.

18 Y.S. Choi, J.S. Park, H.D. Park, Y.H. Song, J.S. Jung, S.G. Kang, *Sens. Actuators B* 2003, **108**, 201.

19 X. Ma, B. Gierhart, S.D. Collins, R.L. Smith, Final report 1998-99 for MICRO Project 98-144.

20 J.C. McDonald, D.C. Duffy, J.R. Anderson, D.T. Chiu, H. Wu, O.J.A. Schueller, G.M. Whitesides, *Electrophoresis* 2000, **21**, 27.

21 D. Armani, C. Liu, N. Aluru, 12th IEEE International Conference on Micro Electro Mechanical Systems 1999, pp. 222-227.

22 G.J. Schwartz, *J. Nephrol.* 2002, **15**, 61.

23 S.J. Dofgson, R.E. Tashian, G. Gross, N.D. Carter, The Carbonic Anhydrases, 1991, Plenum, New York, USA.

24 T. Miyata, T. Uragami, K. Nakamae, *Advanced Drug Delivery Reviews* 2002, **54**, 79.

25 Y. Qui, K. Park, *Advanced Drug Delivery Reviews* 2001, **53**, 321.

26 T. Miyata, N. Asami, T. Uragami, *Nature* 1999, **399**, 766.

27 G. Mayes, J. Blyth, R.B. Millington, C.R. Lowe, *Anal. Chem.* 2002, **74**, 3649.

28 H. Holtz and S.A. Asher, *Nature* 1997, **389**, 829.

29 J. H. Holtz, J. S. Holtz, C. H. Munro, S. A. Asher, *Anal. Chem.* 1998, **70**, 780.

30 H. van der Linden, Investigation of the potentials of stimulus-sensitive hydrogels for microactuator applications (thesis), 2003, Enschede, The Netherlands.

SUMMARY

In this thesis the development of a new type of CO_2 sensor is described. The main application of the sensor is measuring the partial pressure of CO_2 in the stomach to diagnose gastrointestinal ischemia, which occurs when blood flow is insufficient to deliver oxygen to the stomach and intestines.

The sensor exploits a pH-sensitive hydrogel as sensing material and a micro pressure sensor as transducer. A pH-sensitive hydrogel swells and shrinks in response to pH changes. In this case, however, it is enclosed between the pressure sensor and a porous, silicon cover. The cover contains a reservoir being completely filled with bicarbonate electrolyte and is covered by a gas permeable membrane. The operating principle is as follows: CO_2 gas diffuses through the membrane into the electrolyte and starts a reaction resulting in a pH decrease. Consequently, the enclosed pH-sensitive hydrogel generates pressure, which is measured by the pressure sensor. The described process is fully reversible.

The overall dimensions of the final sensor are 2.92x0.95x0.70 mm^3 and the hydrogel thickness is 5 µm. The best qualities of the sensor are the lack of a reference electrode and the use of an existing pressure sensor that is easily accepted in the medical field.

The sensor responds well to carbon dioxide with a response time between 2 and 4 minutes per CO_2 step showing little hysteresis. A maximum pressure of 0.29×10^5 Pa is generated at 20 kPa CO_2. The sensor enables detection of steps smaller than 0.5 kPa CO_2 (limited by the used measurement setup). The sensor shows temperature sensitivity due to the applied construction manner, whereas the kinetics of the hydration of carbon dioxide is the response time limiting factor. However, both effects can relatively easily be compensated for respectively be improved. The sensor is considered to fulfill most of the medical requirements.

A major improvement will be to manufacture the complete sensor with standard cleanroom techniques to increase the yield and reproducibility, and to eliminate the temperature sensitivity. Furthermore, clinical trials should be performed with the sensor mounted in a catheter to verify its working as diagnostic tool.

SAMENVATTING

In dit proefschrift is de ontwikkeling van een nieuw type CO_2 sensor beschreven. De hoofdtoepassing van de sensor is het meten van de partiële CO_2 druk in de maag om maagdarm-ischemie te diagnosticeren. Deze ontstaat wanneer de doorbloeding onvoldoende is om zuurstof te leveren aan de maag en darmen.

De sensor gebruikt een pH-gevoelige hydrogel als gevoelig materiaal en een micro druksensor als transducent. Een pH-gevoelige hydrogel zwelt en krimpt ten gevolge van pH veranderingen. In dit geval is de gel echter opgesloten tussen de druksensor en een poreus, silicium deksel. De deksel bevat een reservoir, dat volledig gevuld is met bicarbonaat elektrolyt en is afgedekt met een gasdoorlatend membraan. Het werkingsprincipe is als volgt: CO_2 gas diffundeert door het membraan in de elektrolyt en start een reactie resulterende in een pH verlaging. Dientengevolge bouwt de opgesloten pH-gevoelige hydrogel een druk op die gemeten wordt met de druksensor. Het beschreven proces is volledig omkeerbaar.

De buitenafmetingen van de sensor zijn 2.92x0.95x0.70 mm^3 en de hydrogel dikte is 5 µm. De beste eigenschappen van de sensor zijn het ontbreken van een referentie elektrode en het gebruik van een bestaande druksensor, dat gemakkelijke acceptatie waarborgt in de medische wereld.

De sensor reageert naar behoren op koolstofdioxide met een responstijd tussen de 2 en 4 minuten per CO_2 stap, vrijwel zonder hysterese. Een maximum druk van $0.29x10^5$ Pa wordt opgebouwd bij 20 kPa CO_2. Met de sensor is het mogelijk stappen kleiner dan 0.5 kPa CO_2 te detecteren (begrensd door de gebruikte meetopstelling). De sensor vertoont temperatuurgevoeligheid door de gebruikte constructie methode, terwijl de snelheid van de hydratatie van koolstof dioxide de responstijd beperkende factor is. Beide effecten kunnen overigens worden voorkomen respectievelijk verbeterd. De sensor voldoet aan vrijwel alle medische eisen.

Een grote verbetering zal het fabriceren van de complete sensor met standaard cleanroom technieken zijn om zo de opbrengst en reproduceerbaarheid te verhogen en temperatuurgevoeligheid te elimineren. Verder zouden klinische testen met de in een katheter afgemonteerde sensor moeten worden uitgevoerd om zijn werking als diagnostisch gereedschap te toetsen.

LIST OF PUBLICATIONS

Full papers

H. van den Linden, S. Herber, W. Olthuis, P. Bergveld, *Development of stimulus-sensitive hydrogels suitable for actuators and sensors in microanalytical devices*, Sensors and Materials 2002, vol. 14, pp. 129-139.

S. Herber, W. Olthuis, P. Bergveld, *A swelling hydrogel-based Pco_2 sensor*, Sensors and Actuators B 2003, vol. 91, pp. 378-382.

H. van der Linden, S. Herber, W. Olthuis, P. Bergveld, *Stimulus-sensitive hydrogels and their applications in chemical (micro)analysis*, The Analyst 2003, vol. 128, pp. 325-331.

S. Herber, W. Olthuis, P. Bergveld, A. van den berg, *Exploitation of a pH-sensitive hydrogel disk for CO_2 detection*, Sensors and Actuators B 2004, vol. 103, pp. 284-289.

S. Herber, J. Eijkel, W. Olthuis, P. Bergveld, A. van den Berg, *Study of chemically induced pressure generation of hydrogels under isochoric conditions using a microfabricated device,* Journal of Chemical Physics 2004, vol. 121, pp. 2746-2751.

S. Herber, J. Bomer, W. Olthuis, P. Bergveld, A. van den Berg, *A miniaturized carbon dioxide gas sensor based on sensing of pH-sensitive hydrogel swelling with a pressure sensor*, Biomedical Microdevices 2005, vol. 7, issue 3.

Conference contributions

S. Herber, H. van der Linden, W. Olthuis, P. Bergveld, *The use of hydrogels for micro sensors and actuators,* Annual MESA$^+$ meeting 2001, Hengelo, the Netherlands, poster presentation.

S. Herber, W. Olthuis, P. Bergveld, *A swelling hydrogel-based carbon dioxide sensor*, The 9th International Meeting on Chemical Sensors 2002, Boston, USA, oral presentation and proceedings contribution.

S. Herber, H. van der Linden, W. Olthuis, P. Bergveld, *The use of hydrogels for sensors and actuators*, The Sense of Contact 4 2002, Woudschoten, the Netherlands, poster presentation and proceedings contribution.

S. Herber, W. Olthuis, P. Bergveld, A. van den Berg, *Exploration of stimulus-sensitive hydrogels as sensor material*, NWO congres Studiegroep Analytische Scheikunde 2002, Lunteren, the Netherlands, poster presentation.

S. Herber, W. Olthuis, P. Bergveld, A. van den Berg, *Exploitation of a pH-sensitive hydrogel for CO_2 detection*, Eurosensors XVII 2003, Guimarães, Portugal, oral presentation and proceedings contribution.

S. Herber, W. Olthuis, P. Bergveld, A. van den Berg, *A hydrogel-based CO_2 sensor*, The Sense of Contact 5 2003, Veldhoven, the Netherlands, poster presentation and proceedings contribution.

S. Herber, W. Olthuis, P. Bergveld, A. van den Berg, *Hydrogel-based sensor for CO_2 measurements*, The Sensor of Contact 6 2004, Wageningen, the Netherlands, poster presentation and proceedings contribution.

S. Herber, J. Bomer, W. Olthuis, P. Bergveld, A. van den Berg, *A hydrogel-based CO_2 microsensor for diagnosing gastrointestinal ischemia*, Annual MESA+ meeting 2004, Enschede, the Netherlands, poster presentation.

S. Herber, W. Olthuis, P. Bergveld, A. van den Berg, *Hydrogel-based sensor for CO_2 measurements*, Eurosensors XVIII 2004, Rome, Italy, oral presentation and proceedings contribution.

S. Herber, J. Bomer, W. Olthuis, P. Bergveld, A. van den Berg, *Development of a hydrogel-based carbon dioxide sensor*, The Sense of Contact 7 2005,

Wageningen, the Netherlands, oral presentation and proceedings contribution.

S. Herber, J. Bomer, W. Olthuis, P. Bergveld, A. van den Berg, *A micro CO_2 gas sensor based on sensing of pH-sensitive hydrogel swelling by means of a pressure sensor*, Transducers 2005, Seoul, Korea, accepted for oral presentation and proceedings contribution.

Lectures

S. Herber, J. Bomer, W. Olthuis, P. Bergveld, A. van den Berg, *The hydrogel-based CO_2 sensor*, 2004, Dresden, Germany, lecture.

DANKWOORD

Toen ik begon met promoveren, vers van het HBO met een dosis enthousiasme voor de micro wereld dankzij Rob Sillen, had ik geen flauw idee waar ik eigenlijk echt aan begon. Naar verloop van tijd bleek het toch wel een hele grote klus te zijn, maar mede dankzij de hulp en steun van anderen is het tot een succesvol einde gekomen en ben ik de trotse auteur van dit proefschrift. In dit hoofdstuk wil ik graag iedereen bedanken die hoe dan ook heeft bijgedragen.

Allereerst wil ik graag de mensen bedanken die direct met mijn onderzoek te maken hadden en mij hebben geholpen middels sturen en adviseren. Dat zijn de promotor Piet Bergveld, co-promotor Albert van den Berg en assistent promotor Wouter Olthuis. Dankzij jullie kans om te promoveren heb ik veel geleerd op allerlei vlakken, niet alleen het fysische en chemische maar ook het sociale.

Verder ben ik dank verschuldigd aan de mensen die de technische ondersteuning hebben geleverd. De grootste rol daarin is vertegenwoordigd door cleanroom-goeroe Johan Bomer die de sensoronderdelen heeft gemaakt waarmee het allemaal mogelijk is geweest. Ook heb ik vele praktische tips mogen ontvangen van Ton Verloop en Sjouke Hornstra. Allen hartelijk bedankt.

Bij aanvang van de promotie balanceerde mijn kennis van de chemie zo rond het nulpunt. Dankzij het didactisch vermogen van een aantal personen is deze kennis gelukkig voldoende opgekrikt. Heiko van der Linden heeft mij uitgebreid geïntroduceerd in de hydrogel wereld. Voor ik het wist synthetiseerde ik mijn eerste hydrogel terwijl ik daarvoor niet eens wist hoe een pipet vast te houden. Verder ben ik erg veel geholpen door Geert Besselink en vraagbaak Jan “fruit of the oak tree” Eijkel. Bij deze hartelijk bedankt.

Natuurlijk mag ik de studenten niet vergeten die een opdracht bij mij hebben gedaan. Dat waren Arnoud van den Dobbelsteen en Erik Staijen. Beiden hebben met hun IOO een leuke bijdrage geleverd en worden hiervoor hartelijk bedankt.

Vooral de goede werksfeer binnen BIOS heeft er voor gezorgd dat deze periode zeer plezierig is verlopen. Het grootste gedeelte van de dag werd

deze bepaald door mijn werkkamergenoten waarvan er inmiddels al wat zijn geweest: Heiko van der Linden, Geert Besselink, Erik “hihi” Krommenhoek, Edwin Oosterbroek, Monica Brivio en Björn Timmer. Ik hoop dat jullie het ook plezierig met mij op de kamer vonden ondanks mijn voorliefde voor metal muziek. De goede werksfeer werd verder versterkt door de vele onvergetelijke lunch- en koffiepauzes in de BIOS-hoek waarin soms de meest onmogelijke dingen werden besproken. Hiervoor wil ik graag mijn dank uiten aan alle Bio boyz ’n girlz, zoals de Erikken, de Jannen, “je weet nog wel eens wat” Adje, Jurjen, Roald, Ana, Patrick, Han, Egbert, Koen, Rob, Steven, Paul, Theo, Dorothee, Björn, Bart, Wojciech, Emiel, Hermine, Ida, Joke, Henk, Regina, conference-mate Thi Van-Anh Dam a.k.a. Annie en alle anderen.

Het belang van een goede privé situatie naast het promoveren mag niet onderschat worden. Natuurlijk zijn mijn ouders Otto & Miranda, mijn broertje Niels en mijn vriendin Dorothee hierin sterk betrokken en wil ik hen graag bedanken voor alle interesse, steun en gezellige momenten.

Het bleek verder af en toe noodzakelijk in het weekend de slechte hersencellen te elimineren middels bieravonden in Utrecht om er weer goede voor terug te krijgen. De centrale hoofdpersonen hierin zijn Randy, Marc en “kroegtijger” Ernesto. Niet alleen bedankt voor het tonen van jullie interesse in mijn onderzoek, maar ook voor het voeren van de vele uitgebreide gesprekken over van alles en nog wat.

Op een zondagavond of tijdens een LAN-party mocht ik graag een potje gamen met, of beter gezegd tegen Ed ⌖ Droog. Het was me een waar genoegen je altijd maar weer te sniperen. En onze dagelijkse lunchwandeling naar de campus supermarkt niet te vergeten natuurlijk.

Iedereen bedankt voor de plezierige en leerzame tijd!

Enschede, mei 2005